Microwave Laboratory

W. W. HANSEN LABORATORIES OF PHYSICS

STANFORD UNIVERSITY · STANFORD, CALIFORNIA

Microwave Laboratory
W. W. Hansen Laboratories of Physics
Stanford University
Stanford, California

THE THEORY AND APPLICATION OF SOME TRANSVERSE-WAVE INTERACTIONS

by

Russell E. Hayes

M. L. Report No. 1025

Technical Report
April 1963

Prepared under Office of Naval Research
Contract Nonr 225(48)(NR 373-361)
Jointly supported by the U. S. Army Signal Corps,
the U. S. Air Force, and the U. S. Navy
(Office of Naval Research)

ABSTRACT

The results of a theoretical and experimental investigation of transverse-wave couplers, and of frequency doublers employing these couplers in conjunction with a resonant quadrupole circuit, are described.

The theoretical description of transverse-wave couplers is based upon the well known coupled mode formalism which describes the interaction between the normal modes on a filamentary electron beam immersed in a longitudinal dc magnetic field and the normal modes on a periodic circuit. The theory of both traveling-wave and resonant couplers is developed in detail so that the significant characteristics of the coupling interactions are described in terms of known quantities. The coupled mode theory has been extended to include twisted transverse-wave couplers with a resulting clarification of this important class of interactions.

The theory shows that the traveling-wave couplers may have a large bandwidth but generally tend to be quite long due to the low interaction impedance characterizing this type of circuit. Much stronger coupling per unit length is obtained by the use of resonant circuits with a resulting decrease in the length and bandwidth of the coupler. The type of coupler to be used in a particular device depends upon the requirements and restrictions involved.

The theory of transverse-wave frequency doublers using a resonant quadrupole cavity is developed in detail from a coupled mode approach. It is found that the fast cyclotron wave doubler which has been investigated previously is a special case of a general class of interactions. In general, a periodic quadrupole circuit interacting with any one of the four transverse waves can result in a second harmonic output from the quadrupole if the proper synchronism conditions are met. Some of these cases are of particular interest since they involve an active interaction with the beam which can result in frequency conversion efficiencies that are greater than one hundred per cent. The characteristics of the various frequency doubling interactions are presented in terms of normalized curves and equations that may be readily used in the design of devices.

An experimental study of some of the coupling and frequency doubling schemes described in the theoretical analysis was carried out. In the course of this work several new types of transverse-field coupler and quadrupole circuits were investigated and found to be of practical importance. The experimental results were in good qualitative agreement with the theory in all cases, but a quantitative disagreement was observed in the cases in which the beam was an appreciable fraction of a normal mode wavelength in diameter.

Frequency doubling by means of the synchronous waves was observed, although the conversion efficiency was only one per cent of the theoretical value. This discrepancy is attributed to thick beam effects. Doubling by means of a fast cyclotron wave interaction was also observed, and the 25 per cent conversion efficiency in the quadrupole was in good agreement with the theory, as is to be expected since the relative beam diameter was small.

An amplifier consisting of two synchronous wave couplers was also investigated and the net gain of 8 db was 5 db below the predicted value. High values of gain can be expected from this device if a proper design, that takes into account thick beam effects, is used.

ACKNOWLEDGEMENT

I wish to express my gratitude to Professor Marvin Chodorow for the inspiration and guidance which he gave during the course of this work.

I would also like to thank Dr. Tore Wessel-Berg for the many hours of conversation that contributed so much to the author's efforts.

The contribution of Mr. V. Prosper and Mr. A. Moody of the Machine Shop, and of Mr. H. Landsbergen and Mr. W. Holmes of the Tube Shop, can hardly be overestimated.

Finally, I would like to thank Mr. A. Braun and the staff of the Drafting Room and of the Reports Office for their painstaking efforts in the preparation of the manuscript.

TABLE OF CONTENTS

CHAPTER I

INTRODUCTION

The study of transverse-wave electron devices has received widespread attention recently, primarily due to the promise of the higher efficiencies, lower noise figures, and basically new types of interactions which may be obtained by utilizing the transverse modulation of an electron beam. The transverse waves which can exist on a straight electron beam immersed in an axial magnetic field are characterized by transverse displacement and velocity modulation of the electrons as opposed to the longitudinal modulation characteristic of the more familiar space-charge waves. The initial experimental studies of transverse-wave devices by Cuccia,[1,2] Adler,[3] and others[4,5,6] have been notably successful in demonstrating the practicality of this class of devices and have served as an incentive for further work.

The first theoretical studies of interactions between a thin electon beam and a circuit supporting a transverse electric field were based upon a solution of the Lorentz force equation in terms of the dynamical variables for one electron.[7,8,9] This Lagrangian approach, while certainly adequate, does not yield solutions in the simple and intuitive form that is obtainable with a wave formalism. Siegman,[10] and others[11,12] have described the small-signal excitation of the beam in the transverse plane in terms of circularly polarized waves, yielding results which are easily described in terms of the coupling of normal modes. Two of these waves, the fast and slow cyclotron waves, are characterized by a rotation of the individual electrons at the cyclotron frequency. The phase velocities of these waves are greater than, and less than, the dc beam velocity as their names imply. The other two waves are characterized by pure transverse displacement of the electrons and are called synchronous waves since their phase velocities are equal to the beam velocity. Besides these differences the transverse waves are distinguished by the sign of the energy which they carry and their polarization. The applicability of the filamentary beam model, used to

obtain this wave description, to devices employing finite size beams is certainly to be questioned. However, Gordon[13] and Wessel-Berg[14] have demonstrated that, for beams of nominal thickness, the simple results obtained from a filamentary beam theory are approximately correct, although some additional waves are present.

Two classes of circuits have been important in the study of transverse-wave interaction. First are the transverse wave couplers which have a transverse electric field that is uniform over the portions of the transverse plane in which the interaction takes place. The first complete description of a transverse wave coupler was given by Cuccia,[9] although the description was in terms of the electron dynamics rather than waves. This coupler consisted of a parallel resonant circuit with the beam passing through the uniform field of the capacitor plates, or the microwave cavity equivalent of this, and an axial magnetic field with the cyclotron frequency equal to the signal frequency. In terms of the wave formalism this coupler excited the fast cyclotron wave with infinite phase velocity. Essentially all of the experimental devices which have been studied have employed this type of coupler. However, it is of some value to use couplers with other synchronism conditions to obtain new types of interactions, and to avoid the high magnetic field demanded by the use of the Cuccia coupler at microwave frequencies. Several authors have considered the theory of transverse-wave couplers in varying degrees of generality.[10-12, 15,16] These analyses have dealt with the general aspects of coupling to a traveling-wave circuit which can be predicted from the coupled mode equations. However, a detailed description of transverse-wave couplers, both traveling-wave and resonant, has not been given. Such a description would include a discussion of how sensitive the coupling between the circuit and the beam is to errors in the synchronism conditons, the coupler gain, bandwidth, and a comparison of the various types of couplers. One of the purposes of this study is to consider these, and other points, related to transverse-wave couplers.

The second class of circuits which have been of interest in connection with transverse waves are the quadrupole structures. The quadrupole field is characterized by an $r \cos 2\theta$ variation in the transverse plane, where r is the radius from the axis and θ is the angular position. The parametric amplifier developed by Adler, Hrbek and Wade[3] uses a resonant

quadrupole as the pumping cavity. Others have demonstrated that electrostatic quadrupoles of various designs are useful in dc pumped amplifiers.[17-18] The interaction between a thin beam and a general quadrupole circuit may also be analyzed in terms of coupled mode theory, as has been done by Blötekjaer and Wessel-Berg and others.[11,19] The differential equations now have time and space varying coefficients which lead to more complex solutions than in the case of the coupler type circuits.

One of the interesting possible classes of interactions in a quadrupole type cavity leads to frequency doubling. This had been noticed earlier by Cuccia[20] and later by others in connection with the Adler tube.[21] In this case the fast cyclotron wave excitation due to an infinite phase velocity input coupler induces a second harmonic current in the quadrupole cavity due to the difference in angular variation between the cyclotron wave and the quadrupole circuit. Lindsay and Caunter[22] analyzed this situation by means of a ballistic approach and obtained predictions of conversion efficiencies greater than fifty per cent. Cuccia also noted that the basic principle could be extended to higher multiplication ratios by using higher order multipole circuits, and obtained five per cent conversion efficiency in multiplying up to 3.2 kMc with a frequency quadrupler.[20]

The cyclotron wave frequency doubler described above is quite interesting, not only because of the possibility of high conversion efficiency but also because it appears that relatively high power levels could be obtained, and because the circuit dimensions make the device amenable to scaling to high frequencies. The previous work on frequency doublers has been restricted to this special case. One of the purposes of this study will be to carry out a general analysis, based on the coupled mode approach, of the class of frequency doublers employing one or more of the four transverse waves interacting with the electric field in a periodic quadrupole cavity.

In addition to the theoretical studies of coupler and quadrupole interactions that were indicated above, experimental studies of some transverse-wave devices were carried out. One purpose of this part of the research program was to develop some new types of transverse-field circuits that were suitable for use in transverse-wave tubes. A second purpose was to verify some of the interactions that were predicted in the theoretical analysis and have not been investigated by others.

A brief account of the contents of this report is given in this and the following paragraphs. Chapters II and III give a description of the traveling-wave and resonant type couplers which may be used to couple to the various transverse waves. The basic ideas in these chapters are not new, but the complete solutions to the problems discussed have not been given before. The next chapter deals with a new type of coupler circuit which has some interesting applications. These twisted circuits can be used to couple waves together in a manner which could not be obtained with conventional circuits. For example, it is possible to couple equally to the fast and slow cyclotron waves with the appropriate twisted coupler.

The next two chapters give a complete description of frequency doublers using quadrupole circuits. Chapter V is concerned with the cyclotron wave doubler, and the previous work which has been done on this subject is shown to be a special case of the more general device. Chapter VI describes the frequency doublers which employ the synchronous waves. These are particularly interesting devices because of the high conversion efficiency which can be obtained in some cases.

The next two chapters are reports of experimental studies of transverse-wave devices. Chapter VII describes a class of slow wave structures which are suitable for use as coupler and quadrupole circuits. Results of studies of the dispersion characteristics and interaction impedances are given. Finally, Chapter VIII describes results obtained from an experimental device which was used to study transverse-wave frequency doublers and couplers. An amplifier which consists of two synchronous-wave coupler cavities is described and the results of an investigation of frequency doublers based upon the cyclotron and synchronous wave interactions are given. To the author's knowledge, these are the first studies to be carried out, with periodic circuits, at dc power levels of more than 1.0 kilowatts. These results are important since they have a bearing on the question of the use of transverse-wave devices at high power levels.

CHAPTER II

TRAVELING-WAVE COUPLERS

The central purpose of this chapter is to use the coupled mode theory to obtain the information necessary to the understanding and design of traveling-wave couplers which can be used to excite the transverse waves on the beam. The solution of the basic equations is straightforward and others have described some of the results given here. However, a detailed discussion of this class of couplers has not been given, and is required in order to bring out the synchronism requirements, the bandwidth, and the scaling properties.

The discussion of interactions between transverse-field circuits and electron beams is restricted to those mechanisms which are usually associated with the excitation or removal of a signal on a beam. No discussion of traveling-wave tubes or backward-wave oscillators is given here, as these devices do not bear on the main purpose of this study.

The first section of this chapter gives a review of the coupled mode theory which is used for much of the analysis in this thesis. Then, in the next two sections this theory is applied to the discussion of coupling to a positive energy wave and then to coupling between both synchronous waves. The properties of an interesting class of traveling-wave couplers which are twisted about their axis will be left until Chapter IV.

A. REVIEW OF COUPLED MODE THEORY

The purpose of this section is to present the important results of the coupled mode theory for transverse-wave interactions in the form which has been used by Siegman.[10] This theory will form the basis of the analytical approach used in this, and the later chapters, to consider the various types of transverse-wave couplers. This review is necessary in order to provide the working equations for the later calculations.

The model which is used to derive the coupled mode equations is one in which the electron beam is considered to be a very thin filament of electrons traveling with a velocity u_0 in the positive z direction as Shown in Fig. 2.1. A magnetic field, B_0, directed along the z axis provides the restoring force for the transverse oscillations which characterize the transverse waves. The equation which describes the dynamics of the electrons which make up the filamentary beam is

$$d\vec{v}/dt = -(e/m)[\vec{E} + \vec{v} \times \vec{B}] \quad . \qquad (2.1)$$

In this equation $\vec{E}$ and $\vec{B}$ are the external vector fields and $\vec{v}$ is the velocity. The electronic charge e is a positive number. The electric field due to the circuit is assumed to have no z component and to be uniform in the transverse plane. This is strictly true only for an infinite phase velocity structure and is approximately true, over the region of interaction, for slow wave circuits if the beam is small in diameter and the beam excursion is small. The force due to the ac magnetic field of the circuit will also be neglected. This assumption is also strictly valid for infinite phase velocity and slow-wave structures.

For a beam of infinitesimal thickness, the modulation of the electrons is independent of the transverse dimensions so that the time derivative may be written as

$$d/dt = \partial/\partial t + u_0 \partial/\partial z \quad , \qquad (2.2)$$

where u_0 is the velocity in the z direction. Upon substituting (2.2) into (2.1) and using the definition of the cyclotron frequency

$$\omega_c = e B_0/m \qquad (2.3)$$

and the definition of velocity

$$v_x = dx/dt \quad , \quad \text{etc.} \quad ,$$

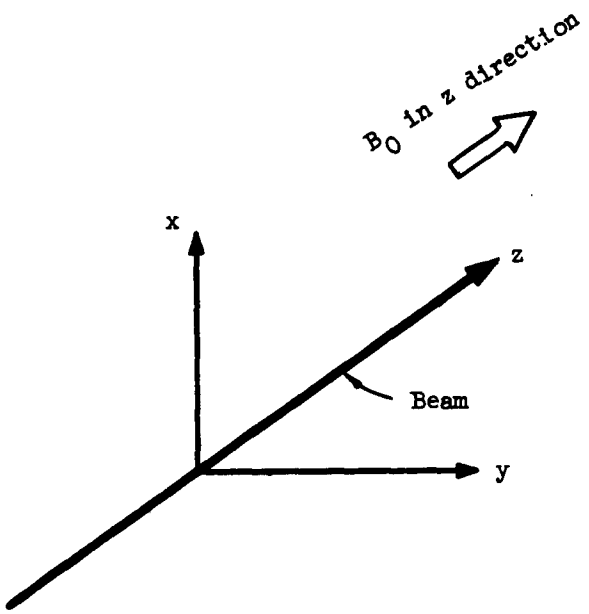

FIG. 2.1--The coordinate system for the coupled mode theory, showing the filamentary beam.

we obtain the four equations describing the motion of the beam. These are cast in a particularly simple formulation by assuming all quantities vary as $e^{j\omega t}$ and defining the circularly polarized variables:

$$r_+ = 1/2\ (x - jy) \quad , \quad v_+ = 1/2\ (v_x - jv_y)$$

$$r_- = 1/2\ (x + jy) \quad , \quad v_- = 1/2\ (v_x + jv_y) \tag{2.4}$$

$$E_+ = 1/2\ (E_x - jE_y)$$

$$E_- = 1/2\ (E_x + jE_y)$$

The beam excitation may then be expressed by the equations

$$\partial v_+/\partial z + j(\beta_e + \beta_c)\ v_+ = -\ e/m\ \frac{E_+}{u_0}$$

$$\partial v_-/\partial z + j(\beta_e - \beta_c)\ v_- = -\ e/m\ \frac{E_-}{u_0} \tag{2.5}$$

$$\partial r_+/\partial z + j\ \beta_e\ r_+ = v_+$$

$$\partial r_-/\partial z + j\ \beta_e\ r_- = v_- \quad ,$$

where

$$\beta_e = \omega/u_0$$

$$\beta_c = \omega_c/u_0 \tag{2.6}$$

It is evident that there are four wave-like solutions with $e^{-j\beta z}$ variation. The four values of β are:

$$\beta_1 = \beta_e + \beta_c$$

$$\beta_2 = \beta_e - \beta_c \qquad (2.7)$$

$$\beta_3 = \beta_e$$

$$\beta_4 = \beta_e \quad .$$

Each of these represents a normal mode on the beam and these will be defined later.

The next step in setting up the coupled mode formulation is to obtain the equation which describes the circuit excitation due to the modulation on the beam. Siegman[10] accomplishes this be considering the transmission line equations relating the circuit voltage and current to the current induced by the beam. This assumes that the circuit phase velocity is much less than the velocity of light, or that the structure is much smaller than the free-space wavelength, so that the electric field can be represented by a scalar potential. This is usually a valid assumption. We then have

$$\partial V/\partial z = \mp j\, \beta_0 Z_0 I$$

$$\partial I/\partial z = \mp j(\beta_0/Z_0)\, V + J \quad , \qquad (2.8)$$

where β_0 and Z_0 are the circuit propagation constant and impedance in absence of the beam and J is the current induced per unit length. The upper sign applies to a wave with positive group velocity, and the lower to a wave with negative group velocity. The transverse electric field at the beam position is defined in terms of the circuit voltage by the complex

polarization coefficients f_+ and f_-, which characterize the circuit:

$$E_+ = - f_+ V/D \qquad (2.9)$$

$$E_- = - f_- V/D \quad , \qquad (2.10)$$

where E_+ and E_- represent the circularly polarized fields given in (2.4), and D is an arbitrary normalizing distance which will not appear in any of the final results. Note that the complex expressions for the fields E_x and E_y are to be used in Eqs. (2.4). To insure that $|E|^2$ is equal to $(V/D)^2$ it follows that

$$f_+ f_+^* + f_- f_-^* = 1 \quad . \qquad (2.11)$$

The induced current per unit length can be represented by the expression given by Siegman:[10]

$$J = - j \frac{2I_0 \omega}{D u_0} (f_+^* r_+ + r_-^* r_-) \quad , \qquad (2.12)$$

where I_0 is the beam current. Equations (2.5), (2.8), and (2.12) are the equations necessary to describe the beam-circuit system for this transverse field case. These are put in the final form by defining the normal modes so that the square of their amplitude represents the power carried:

$$A_0 = V\sqrt{2Z_0} = \text{circuit wave}$$

$$A_1 = j k v_+ = \text{slow cyclotron wave}$$

$$A_2 = j k v_- = \text{fast cyclotron wave} \qquad (2.13)$$

$$A_3 = j k (v_+ + j \omega_c r_+) = \text{positive polarized synchronous wave}$$

and

$$A_4 = j\,k\,(v_- - j\,\omega_c\,r_-) = \text{negative polarized synchronous wave} \quad ,$$

where

$$k = \sqrt{\frac{I_0}{2e/m}\,\frac{\omega}{\omega_c}} \quad . \qquad (2.14)$$

Notice that the beam waves are circularly polarized. Siegman[10] shows that the power carried by the system is

$$P = \pm\,|A_0|^2 - |A_1|^2 + |A_2|^2 + |A_3|^2 - |A_4|^2 \quad . \qquad (2.15)$$

The final form for the coupled mode equations is:

$$\begin{aligned}
&\partial A_1/\partial z + j(\beta_e + \beta_c)\,A_1 = j\,K\,f_+\,A_0 \\
&\partial A_2/\partial z + j(\beta_e - \beta_c)\,A_2 = j\,K\,f_-\,A_0 \\
&\partial A_e/\partial z + j\,\beta_e\,A_3 = j\,K\,f_+\,A_0 \qquad (2.16) \\
&\partial A_4/\partial z + j\,\beta_e\,A_4 = j\,K\,f_-\,A_0 \\
&\partial A_0/\partial z + j\,\beta_0\,A_0 = \pm\,j\,K\,[f_+^*\,(A_3 - A_1) + f_-^*\,(A_2 - A_4)] \quad .
\end{aligned}$$

The coupling coefficient, K, is given by

$$K = \sqrt{\frac{1}{2}\,\frac{\omega}{\omega_c}\,\frac{K_T}{R_0}\,\beta_0^{\,2}} \quad , \qquad (2.17)$$

where K_T is the transverse interaction impedance, defined, in terms of the field and power flow, P, by

$$K_T = \frac{E_+ E_+^* + E_- E_-^*}{2 \beta_0^2 P} \quad , \qquad (2.18)$$

and R_0 is the dc beam impedance V_0/I_0.

In the absence of a circuit ($A_0 = 0$) these equations just give the four transverse waves which an propagate on a filimentary beam. The wave propagation constants are given by (2.7) and the dispersion characteristics are shown in Fig. 2.2. From (2.15) we see that the waves A_2 and A_3 carry positive energy while A_1 and A_4 carry negative energy. Since the subsequent work will be in terms of wave amplitudes, it is convenient to express the induced current and the beam displacement in terms of the wave amplitudes. By using (2.9) and (2.10), we obtain

$$J = - j \frac{2I_0}{Dku_0} \frac{\omega}{\omega_c} [f_+^* (A_1 - A_3) - f_-^* (A_2 - A_4)] \qquad (2.19)$$

and

$$x = \frac{1}{k\omega_c} [A_1 - A_2 - A_3 + A_4]$$

$$y = j \frac{1}{k\omega_c} [A_1 + A_2 - A_3 - A_4] \qquad (2.20)$$

These last equations are useful in the calculation of interception conditions.

The theory presented above has been very successful in predicting the characteristics of the transverse-wave devices which have been tested up to this time. However, the filamentary beam assumption which makes this simple approach possible is very likely to be violated in devices

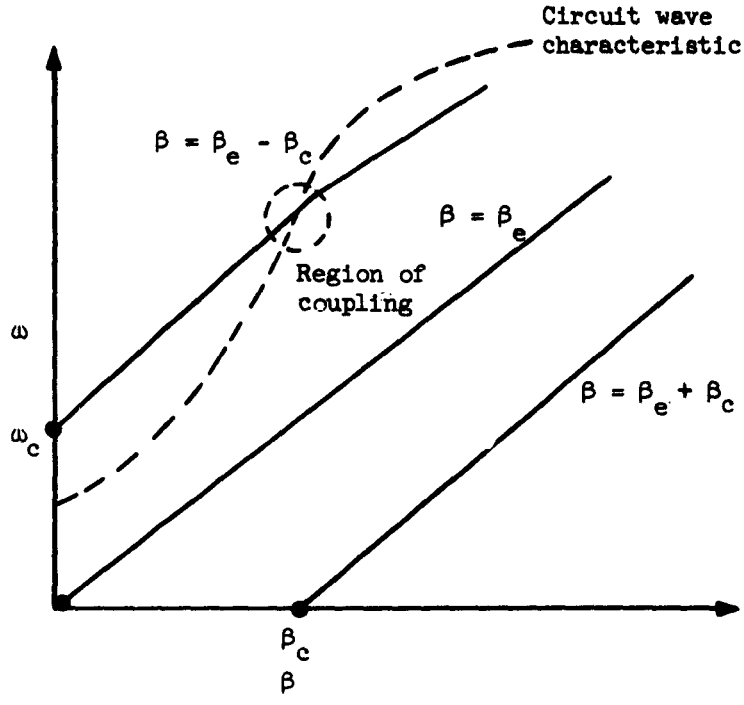

FIG. 2.2--The dispersion characteristics of the transverse waves.

which are intended to operate at dc power levels above the milliwatt region. Gordon[13] considered this problem, utilizing some simplifying assumptions, and found that, for beam radii, a, such that $\beta a \ll 1$, the filamentary beam theory still describes the motion of the center of mass of the beam. In this inequality β is the propagation constant of the beam wave in question. In addition to these solutions, another set of waves, which represent internal motion of the beam, was found. The propagation constants of these waves depend upon the space-charge density of the beam, and are most widely separated from the filamentary beam waves when a Brillouin flow beam is used. Wessel-Berg[14] has analyzed the Brillouin flow problem from a rigorous field approach and obtains results in qualitative agreement with Gordon's. In addition, Wessel-Berg finds higher order transverse waves having azimuthal variations $\exp(in\theta)$, where n is any integer. The conclusion which may be drawn from these results is that the filamentary beam theory still provides a guide for discussing high power interactions, but that additional beam waves with different phase velocities will be present. If care is not taken to avoid exciting these additional waves, the device will not perform in the manner predicted by the simple theory.

B. PASSIVE COUPLING TO ONE WAVE

Here we are interested in using a traveling-wave circuit as a coupler to excite one of the positive energy transverse waves. One application of such a coupler is in parametric amplifiers of the type described by Adler, where the amplifying mechanism is frequency independent and the bandwidth is determined by the couplers. In order to obtain a large bandwidth traveling-wave couplers are used. The alternative choice of resonant couplers and the resulting small bandwidths are discussed in the next chapter.

The circuit is assumed to have only a transverse electric field at the beam position as described in Section II.A. Selective coupling to one of the beam waves is accomplished by employing a circuit which has the appropriate phase velocity as well as a circularly polarized field component which is of the same polarization as the beam wave to be excited.

Because the phase velocities of the transverse waves are widely separated (β_c is usually of the order of magnitude of β_e) , or the waves are separated by their polarization, it is possible to have coupling between the circuit and essentially one beam wave. This simplifies the mathematics considerably.

Rather than consider either the positive energy cyclotron or synchronous wave alone, we will employ the generalized coupled mode equations which both waves obey. From Eqs. (2.16) we may write

$$\partial A_i/\partial z + j\,\beta_i A_i - j\,K\,f\,A_0 = 0$$

$$\partial A_0/\partial z + j\,{}_0A_0 - j\,K\,f^*\,A_i = 0 \qquad (2.21)$$

The subscript i designates which of the positive energy waves is under consideration and f is the polarization factor of that wave. Typical dispersion characteristics for the beam and circuit waves are shown in Fig. 2.2. These equations are solved easily by substituting in the assumed exponential variation $e^{-j\beta z}$ to yield the values of β :

$$\beta = \frac{\beta_0 + \beta_i}{2} \pm \sqrt{\left(\frac{\beta_0 - \beta_i}{2}\right)^2 + ff^*K^2} \qquad (2.22)$$

By matching the conditions imposed at the input end of the circuit and beam (at $z = 0$) the expressions for the circuit and beam waves are obtained:

$$A_0 = \left\{a_0(0)\left[\cos\phi - j\frac{\gamma}{\sqrt{1+\gamma^2}}\sin\phi\right] + a_i(0)\left[j\frac{f^*/|f|}{\sqrt{1+\gamma^2}}\sin\phi\right]\right\} e^{j\left(\omega t - \frac{\beta_0+\beta_i}{2}\right)z}$$

$$A_i = \left\{a_i(0)\left[\cos\phi + j\frac{\gamma}{\sqrt{1+\gamma^2}}\sin\phi\right] + a_0(0)\left[j\frac{|f|/f^*}{\sqrt{1+\gamma^2}}\sin\phi\right]\right\} e^{j\left(\omega t - \frac{\beta_0+\beta_i}{2}\right)z} \qquad (2.23)$$

where we define

$$\gamma = \frac{\beta_i - \beta_0}{2|f|\,K} \tag{2.24}$$

and

$$\phi = K\,|f|\,\sqrt{1+\gamma^2} \tag{2.25}$$

These results are equivalent to those given by Louisell.[23] However, the dependence upon the polarization of the circuit is shown explicitly here. The polarization factor has been retained to emphasize the difference between linearly and circularly polarized circuits.

The usual case of interest is the one in which the initial excitation is either entirely on the circuit (an input coupler) or on the beam (an output coupler). In that case, the complete transfer of power from one wave to the other occurs in the distance

$$\ell = \pi/2|f|K \tag{2.26}$$

at synchronism ($\gamma = 0$). For a circuit which propagates a linearly polarized field, polarized in the x direction, $f_+ = f_- = 1/\sqrt{2}$, while for a circularly polarized field f_+ or f_- is unity. Since the coupling coefficient, K, is small at best, it is desirable to use circularly polarized circuits to reduce the coupler length. However, for practical reasons it is easier to develop linearly polarized structures and the circuits to be discussed in Chapter VII are linearly polarized. It is also true that, for some of the interactions to be discussed later, linearly polarized structures are desirable. It should be noted that the use of linearly polarized couplers for synchronous waves does not fall into the kind of interaction discussed here since the two waves have the same phase velocity. This situation will be discussed in Section II.C.

There are two important points of interest in the consideration of traveling-wave couplers: the synchronization requirements and the bandwidth. From Eqs. (2.23) it is a simple matter to decide how close to

synchronism the beam and circuit waves must be to obtain strong interaction. For example, if an input coupler is designed correctly, its length, ℓ, satisfies (2.26) so that all of the power is transferred to the beam at synchronism. When the beam varies from this correct velocity so that γ is not zero, we have as the ratio of the output beam power to the input power, defined as the transfer efficiency,

$$\eta_T = \frac{P_{beam}}{P_{input}} = \left[\frac{\sin\left(\frac{\pi}{2}\cdot\sqrt{1+\gamma^2}\right)}{\sqrt{1+\gamma^2}}\right]^2 \quad . \quad (2.27)$$

This may be put in a more convenient form by substituting the definition of γ from (4) and using (5). Then the transfer efficiency may be written[1]

$$\eta_T = \left[\frac{\sin\left(\frac{\pi}{2}\cdot\sqrt{1+[(\theta/\pi)\epsilon]^2}\right)}{\sqrt{1+[(\theta/\pi)\epsilon]^2}}\right]^2 \quad , \quad (2.28)$$

where

$\theta = \beta_0 \ell$ = length of coupler in radians ,

$\epsilon = 1 - v_0/v_i$ = fractional velocity error ,

v_0 = circuit phase velocity ,

v_i = beam wave phase velocity .

This result, which is symmetrical in ϵ, is plotted in Fig. 2.3. It is equally applicable to output couplers. We see that the half power points

[1] We have assumed that K is invariant to small changes in the beam velocity. This is valid, for small coupling, even though K is proportional to the beam velocity [as may be seen from (2.17) by noting that the beam current is proportional to the three halves power of the voltage] since the primary change in the transfer coefficient comes from the velocity error multiplied by the large number θ/π and not from the small variation in K. Equation (2.28) is quite correct at $K/\beta_0 = 0.1$, which is strong coupling for a traveling-wave circuit, as can be seen from the results in Chapter VII.

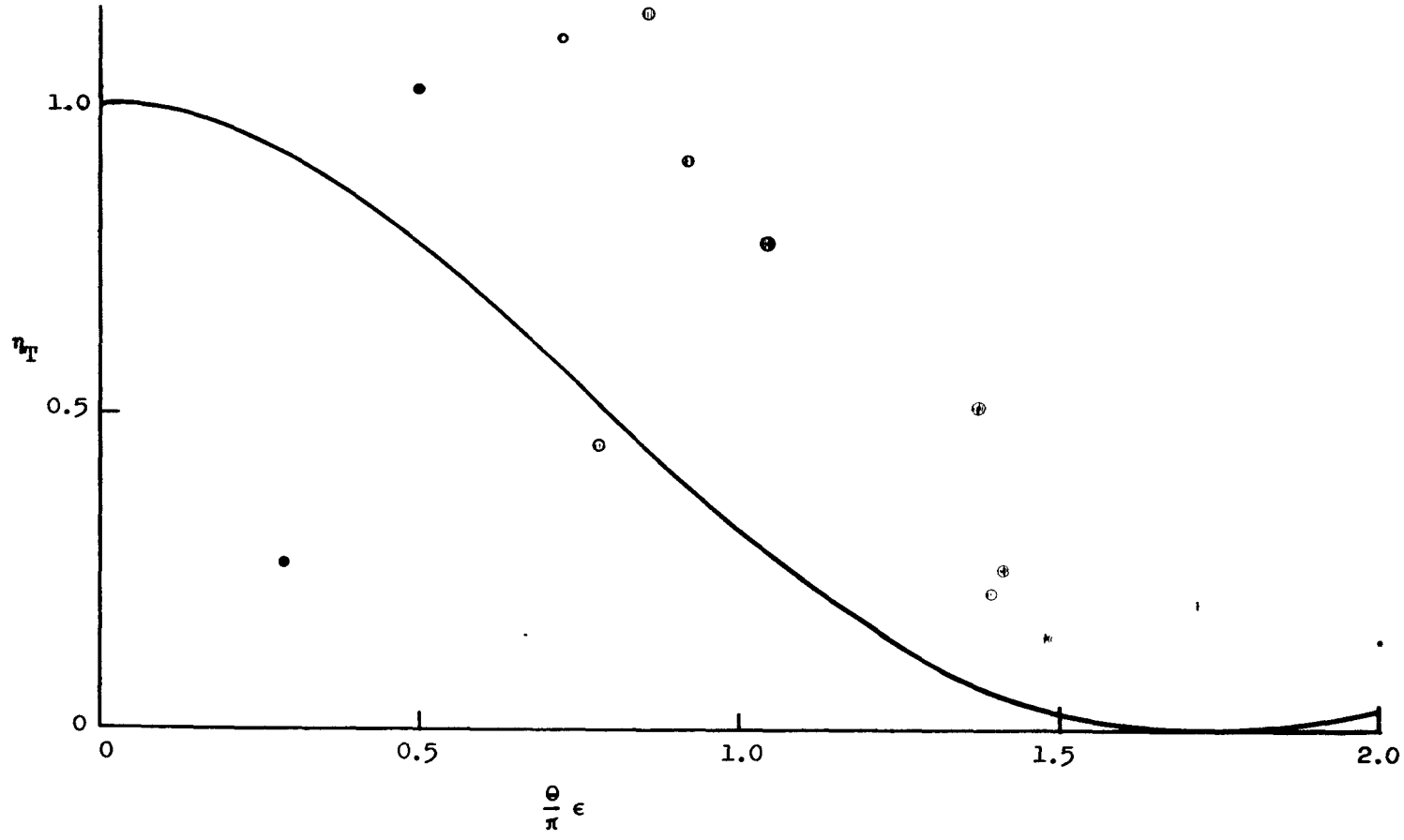

FIG. 2.3--Plot of the transfer efficiency of an optimized coupler vs error in synchronism. The curve is valid for weak coupling, $(K/\beta_0 \leq 0.1)$.

occur when $(\theta/\pi)\epsilon = 0.75$. For a coupler which is five wavelengths long the allowed fractional velocity error is 0.038, which is still quite large. For a linearly polarized coupler, this optimum length corresponds to $K/\beta_0 = 0.1$, which is a relatively large value for the circuits discussed in Chapter VII. Consequently, we see that velocity errors of a few per cent, while being noticeable, still fall in the range of strong interaction for usual couplers.

The bandwidth of the coupler cannot be predicted so simply. The variation of the coupling coefficient with frequency and the error in synchronism both play an important role here and the only valid way of predicting bandwidth is to have the dispersion characteristics and a plot of the interaction impedance for the particular circuit in mind. Then the second of Eqs. (2.23) may be used to compute the frequency dependence of the power transferred to the beam. This is done in Chapter VII where experimental circuits are discussed. It is seen there that bandwidths of 30 per cent are easily obtainable in fast cyclotron wave couplers. If the reduction in power transfer as a result of frequency deviation is due to the variation of the coupling coefficient related to change in circuit impedance rather than falling out of synchronism, then the half-power point bandwidth is determined by the frequency range for which

$$\frac{\pi}{4} \leq |f|\, K\ell \leq 3\pi/4 \quad , \qquad (2.29)$$

as can be seen from (2.23). The optimum situation would be for the coupling coefficient to be independent of frequency. Equation (2.17) shows that this places a restriction on the circuit impedance. The impedance of the optimum circuit would vary so that E^2/P is inversely proportional to the frequency. While the impedance of experimental circuits studied in Chapter VII does decrease with increasing frequency, it is generally at a rate greater than that indicated above.

C. COUPLING EQUALLY TO THE SYNCHRONOUS WAVES

In this section we are interested in studying the conditions in which a traveling-wave circuit may be used to couple to both of the synchronous waves. The distinction between this and the previous case is that here,

two-wave coupling is possible. That is, it is possible to excite two beam waves simultaneously because both have the same phase velocity. This case is interesting for two reasons. First, the optimum coupler for the synchronous wave amplifier described by Nordbotten[24] is one which excites both synchronous waves. This results in an improvement of the gain in the amplifying section of 6 db. Second, the amplitude of the synchronous waves excited in such a coupler is shown below to be proportional to the length of the coupler. Consequently, it is possible to excite large wave amplitudes with little expenditure of power since the synchronous waves carry energy of opposite signs.

The coupling is described by the equations

$$\begin{aligned} \partial A_3/\partial z + j\,\beta_e A_3 - j\,K\,f_+\,A_0 &= 0 \\ \partial A_4/\partial z + j\,\beta_3 A_4 - j\,K\,f_-\,A_0 &= 0 \\ \partial A_0/\partial z + j\,\beta_0 A_0 \mp j\,K\,[f_+^*\,A_3 - f_-^*\,A_4] &= 0 \end{aligned} \tag{2.30}$$

where the upper sign is for a forward wave circuit. The cyclotron waves have been neglected since they will usually be very far from synchronism with the coupler circuit in this case. In order to couple strongly to the synchronous waves the phase velocity of the circuit should be close to the beam velocity. From Eqs. (2.30) we see that, by using circularly polarized circuits so that either f_+ or f_- is zero, coupling to either synchronous wave may be achieved. This case is the problem discussed in the previous section. A more interesting case is when a linearly polarized circuit is used so that we couple equally to both synchronous waves. We may solve Eqs. (2.30) in general by assuming solutions of the form

$$\begin{aligned} A_3 &= a_3(z)\,e^{j(\omega t - \beta_e z)} \\ A_4 &= a_4(z)\,e^{j(\omega t - \beta_e z)} \\ A_0 &= a_0(z)\,d^{j(\omega t - \beta_0 z)} \end{aligned} \tag{2.31}$$

two-wave coupling is possible. That is, it is possible to excite two beam waves simultaneously because both have the same phase velocity. This case is interesting for two reasons. First, the optimum coupler for the synchronous wave amplifier described by Nordbotten[24] is one which excites both synchronous waves. This results in an improvement of the gain in the amplifying section of 6 db. Second, the amplitude of the synchronous waves excited in such a coupler is shown below to be proportional to the length of the coupler. Consequently, it is possible to excite large wave amplitudes with little expenditure of power since the synchronous waves carry energy of opposite signs.

The coupling is described by the equations

$$\partial A_3/\partial z + j\,\beta_e A_3 - j\,K\,f_+\,A_0 = 0$$

$$\partial A_4/\partial z + j\,\beta_3 A_4 - j\,K\,f_-\,A_0 = 0 \qquad (2.30)$$

$$\partial A_0/\partial z + j\,\beta_0 A_0 \mp j\,K\,[f_+^*\,A_3 - f_-^*\,A_4] = 0$$

where the upper sign is for a forward wave circuit. The cyclotron waves have been neglected since they will usually be very far from synchronism with the coupler circuit in this case. In order to couple strongly to the synchronous waves the phase velocity of the circuit should be close to the beam velocity. From Eqs. (2.30) we see that, by using circularly polarized circuits so that either f_+ or f_- is zero, coupling to either synchronous wave may be achieved. This case is the problem discussed in the previous section. A more interesting case is when a linearly polarized circuit is used so that we couple equally to both synchronous waves. We may solve Eqs. (2.30) in general by assuming solutions of the form

$$A_3 = a_3(z)\,e^{j(\omega t - \beta_e z)}$$

$$A_4 = a_4(z)\,e^{j(\omega t - \beta_e z)} \qquad (2.31)$$

$$A_0 = a_0(z)\,e^{j(\omega t - \beta_0 z)}$$

No generality has been lost in assuming the unperturbed propagation constants above, because no restrictions have been placed upon the z dependence of the amplitudes. Substituting these assumed solutions into the coupled mode equations gives the differential equations for the amplitudes:

$$\frac{da_3(z)}{dz} = j\,K\,f_+\,a_0(z)\,e^{-j(\beta_0 - \beta_e)z}$$

$$\frac{da_4(z)}{dz} = j\,K\,f_-\,a_0(z)\,e^{-j(\beta_0 - \beta_e)z} \qquad (2.32)$$

$$\frac{da_0(z)}{dz} = +\,j\,K\,[f_+^*\,a_3(z) - f_-^*\,a_4(z)]\,e^{+j(\beta_0 - \beta_e)z}$$

Integration of these equations yields the general solution. When either f_+ or f_- is zero we have the simple solutions obtained for two coupled waves as before. In the case of linear polarization (polarized in the x direction) we have $f_+ = f_- = 1/\sqrt{2}$, and the solutions are:

$$a_0(z) = a_0(0) \pm j\frac{K}{\sqrt{2}}M_1^*\,z\,[a_3(0) - a_4(0)]$$

$$a_3(z) = a_3(0) + j\frac{K}{\sqrt{2}}M_1 z\,a_0(0) \mp \frac{K^2}{4}M_2\,[a_3(0) - a_4(0)]\,z^2 \qquad (2.33)$$

$$a_4(z) = a_4(0) + j\frac{K}{\sqrt{2}}M_1\,a_0(0)z \mp \frac{K^2}{4}M_2\,[a_3(0) - a_4(0)]\,z^2$$

where

$$M_1 = e^{-j\,\Delta z/2}\,\frac{\sin \Delta z/2}{\Delta z/2} \qquad (2.34)$$

$$M_2 = +\,j\,\frac{e^{-j\,\Delta z/2}}{(\Delta z/2)^2}\,[\sin \Delta z/2 - e^{+j\,\Delta z/2}\cdot \Delta z/2] \qquad (2.35)$$

and

$$\Delta = \beta_0 - \beta_e \qquad (2.36)$$

The coefficients M_1 and M_2 give the sensitivity of the coupling to the error in synchronism and are shown in Figs. 2.4 and 2.5. Conservation of energy requires that

$$|a_0(z)|^2 + |a_3(z)|^2 - |a_4(z)|^2 = |a_0(0)|^2 + |a_3(0)|^2 - |a_4(0)|^2. \qquad (2.37)$$

Substituting (2.33) into this relation shows that there is indeed conservation.

In the case of an input coupler for a transverse wave device $a_3(0)$ and $a_4(0)$ would be zero. The situation is then one in which the circuit wave is undisturbed and the beam waves both grow linearly with distance. Energy is conserved since one synchronous wave carries negative power. By substituting these mode expressions into Eqs. (2.20), we obtain the beam excursion at a fixed plane indicated in Fig. 2.6a. Note that large excursions (large mode amplitudes) may be obtained without the beam striking the circuit since the beam displacement is perpendicular to the circuit field. This will be important later when we discuss some particular devices.

In the case of a general output coupler $a_3(0)$ and $a_4(0)$ will not be zero while $a_0(0)$ will be zero, giving rise to more complex expressions than before. It is evident from the first part of (2.33) that, in order to maximize the transfer of energy to the circuit, the entrance conditions should be such that

$$a_3(0) = - a_4(0).$$

This means that the transverse beam velocity at the entrance plane is parallel to the electric field supported by the circuit as shown in Fig. 2.6b. The current induced in the circuit may be calculated from Eq. (2.19), and it is indeed maximum for the above entrance conditions. Assuming these

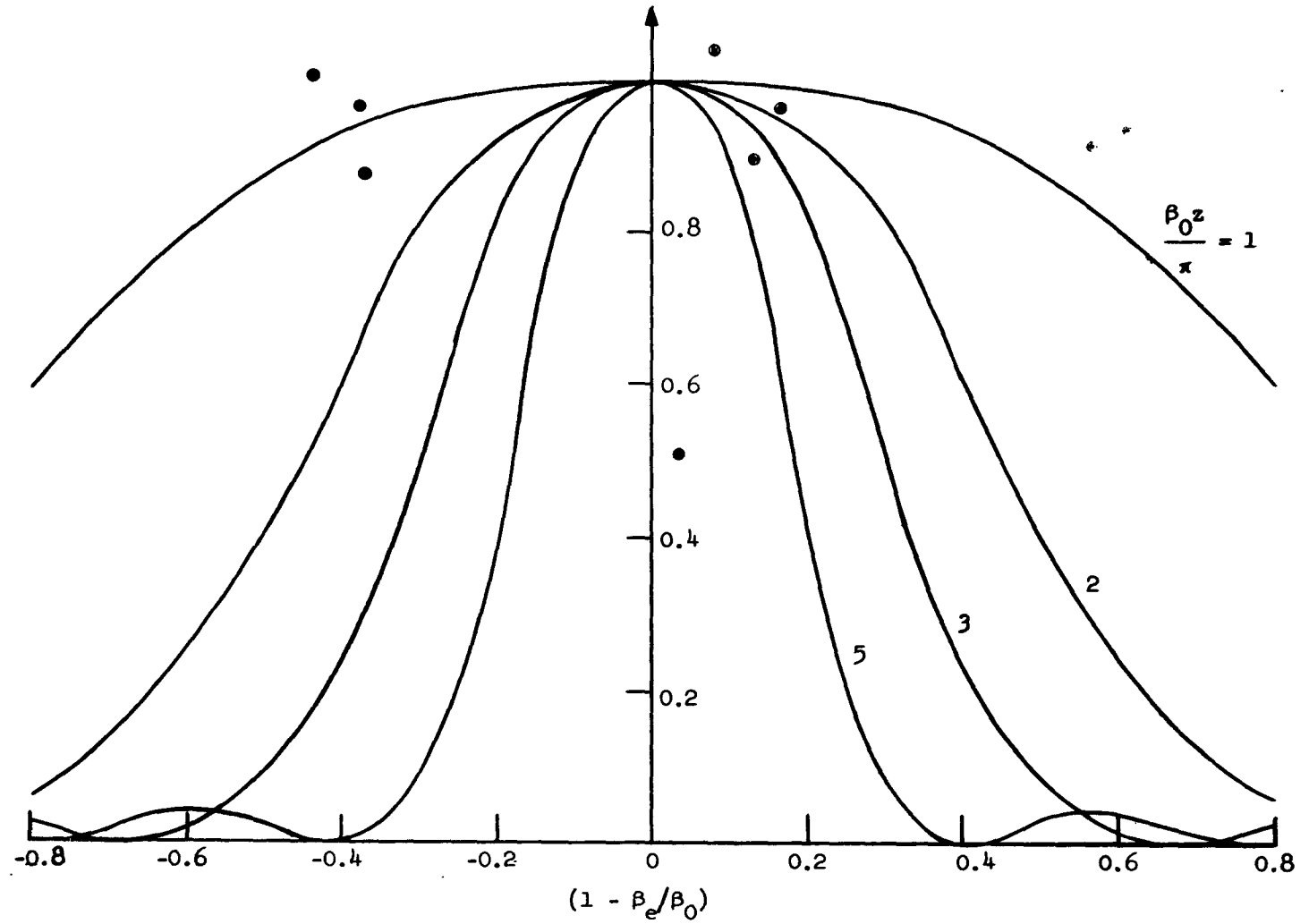

FIG. 2.4--Plot of the coupler modulation coefficients $\mathrm{Re}\,(M_2) = |M_1|^2$ for various length couplers.

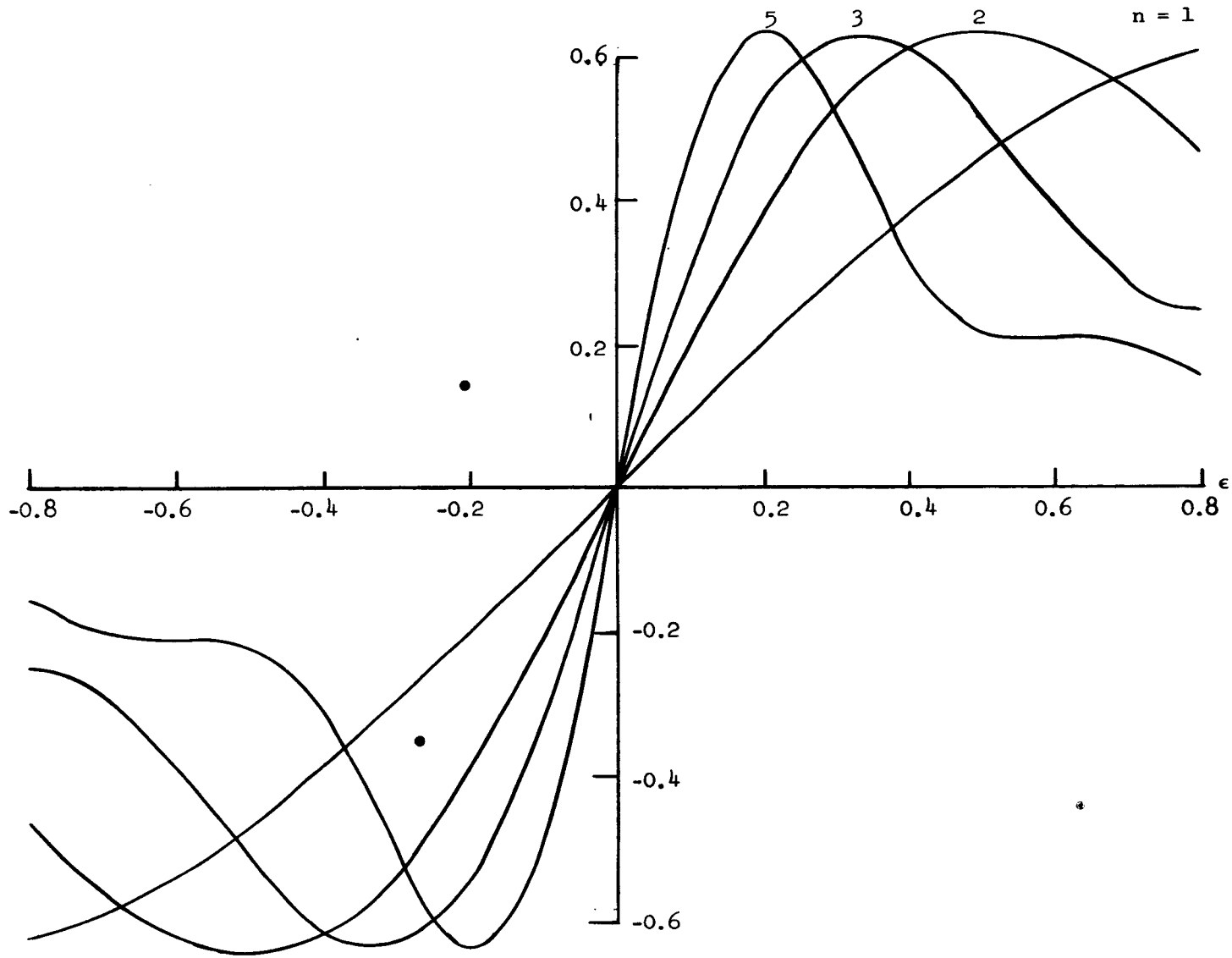

FIG. 2.5--Plot of the coupler modulation coefficient $-\mathrm{Im}(M_2)$.

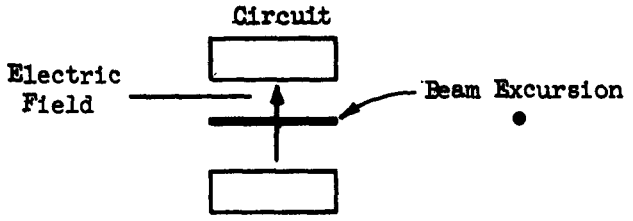

FIG. 2.6a--The beam excursion in a linearly polarized synchronous wave input coupler. The solid line shows the trace of the beam as it would appear on a screen in a fixed plane.

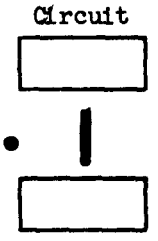

FIG. 2.6b--The beam excursion for the output synchronous wave coupler at the entrance plane. The transverse motion of the beam is toward the circuit so as to induce the maximum current.

entrance conditions, the wave amplitudes are, in the case of a forward circuit wave,

$$a_0(z) = a_3(0)\ (j\sqrt{2}\, M_1^*\, Kz)$$

$$a_3(z) = a_3(0)\ \left(1 - \frac{M_2}{2} K^2 z^2\right) \qquad (2.38)$$

$$a_4(z) = -\, a_3(0)\ \left(1 + \frac{M_2}{2} K^2 z^2\right)$$

A plot of the normalized power carried by each wave, as a function of the axial distance, z, is computed from these amplitudes and shown in Fig. 2.7. Note that there is a critical length at which there is only negative energy wave excitation on the beam. Beyond this, both waves grow quadratically with distance. The circuit power grows quadratically from the input. In Chapter VII we will discuss experimental circuits which have coupling coefficients of the order $K/\beta_0 = 0.1$, so that the Kz scale in Fig. 2.7 would typically be $0.6N$ where N is the number of wavelengths in the coupler. The circuit power may thus become much larger than the input beam wave powers in reasonable distances.

The bandwidth of this class of couplers cannot be calculated simply since both deviation in propagation constants and impedance variations give rise to a frequency dependence of the wave excitation. It is necessary to have these characteristics for the actual circuit under consideration. The reduction in coupling due to velocity errors is expressed by (2.34) and (2.35). The dependence upon interaction impedance appears in the coupling coefficient in Eqs. (2.33). Usually, it will be the first factor which is most important. Generally, it is found that the bandwidth of practical synchronous wave couplers is about the same as that of the cyclotron wave coupler described in the last section.

One practical aspect of the type of coupler considered in this section is that an input coupler must be terminated in a well-matched load. In the case of the one-wave couplers described in the previous section, the power is transferred from the circuit to the beam and there is a length for which complete transfer takes place. However, (2.33)

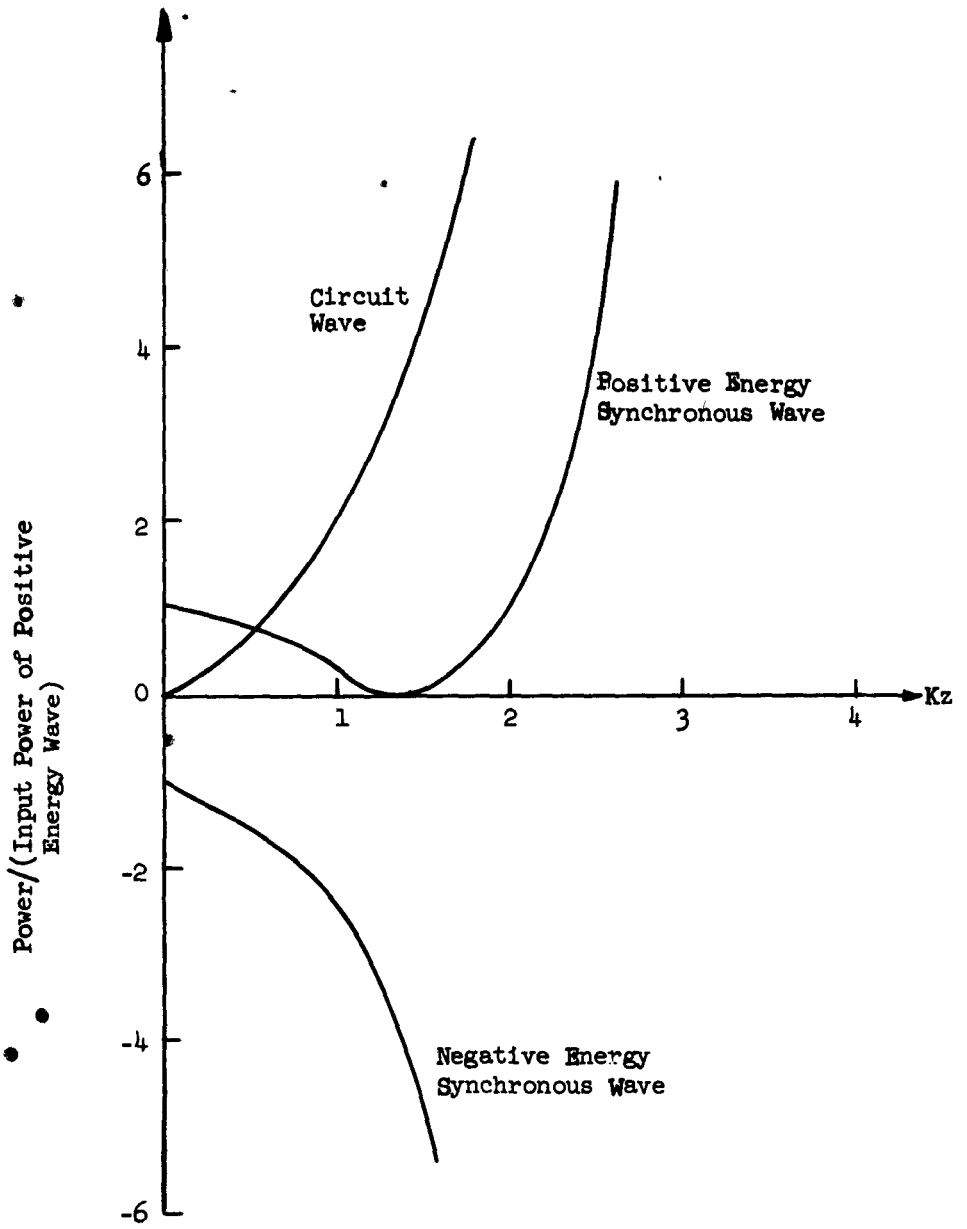

FIG. 2.7--A plot of the normalized power on the waves for the case in which synchronous waves of equal amplitude enter an output coupler with the optimum entrance conditions. The coupler is synchronous with the beam.

shows that the circuit wave on an input coupler considered in this section has a constant amplitude throughout the coupler length and must therefore be dissipated in a load at the end of the coupler.

CHAPTER III

RESONANT COUPLERS

The traveling-wave couplers considered in the previous chapter tend to be quite long, if optimum coupling is achieved, and it is therefore worth considering the exchange of bandwidth for length by employing traveling-wave circuits which have been shorted to make resonant couplers. It is also true that interesting circuit interactions which are not found in traveling-wave circuits are obtained with resonant circuits.

The resonant cavities considered in this chapter are made by placing shorting planes an even number of half-wavelengths apart on a general periodic traveling-wave circuit which supports a transverse electric field. The coupled mode equations described in Section II.A may be used to describe the interaction phenomena just as before. In this case the field is broken down into its forward and reverse propagating wave components in order to fit into the coupled mode approach. In the first section of this chapter we calculate the beam wave amplitude resulting from an assumed cavity field. The calculation is not complete until the circuit field is found from the power exchanged between the beam and the external cavity load. The next three sections of this chapter consider this half of the analysis for the different synchronization conditions. A comparison of the characteristics of resonant and traveling-wave couplers is given in the final section.

A. CALCULATION OF WAVE AMPLITUDES

The procedure followed here is the usual one in which two constant-amplitude counter-propagating circuit waves are assumed and the beam waves resulting from this field are calculated. Because of the constant amplitudes of the circuit fields the last of Eqs. (2.16) is not required. The coupled mode equations are simply

$$\frac{\partial A_1}{\partial z} + j\beta_1 A_1 = jKf_+ A_0$$

and

$$\frac{\partial A_2}{\partial z} + j\beta_2 A_2 = jKf_- A_0$$

$$\frac{\partial A_3}{\partial z} + j\beta_e A_3 = jKf_+ A_0$$

$$\frac{\partial A_4}{\partial z} + j\beta_e A_4 = jKf_- A_0 \qquad (3.1)$$

The two propagating waves which make up the resonant field configuration must be of equal amplitude to satisfy the boundary conditions at the shorting planes. Choosing one shorting plane (the entrance to the cavity) to be at $z = 0$, the circuit mode A_0 is written

$$A_0 = \left[a_0 e^{-j\beta_0 z} - a_0 e^{+j\beta_0 z}\right] e^{j\omega t} \qquad (3.2)$$

If the cavity field requires space-harmonics for its representation there will be similar terms for each space-harmonic. Usually only one will be of importance due to the synchronism conditions. However, superposition holds here and the calculations described in the following sections may be carried out for each space-harmonic and the results combined to give the complete solution as described at the end of this section. It is evident that the solution of any one of (3.1) will be the same as the others. The difference between the various interaction schemes will come out in the later sections of this chapter when we consider the power relations

The equation that is to be solved is

$$\frac{\partial A_1}{\partial z} + j\beta_1 A_1 = jKfA_0 \quad , \qquad (3.3)$$

along with the expression for A_0 as given by (3.2). In the above expression we have dropped the subscript on the polarization factor and f represents f_+ or f_- in agreement with the polarization of the wave indicated by the subscript i . The perturbed beam mode amplitude is assumed to vary as

$$A_i = a_i(z)\, e^{j(\omega t - \beta_i z)} \quad . \tag{3.4}$$

Just as in the previous chapter, no generality has been lost by assuming this specific form since the arbitrary z variation of a_i still allows a modification of the propagation constant. By substituting (3.4) into (3.3) we obtain a simple differential equation for $a_i(z)$ which may be integrated immediately to yield

$$a_i(\ell) = a_i(0) + a_0(jM_3 fK\ell) \quad , \tag{3.5}$$

where ℓ is the coupler length,

$$M_3 = \left[e^{-j\frac{\Delta}{2}\ell} \frac{\sin \frac{\Delta}{2}\ell}{\frac{\Delta}{2}\ell} - e^{j\left(\beta_j + \frac{\Delta}{2}\right)\ell} \frac{\sin \left(\beta_i + \frac{\Delta}{2}\right)\ell}{\left(\beta_i + \frac{\Delta}{2}\right)\ell} \right] \tag{3.6}$$

and $\Delta = \beta_0 - \beta_i$. The first term in M_3 (the subscript is to separate it from the similar coefficients found in Chapter III) represents coupling to the forward wave and the second represents coupling to the reverse wave on the circuit. The coefficient M_3 can be put in a more useful form by defining the fractional velocity deviation from synchronism to be

$$\epsilon = \left(1 - \frac{v_0}{v_i}\right) \quad , \tag{3.7}$$

where v_0 is the phase velocity of the traveling wave circuit which has been shorted to make the cavity and v_i is the phase velocity of the beam wave. Then, noting that a resonant cavity is an integral number of half wavelengths long, $\beta_0 \ell = n\pi$, and we finally obtain the expression

$$M_3 = e^{\frac{-jn\pi\epsilon}{2}} \left[\frac{1}{1 - \frac{\epsilon}{2}} \frac{\sin \frac{n\pi\epsilon}{2}}{\frac{n\pi\epsilon}{2}} \right] . \tag{3.8}$$

In this notation Eq. (3.5) is conveniently written as

$$a_i = a_i^{(0)} + j \left(f \frac{K}{\beta_0} n\pi M_3 \right) a_0 . \tag{3.5a}$$

A plot of $|M_3|^2$, which shows how the coupling depends upon synchronism between the beam wave and circuit wave phase velocities, is shown in Fig. 3.1. The asymmetry in the curves is due to the interaction with the backward propagating wave in the cavity. The effect of this wave is quite noticeable for short cavities. For longer cavities the interaction no longer involves the reverse wave to any great extent. These results are similar to those obtained for longitudinal wave coupling in resonant slow-wave structures by Wessel-Berg,[25] except that the coefficient M_3 has a slightly different form in that case.

Having derived (3.5) and (3.6), which are valid for any of the four beam waves (the correct polarization coefficient must be used), the next step is to calculate the power exchange between the beam and the circuit and, taking into account the losses in the cavity and the external load, to calculate the power which the external circuitry must supply to or receive from the cavity. The nature of these considerations depends upon which beam wave is in synchronism with the forward propagating wave in the cavity. The next sections are devoted to these calculations for the various synchronism conditions. Although only those waves which are near synchronism with the circuit are considered, this does not place a restriction on the validity of the analysis since the couplers are described by linear equations. This means that the beam admittances found for each

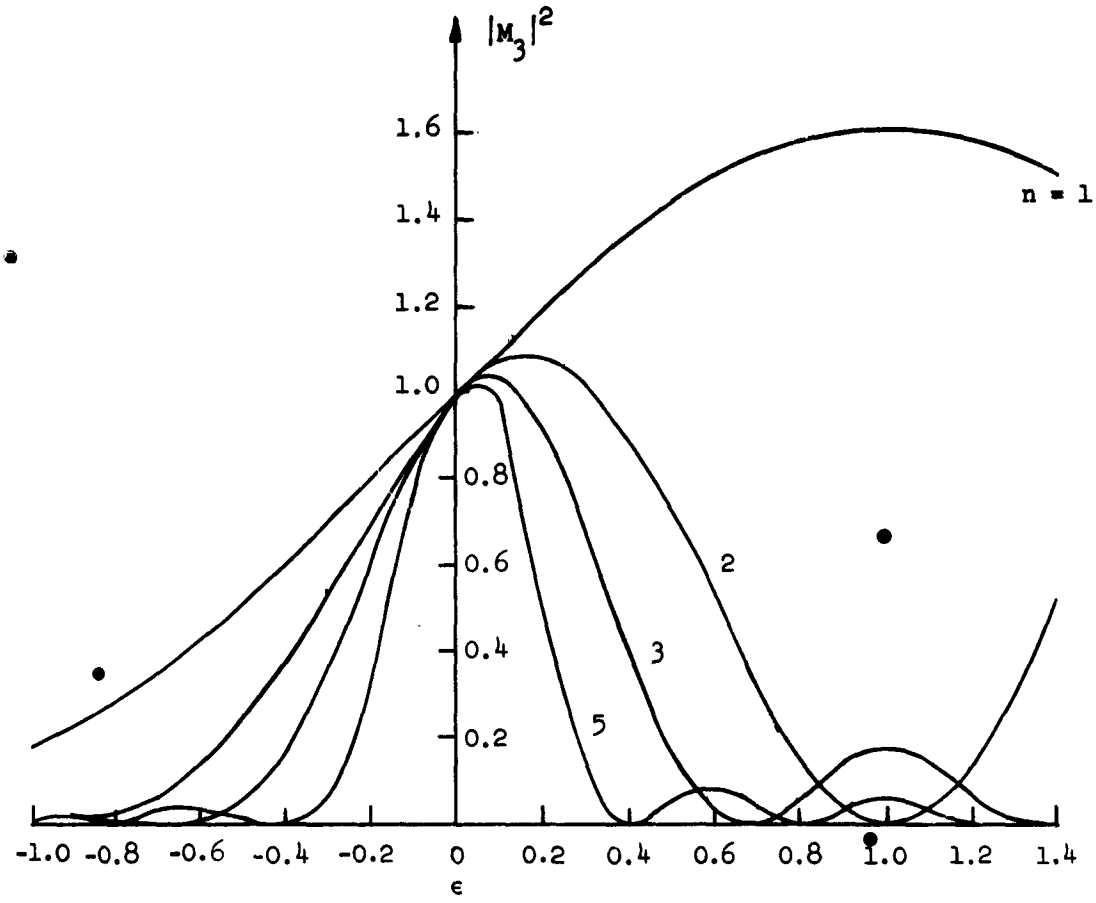

FIG. 3.1--The square of the coupler modulation coefficient as a function of the fractional velocity error.

wave may be added to give the total beam admittance if necessary. This will usually not be required since most couplers are long enough to make the modulation coefficient M_3 small except for the wave in question.

The results that have been obtained above, and the relations derived from them in the next sections, can also be used if more than one space-harmonic of the circuit field couples to one of the beam waves. This can be seen by returning to (2.5). For example, by writing velocity components in (2.5) in the same way as (2.31), we obtain expressions such as

$$v_+ = \underline{v}_+ \, e^{-j(\beta_e + \beta_c)z} \quad ,$$

where the solution for $\underline{v}_+$ is

$$\underline{v}_+ = \frac{\frac{-e}{m}}{u_0} \int_0^{\ell} E_+ \, e^{+j(\beta_e + \beta_c)z} \, dz \quad .$$

Then if E_+ is composed of space-harmonics we can interchange the order of integration and summation to obtain

$$\underline{v}_+ = \sum_{\text{all } n} \frac{-\frac{e}{m}}{u_0} \int_0^{\ell} E_{+n} \, e^{+j(\beta_e + \beta_c)z} \, dz \quad .$$

Thus, the total excitation of a particular beam mode can be represented as the sum of the excitations due to each space-harmonic. Finally, to apply these results to the present situation, the second term in (3.5) should be replaced by a sum of terms like

$$a_0 \sum_{\text{all } n} (jf\ell K_n M_{3n}) \quad ,$$

where K_n is the coupling coefficient for each space harmonic and M_{3n} is the corresponding coupler modulation coefficient. In general the results that have been derived in this chapter are made valid for interaction with a number of space harmonics by replacing KM_3 by $\sum_{\text{all } n} K_n M_{3n}$ in the various equations.

B. PASSIVE COUPLING TO ONE WAVE

The term "passive coupling" means the circuit is coupled to a positive energy beam wave. In this section we consider the synchronization conditions which bring about strong coupling to the positive energy cyclotron or synchronous wave. Couplers of this type are important because of their application as the input and output couplers in parametric amplifiers employing the positive energy transverse waves. To couple strongly to the cyclotron wave, the circuit propagation constant should nearly satisfy the condition $\beta_0 = \beta_e - \beta_c$ and the polarization coefficient f_- should be nonzero. That is, the circuit must have a negative, circularly polarized field component. In order to couple strongly to the synchronous wave the condition $\beta_0 = \beta_e$ should be satisfied and the circuit should have only a positively polarized field component. Since the two synchronous waves have the same propagation constant, a negatively polarized field component would result in the active coupling situation which will be considered in the next section.

The complex power delivered by the beam to the circuit may be computed from

$$\frac{d\mathcal{P}}{dz} = \frac{1}{2} V^* J \quad , \tag{3.9}$$

where V is the circuit voltage of (2.13) and J is the current per unit length induced in the circuit. The induced current is, from (2.19),

$$J = +j \frac{2\rho_0 \omega}{Dk\omega_c} f^* a_i \, e^{j(\omega t - \beta_i z)} \quad , \tag{3.10}$$

where a_i is either the positive energy cyclotron or synchronous wave amplitude (a_2 or a_3), β_i is the appropriate propagation constant, and f is f_- or f_+, respectively. From (3.2) and (2.13) the circuit voltage is

$$V = \sqrt{2Z_0}\, a_0 \left[e^{-j\beta_0 z} - e^{+j\beta_0 z} \right] e^{j\omega t} \quad . \tag{3.11}$$

To eliminate D from the power expression we combine (2.9), (2.10), and (2.18) and the definition of the circuit impedance Z_0 to obtain

$$D = \frac{1}{\beta_0} \sqrt{\frac{Z_0}{K_t}} \quad . \tag{3.12}$$

Finally, using

$$u_0 = \sqrt{\frac{2e}{m} V_0} \quad , \tag{3.13}$$

and Eqs. (2.14), (2.17), and (3.5), we obtain

$$\frac{d\underline{P}}{dz} = +j2f^* K \left[a_0^* a_i(0) - jf a_0 a_0^* M_3(z) Kz \right] \cdot \left[e^{+j\beta_0 z} - e^{-j\beta_0 z} \right] e^{-j\beta_i z} \quad . \tag{3.14}$$

Note that this is a point statement and M_3 is a function of z, requiring the use of (3.6) with z replacing ℓ, rather than (3.8). The complex power given up to a resonant coupler $n\pi$ radians long is found by integrating (3.14):

$$\underline{P} = +j2f^* \frac{K}{\beta_0} M_3^* n\pi a_0^* a_i(0) - j4ff^* \left(\frac{K}{\beta_0} \right)^2 n\pi \left[\frac{1 - \epsilon - M_3^*}{\epsilon(2 - \epsilon)} \right] a_0 a_0^* \quad , \tag{3.15}$$

where ϵ is defined by Eq. (3.7). The real part of this expression should be the negative of the power gained by the fast cyclotron wave in the coupler. From (3.5a) we see that

$$R_e(\underset{\sim}{P}) = -a_1 a_1^* \ ,$$

which is the required result. If the only purpose of the above calculation was to compute the real power exchanged, the wave amplitude could have been squared immediately and a lot of effort would have been saved. However, by using the expression for complex power we will be able to discuss the effects of beam loading on the coupler operation.

An electronic admittance may be defined in terms of the complex power absorbed by the beam and the voltage of the forward circuit wave,

$$\underset{\sim}{P}_{beam} = \frac{1}{2} V_c V_c^* Y_b = Z_0 a_0 a_0^* Y_b \ , \qquad (3.16)$$

where the circuit voltage is the complex amplitude of the traveling-wave voltage. From (2.13) we have

$$V_c = \sqrt{2 Z_0}\, a_0 \ . \qquad (3.17)$$

By substituting the negative of the power absorbed by the circuit from (3.15), we have the ratio of the admittance presented to the coupler cavity by the beam to the characteristic admittance of the unshorted traveling-wave circuit:

$$\frac{Y_b}{Y_0} = -j2f^* \frac{K}{\beta_0} n\pi M_3^* \left(\frac{a_1(0)}{a_0}\right)$$

$$+ j4ff^* \left(\frac{K}{\beta_0}\right)^2 n\pi \frac{1 - \epsilon - M_3^*}{\epsilon(2 - \epsilon)} \ . \qquad (3.18)$$

This expression is particularly simple in the case of an input coupler since the initial wave amplitude is zero. Then the electronic admittance is determined by the second term in (3.18). This is referred to as the electronic admittance, and its normalized conductance and susceptance are:

$$R_e\left(\frac{Y_e}{Y_0}\right) \equiv g_e = |f|^2 \left(\frac{K}{\beta_0}\right)^2 (n\pi)^2 |M_3|^2 \qquad (3.19)$$

and

$$I_m\left(\frac{Y_e}{Y_0}\right) \equiv b_e = - |f|^2 \left(\frac{K}{\beta_0}\right)^2 (n\pi)^2 M_4 , \qquad (3.20)$$

where

$$M_4 = |M_3|^2 \cot \frac{n\pi\epsilon}{2} - \frac{1}{\frac{n\pi\epsilon}{2}} \left(\frac{1 - \epsilon}{1 - \epsilon/2}\right) . \qquad (3.21)$$

A plot of $|M_3|^2$ was given in Fig. 3.1 and M_4 is shown in Fig. 3.2. The beam susceptance, b_e, is not zero at synchronism due to the interaction with the reverse circuit wave. The ratio of the beam susceptance to conductance at synchronism is

$$\frac{b_e}{g_e} = \frac{3}{n\pi} . \qquad (3.22)$$

For couplers of usual length the electronic susceptance at synchronism will be much smaller than the conductance. By comparing the curves in Figs. 3.1 and 3.2 we see that it is distinctly advantageous to operate short resonant couplers off of synchronism. The value of ϵ which yields maximum conductance also reduces the susceptance to essentially zero. For example, a one-half wavelength long cavity designed to couple optimally to the fast cyclotron wave should have $\epsilon = 1.0$. From (3.7) it is obvious that this requires the cyclotron wave to have infinite phase

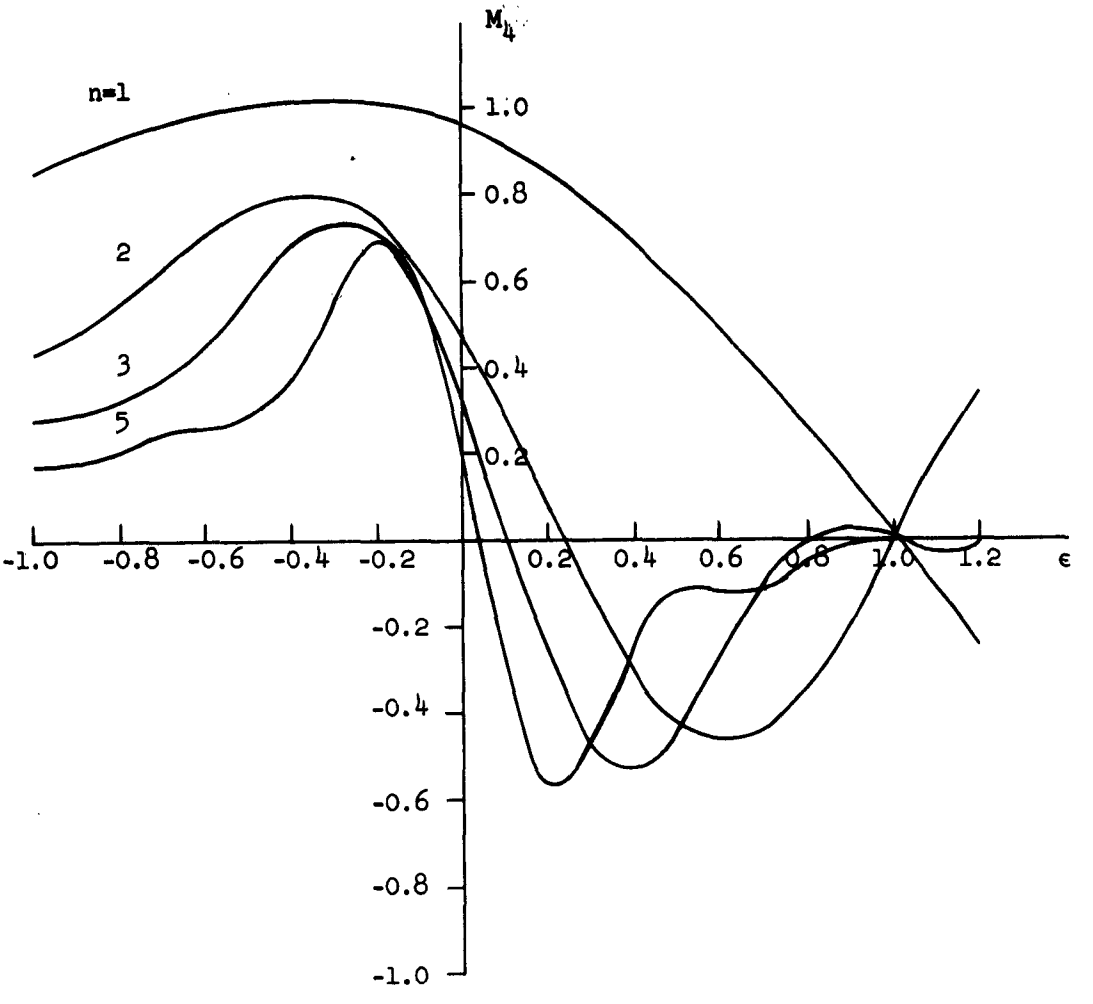

FIG. 3.2 -- A plot of the coupler modulation coefficient M_4 showing the relative magnitude of the reactive component of the beam admittance.

velocity, that is, ω_c/ω should be unity. This interesting result shows that the beam conductance in a half-wavelength coupler is maximum, and independent of the circuit phase velocity, for $\omega_c/\omega = 1$. Also, we see that the susceptance is zero in this situation. This example is valid only when the circuit phase velocity is such that the coupling to the other transverse waves is negligible; otherwise there will be other contributions to the admittance.

The above results give the effects of the loading of the input coupler by the beam, and show the dependence on the fractional velocity error ϵ . Another formulation of this problem is to determine the Q of the cavity loaded by the beam. In order to do this we calculate the power which must be supplied to the lossy coupler in order to sustain fields of a given amplitude. Since $|a_0|^2$ represents the power carried in either the forward or reverse propagating circuit waves, we find from the definition of the Q of a cavity that

$$Q_0 = \frac{\omega\left(\frac{2|a_0|^2 \ell}{|v_g|}\right)}{P_{ckt}} , \qquad (3.23)$$

where v_g is the group velocity of the shorted transmission forming the resonant cavity, ℓ is the length of the cavity, and P_{ckt} is the power dissipated in the cavity losses. The Q_0 is then the unloaded Q of the coupler cavity. Using the definition of the circuit propagation constant, the power lost to a coupler which is $n\pi$ radians long is

$$P_{ckt} = \frac{2n\pi}{Q_0}\left|\frac{v_p}{v_g}\right| |a_0|^2 , \qquad (3.24)$$

where v_p is the phase velocity of the traveling-wave circuit. The power delivered to the beam in the coupler is the real part of (3.15) with $a_2(0) = 0$, or it may be obtained from (3.17) and (3.19);

$$P_{beam} = |f|^2 \left(\frac{K}{\beta_0}\right)^2 (n\pi)^2 |M_3|^2 |a_0|^2 . \qquad (3.25)$$

Then, using

$$\frac{P_{beam}}{P_{ckt}} = \frac{Q_0}{Q_b} , \tag{3.26}$$

the Q of the cavity loaded by the beam only, Q_b, is found to be

$$\frac{1}{Q_b} = \frac{n\pi}{2} |f|^2 \left(\frac{K}{\beta_0}\right)^2 |M_3|^2 \left|\frac{v_g}{v_p}\right| . \tag{3.27}$$

This shows that Q_b is inversely proportional to the length of the cavity. On the other hand, Q_0 does not depend on the length of the cavity, so

$$\frac{Q_0}{Q_b} \propto \ell .$$

Hence, the ratio of the power lost in the cavity to that which goes into the beam inqreases linearly with distance. The bandwidth of the coupler is simply the inverse of the Q :

$$\frac{1}{Q} = \frac{1}{Q_0} + \frac{1}{Q_b} + \frac{1}{Q_{ext}} , \tag{3.28}$$

where Q_{ext} is the Q of the cavity loaded by the external circuit. The gain of the coupler, defined to be the ratio of the beam output power to the input power to the cavity, is

$$G_{in} = \frac{1}{1 + \frac{Q_b}{Q_0}} . \tag{3.29}$$

The discussion up to this point has dealt with the application of Eq. (3.18) to the study of an input coupler. That is, we neglected the first term which represents the initial beam excitation. We now consider the case of an output coupler in which this driving term is not zero. To aid in the interpretation of (3.18) the equivalent circuit of Fig. 3.3 is shown. All of the admittances appear in parallel at the terminals across which the voltage V_c appears. The term in the beam admittance that represents initial excitation has been separated off and is called Y_d :

$$\frac{Y_d}{Y_0} = - j2f^* \frac{K}{\beta_0} n\pi M_3^* \frac{a_i(0)}{a_0} \quad . \tag{3.30}$$

The remaining portion, Y_e , represents power absorbed by the beam and is given by Eqs. (3.19) and (3.20). As shown in Fig. 3.3, the driving admittance can be interpreted as a constant signal generator. The driving current is

$$I_d = - V_c Y_d \quad , \tag{3.31}$$

and by using (3.17), we have

$$I_d = + j \frac{2\sqrt{2}}{\sqrt{Z_0}} f^*(n\pi) \frac{K}{\beta_0} M_3^* a_i(0) \quad . \tag{3.32}$$

The wave amplitude excited on the circuit by this current is

$$a_0 = \frac{I_d}{Y_e + Y_L} \frac{1}{\sqrt{2Z_0}} \quad , \tag{3.33}$$

yielding

$$a_0 = \left[\frac{- j2f^* \left(\frac{K}{\beta_0}\right) n\pi M_3^*}{g_e + j\, b_e + y_L} \right] a_i(0) \quad , \tag{3.34}$$

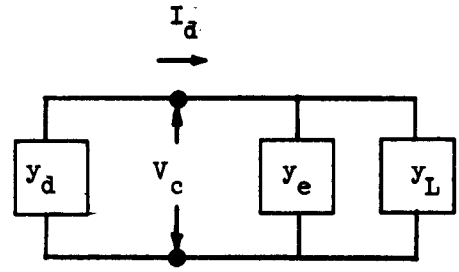

(a)

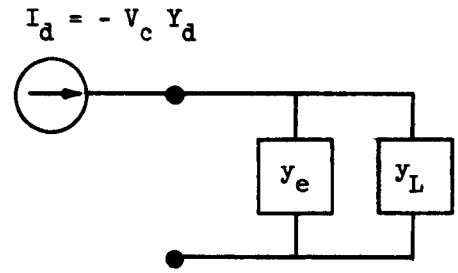

(b)

FIG. 3.3--Equivalent circuits for a resonant output coupler.

where

$$y_L = \frac{Y_L}{Y_0} = g_L + jb_L \quad . \tag{3.35}$$

The real power which is given up to the load admittance is

$$P_L = \frac{1}{2} V_c V_c^* \mathrm{Re}(Y_L) = a_0 a_0^* g_L \quad . \tag{3.36}$$

By substituting (3.32) in (3.34) we obtain

$$P_L = 4 \left| f \frac{K}{\beta_0} (n\pi) M_3 \right|^2 \frac{g_L}{|g_e + g_L + j(b_e + b_L)|^2} |a_1(0)|^2 \quad . \tag{3.37}$$

In order to transfer maximum power to the load the load admittance should be the complex conjugate of the electronic admittance. If this is the case, (3.19) and (3.37) yield

$$P_L = |a_1(0)|^2 \quad , \tag{3.38}$$

which is just the initial power on the fast cyclotron wave. Of course, the load admittance is made up of the cavity and external admittances,

$$Y_L = Y_{ext} + Y_c \quad , \tag{3.39}$$

so that the actual power to the external load under these optimum conditions is

$$P_{ext} = \frac{g_{ext}}{g_{ext} + g_c} |a_1(0)|^2 \quad , \tag{3.40}$$

which may be written

$$G_{out} = \frac{1}{1 + \frac{Q_{ext}}{Q_0}} , \tag{3.41}$$

where G_{out} is the ratio of the power delivered to the external load to the input power on the beam, and Q_{ext} is the Q of the cavity loaded by the external load conductance. The bandwidth of the output cavity assuming constant driving current is given by (3.28).

The above results have been kept general in the sense that they are valid for either positive energy cyclotron or synchronous wave couplers. To obtain the desired characteristics for one of the couplers it is only necessary to employ the appropriate propagation constant and polarization factor. It should be noted however, that, while a linearly polarized coupler for the fast cyclotron wave obeys these equations, another set of equations must be used if a linearly polarized synchronous wave coupler is to be considered. This is considered in the next section.

C. COUPLING TO THE TWO SYNCHRONOUS WAVES

Because the two synchronous waves have the same phase velocity, but opposite polarization, it is possible to couple equally to them by the simple expedient of using a linearly polarized coupler. Such a situation was considered for a traveling-wave coupler in the previous chapter and now we consider the case of a resonant coupler.

In a linearly polarized coupler, polarized in the x direction, $f_+ = f_- = 1/\sqrt{2}$ and the synchronous waves excited in such a coupler are given by Eq. (3.5) or (3.5a). The circuit should have a propagation constant β_0 approximately equal to β_e to yield strong coupling. For the positive energy wave f_+ is used, and for the negative energy wave f_- is used. Then

$$\begin{aligned} a_3(\ell) &= a_3(0) + jf_+M_3K\ell a_0 \\ a_4(\ell) &= a_4(0) + jf_-M_3K\ell a_0 , \end{aligned} \tag{3.42}$$

and it is obvious that if $f_+ = f_-$, the two waves are excited equally. If the circuit is elliptically rather than linearly polarized, one wave will be excited more strongly than the other. The complex power delivered by the beam to the circuit is computed from Eq. (3.9) as before. The induced current per unit length in the circuit is obtained from (2.19) and is, for this case,

$$J = j \frac{2\omega}{Dk\omega_c} \frac{I_0}{u_0} \left[f_+^* a_3 - f_-^* a_4 \right] e^{j(\omega t - \beta_e z)} \quad . \tag{3.43}$$

By using exactly the same steps outlined from Eqs. (3.11) to (3.15) we obtain the expression for the power exchanged in a coupler which is $n\pi$ radians long:

$$\underset{\sim}{P} = + j2 \frac{K}{\beta_0} n\pi M_3^* a_0 \left[f_+^* a_3(0) - f_-^* a_4(0) \right]$$

$$+ j4 \left(f_+ f_+^* - f_- f_-^* \right) \left(\frac{K}{\beta_0} \right)^2 (n\pi) \left[\frac{1 - \epsilon - M_3^*}{\epsilon(2 - \epsilon)} \right] . \tag{3.44}$$

Upon comparing this with (3.15) we see that each beam wave gives a power contribution of the same form as if it alone were present (there is a minus sign with the expression involving the negative energy wave). This is a consequence of the initial assumption of a linear system. While (3.44) is general, and even contains (3.15) as a special case, we now restrict our interest to the linearly polarized case. When $f_+ = f_- = 1/\sqrt{2}$, we have from (3.44)

$$\underset{\sim}{P} = + j\sqrt{2} \frac{K}{\beta_0} M_3^* n\pi a_0^* \left[a_3(0) - a_4(0) \right] \quad . \tag{3.45}$$

The beam admittance presented to the circuit may be calculated in the same way as was (3.18), yielding

$$\frac{Y_b}{Y_0} = -j\sqrt{2}\,\frac{K}{\beta_0}\,n\pi M_3^*\left[\frac{a_3(0)}{a_0} - \frac{a_4(0)}{a_0}\right]. \tag{3.46}$$

This expression just represents a current generator due to the input signal on the beam. There is no electronic loading and therefore the bandwidth of this type of coupler is determined by the cavity losses and the external circuit.

In the case of an input coupler in which there is no excitation of either wave at the input to the coupler, the wave amplitudes grow as predicted by (3.42) without loading the circuit. In the design of such a coupler the input matching and bandwidth are determined by the cold cavity. Equation (3.24) is valid in this case and substitution into (3.42) yields the wave amplitudes excited in the linearly polarized input coupler in terms of the input power to the circuit:

$$a_3 = a_4 = j\,\frac{1}{2}\,M_3\,\frac{K}{\beta_0}\left(n\pi Q_0\left|\frac{v_g}{v_p}\right|\right)^{\frac{1}{2}} P_{ckt}^{1/2}\,, \tag{3.47}$$

where we have chosen the phase of a_0 to be zero. If the power "gain" of an input coupler is defined as the ratio of the output power on the positive energy beam wave to the input power to the cavity, we have

$$G_{in} = \frac{n\pi}{4}\,|M_3|^2\left(\frac{K}{\beta_0}\right)^2\left|\frac{v_g}{v_p}\right| Q_0\,. \tag{3.48}$$

The gain is linearly proportional to the length of the cavity, and may be greater than unity.

When there is initial excitation on the beam, such as would be the case in an output coupler, the beam admittance given in (3.46) may not be zero. Just as in Eqs. (3.31) and (3.32), the beam excitation may be

represented by a constant current generator

$$I_d = + j \frac{2}{\sqrt{Z_0}} n\pi \frac{K}{\beta_0} M_3^* \left| a_3(0) - a_4(0) \right| \quad . \tag{3.49}$$

This current causes a voltage across the electronic and load admittances. Corresponding to (3.34), the wave amplitudes excited in the cavity are:

$$a_0 = - j \sqrt{2} \frac{K}{\beta_0} \frac{n\pi M_3^*}{y_L} \left[a_3(0) - a_4(0) \right] \quad . \tag{3.50}$$

The power which is given up to the external load admittance is easily found from (3.36), (3.39) and (3.50):

$$P_{ext} = \frac{g_L^2}{|y_L|^2} \frac{n\pi Q_0}{\left(1 + \frac{Q_0}{Q_{ext}}\right)\left(1 + \frac{Q_{ext}}{Q_0}\right)} |M_3|^2 \left(\frac{K}{\beta_0}\right)^2 \left|\frac{v_g}{v_p}\right| |a_3(0) - a_4(0)|^2 \quad . \tag{3.51}$$

Note that there is no difference in the power exchange in the case of only a positive or negative energy wave at the entrance plane. The maximum power is transferred when the total load admittance is real and $Q_{ext}/Q_0 = 1$. Equation (3.46) shows that the optimum entrance conditions are attained when $a_3(0)$ and $a_4(0)$ have opposite signs.

A particularly interesting case arises when $a_3(0) = - a_4(0)$. This is the same entrance condition that is shown in Fig. 2.6b, and Fig. 2.6a shows that this is the beam excitation provided by a linearly polarized coupler whose plane of polarization is rotated by an angle of 90° with respect to the present coupler. If the gain of the output coupler is defined to be the ratio of the output power to the initial input power on one of the equal amplitude synchronous waves, it is found that

$$G_{out} = \frac{4Q_0}{\left(1 + \frac{Q_0}{Q_{ext}}\right)\left(1 + \frac{Q_{ext}}{Q_0}\right)} n\pi |M_3|^2 \left(\frac{K}{\beta_0}\right)^2 \left|\frac{v_g}{v_p}\right| |\cos \theta_0| \quad , \tag{3.52}$$

where θ_0 is the angle between the initial polarization of the beam and the plane of polarization of the circuit. It has been assumed that the loaded coupler is resonant at the signal frequency so that $g_L/|y_L|$ is unity. The gain is linearly proportional to the length of the cavity and, just as in (3.48), it may be greater than unity.

It is apparent that an amplifier could be made by using two linearly polarized synchronous wave couplers. The input coupler should be rotated by 90° with respect to the output coupler so that θ_0 in (3.52) is zero. The gain of the two couplers is the product of (3.48) and (3.52). This device, which is shown in Fig. 3.4, is a synchronous wave analog of the extended interaction klystron. Wessel-Berg noted the feasibility of this synchronous-wave klystron earlier[12,16] and pointed out that it has several advantages over the usual extended interaction klystron. In particular, it should not suffer from the oscillations that arise in the usual case when the length of the cavities is increased in order to obtain large values for the gain. This is a result of the fact that the beam loading is zero, as was shown in (3.46). The calculations given by Wessel-Berg in the above reference are more general than those presented here, but they are concerned with the electronic equations only and the gain of the klystron was not obtained. The gain has been obtained explicitly here in the form of Eqs. (3.48) and (3.52).

For purposes of calculating the beam excursion in order to determine when saturation will take place, it is necessary to have the expressions for the synchronous wave amplitudes on the beam. Substituting (3.50) into (3.42) gives

$$a_3(\theta) = a_3(0) - \left|M_3\right|^2 \frac{Y_0}{Y_L}\left[a_3(0) - a_4(0)\right]\left(\frac{K}{\beta_0}\right)^2 \theta^2$$

$$a_4(\theta) = a_4(0) - \left|M_3\right|^2 \frac{Y_0}{Y_L}\left[a_3(0) - a_4(0)\right]\left(\frac{K}{\beta_0}\right)^2 \theta^2, \qquad (3.53)$$

where $\theta = \beta_0 z$ is the axial distance in radians from the entrance plane.

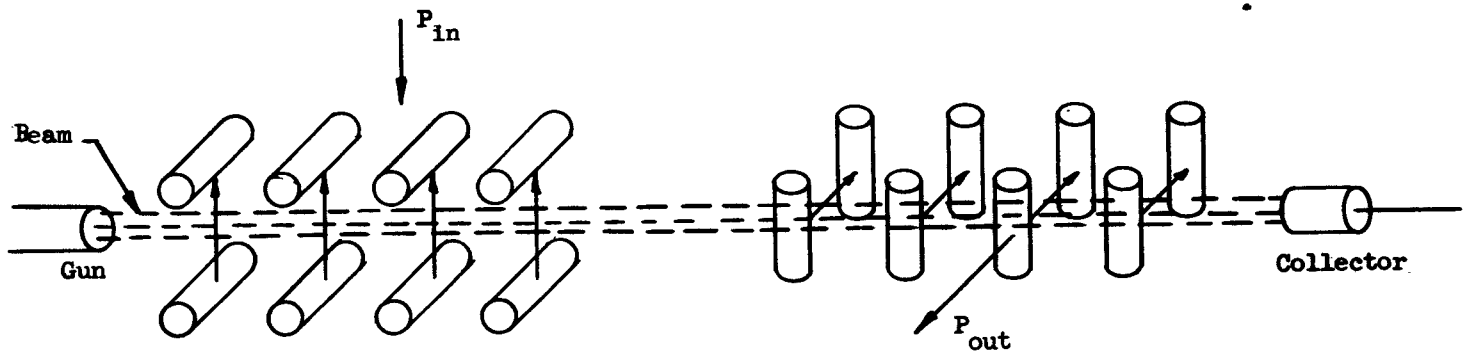

FIG. 3.4--Schematic representation of the synchronous-wave klystron. The structures of rods shown indicate periodic resonant circuits that support a transverse field with the polarization indicated by the arrows.

D. ACTIVE COUPLING TO ONE WAVE

The last case of interest in the study of resonant couplers is the synchronization condition which leads to strong interaction with one of the two negative energy waves. This condition is important since it can result in the transverse wave equivalent of the space-charge wave monotron. The synchronization conditions are: $\beta_0 = \beta_e + \beta_e$ for the slow cyclotron wave interaction, and $\beta_0 = \beta_e$ for the negative energy synchronous wave interaction. In the cyclotron wave case the circuit can be linearly or circularly polarized $(f_+ \neq 0)$, while in the synchronous wave case the coupler circuit must be circularly polarized $(f_- \neq 0)$ since a linearly polarized circuit with $\beta_0 = \beta_e$ leads to the type of interaction considered in the last section.

The notation used here is the same as before: the amplitude a_i is used to denote one of the negative energy waves, a_1 or a_4, and the polarization coefficient f is f_+ when a_1 is considered and f_- for a_4. The current induced in the circuit due to wave excitation on the beam is, from (2.19),

$$J = -j \frac{2\rho_0 \omega}{Dk\omega_c} f^* a_i \quad . \tag{3.54}$$

By using exactly the same steps outlined in Section III.B, we obtain the expression for the complex power exchanged in a coupler which is $n\pi$ radians long:

$$\underset{\sim}{P} = -j2f^* \left(\frac{K}{\beta_0}\right) n\pi M_3^* a_0^* a_i(0) + j4ff^* \left(\frac{K}{\beta_0}\right)^2 n\pi \left[\frac{1 - \epsilon - M_3^{*2}}{\epsilon(2 - \epsilon)}\right] a_0 a_0^* \; ; \tag{3.55}$$

The coefficient M_3 is evaluated for the β_i under consideration. The admittance presented by the beam to the circuit is calculated in the same

manner as (3.18), yielding

$$\frac{Y_b}{Y_0} = + j2f^* \frac{K}{\beta_0} n\pi M_3^* \frac{a_i(0)}{a_0} - j4|f|^2 \left(\frac{K}{\beta_0}\right)^2 n\pi \left[\frac{1 - \epsilon - M_3^*}{\epsilon(2 - \epsilon)}\right] . \quad (3.56)$$

Note that this is just the negative of (3.18) which is the admittance for positive energy wave interactions.

In the case of a beam with no excitation entering a cavity the first term in (3.56) is zero and the electronic conductance and susceptance are:

$$g_e = - |f|^2 \left(\frac{K}{\beta_0}\right)^2 (n\pi)^2 |M_3|^2 \quad (3.57)$$

$$b_e = + |f|^2 \left(\frac{K}{\beta_0}\right)^2 (n\pi)^2 M_4 , \quad (3.58)$$

where M_4 is given by (3.21). The negative conductance means that power is given up to the circuit in the interaction region. The Q of the cavity loaded by the beam only is defined as in (3.26) and in this case we obtain

$$\frac{1}{Q_b} = - \frac{n\pi}{2} |f|^2 \left(\frac{K}{\beta_0}\right)^2 \left|\frac{v_g}{v_p}\right| |M_3|^2$$

Note that Q_b is a negative quantity due to the negative conductance. This results in a decrease of the bandwidth below that determined by the losses of the cavity and external circuit. The gain of the input coupler is given by (3.29):

$$G_{in} = \frac{1}{1 + \frac{Q_b}{Q_0}} , \quad (3.60)$$

and we see that it is greater than unity. Although (3.60) becomes infinite at $Q_b/Q_q = -1$, this is not where oscillation sets in since the external circuit loading was not included in the definition of gain. Oscillation starts when

$$\frac{Q_b}{Q_L} = -1 \quad , \tag{3.61}$$

where Q_L is the loaded Q of the cavity. At this point the negative energy on the beam at the exit plane of the cavity is just equal to the power dissipated in the cavity and its load due to the assumed fields. By combining (3.59), (3.61) and (2.17), we obtain the expression for the beam conductance required to start oscillation:

$$G_0 = \frac{1/Q_L}{\frac{n\pi}{4}\left|f\right|^2 \frac{\omega}{\omega_c}\left(\frac{v_g}{v_p}\right) K_t \left|M_3\right|^2} \quad . \tag{3.62}$$

If a signal is on the beam initially, it can be represented by a constant current generator driving the cavity. The driving current is derived from the first term of (3.56) just as in Eqs. (3.31) and (3.32):

$$I_d = -j \frac{2\sqrt{2}}{\sqrt{Z_0}} f^* n\pi \frac{K}{\beta_0} M_3^* a_i(0) \quad . \tag{3.63}$$

The wave amplitudes induced in the cavity are found in the same way as in the previous cases:

$$a_0 = \left[\frac{+ j2f^* \frac{K}{\beta_0} n\pi M_3^*}{g_e + j\, b_e + y_L}\right] a_i(0) \quad . \tag{3.64}$$

The power to the load is exactly the same as (3.37) where we now use the negative admittances in (3.57) and (3.58). These expressions are valid only if g_L is greater than g_e . Otherwise, the system oscillates as described for the case with zero initial excitation and the energy conservation statements implicit in the derivation of (3.64) are violated in the linear system.

E. COMPARISON WITH TRAVELING-WAVE COUPLERS

It was stated at the beginning of this chapter that one of the important reasons for interest in resonant couplers is that circuit length required for a given gain is less than it is in the case of the traveling-wave couplers. This is an important factor because of the difficulty of focusing the electron beam for large distances. The purpose of this section is to compare the length and bandwidth of some typical traveling-wave and resonant couplers.

The optimum length of a traveling-wave coupler that excites one of the positive energy waves is given by (2.26). This can be written in terms of the circuit length in radians as

$$\theta = \frac{\pi}{2} \frac{1}{|f|} \frac{\beta_0}{K} \quad .$$

The gain of the coupler is unity in this case. In order to make a resonant coupler with unity gain it is necessary to have Q_b/Q_0 be zero. This is not practical, but $Q_b/Q_0 = 0.1$ would give a gain of 0.91 which is close enough to unity for comparison purposes. In that case (3.27) gives, at synchronism,

$$n\pi = \frac{1}{|f|^2} \frac{20}{Q_0} \left|\frac{v_p}{v_g}\right| \left(\frac{\beta_0}{K}\right)^2 \quad .$$

Typical values for linearly polarized circuits described in Chapter VII are: $Q_0 = 1000$, $|K/\beta_0| = 0.1$, and a v_p/v_g of about two. The

ratio of the length of a traveling-wave coupler to a resonant coupler, each having unity gain, is approximately three. Thus, while the S-band traveling-wave coupler described in Chapter VII is about six inches long, its resonant counterpart need be only two inches long to yield the same gain. This is certainly a significant difference. However, a large sacrifice in bandwidth must be made in order to achieve these results. For example, the bandwidth of the traveling-wave coupler described in Chapter VII is about 30 per cent. The bandwidth of the resonated coupler can be computed from (3.27), (3.28), and the above assumption that $Q_b/Q_0 = 0.1$. If the coupler is matched to the external circuit, we have $Q_{ext}\left|1/Q_0 + 1/Q_b\right| = 1$, and we obtain a bandwidth of about two per cent.

Linearly polarized synchronous wave couplers can be compared in the same way. It is found that the ratio of the length of a traveling-wave coupler to a resonant coupler, each giving the same gain, is

$$\frac{\ell_{TW}}{\ell_{Res}} = \frac{1}{2}\left|\frac{v_g}{\gamma_p}\right| Q_0 \quad .$$

Since Q_0 is generally of the order of 10^3 , there is a significant difference in these two cases. Again it is true that a sacrifice in bandwidth must be made. The bandwidth of the matched resonant coupler is simply $2/Q_0$, since there is no beam loading, while the bandwidth of the traveling-wave coupler will typically be about the same as the thirty per cent value calculated in the previous case.

In conclusion, the choice between traveling-wave and resonant couplers must be based entirely upon the application. If the important factor is bandwidth, then the traveling-wave couplers should be used. However, if coupler length, or gain in the case of the linearly polarized synchronous-wave coupler, is a limiting factor, then resonant structures may be indicated. In particular, it is desirable to employ resonant couplers in the synchronous-wave klystron described in Section III.C in order to produce a large gain.

CHAPTER IV

TWISTED COUPLERS

The purpose of this chapter is to describe the interactions which may occur between the transverse waves on an electron beam and a circuit in which the plane of polarization of the transverse electric field rotates uniformly along the axis of the circuit. This type of field corresponds to the transverse electric field of a wave propagating in a medium characterized by Faraday rotation. Because the circuits which support such a field look like linearly polarized structures which have been twisted about their axis, the name "twisted couplers" seems appropriate for this class of circuits. The special properties of these couplers make it worth while to treat them separately in this chapter rather than in Chapters II and III.

The interest in the twisted couplers arises from the fact that the two circularly polarized fields which make up the propagating circuit wave have different propagation constants. This means that it is possible to obtain coupling conditions which could not be obtained with ordinary circuits. For example, with this new class of couplers it is possible to couple equally to the cyclotron waves, or to a cyclotron and synchronous wave. Bernstein and Feinstein[26] have considered the special case of equal excitation of the cyclotron waves in connection with an electrostatically pumped cyclotron-wave amplifier. A more general treatment including all four of the transverse waves will be given here.

The first section of this chapter describes the interaction of the beam with a twisted electric field which propagates along a circuit, and gives the coupled mode equations which describe the interaction. Then, in the next section, the various possible synchronism conditions are discussed. The following section describes the important case in which traveling-wave or resonant couplers are used to excite both cyclotron waves. Finally, in the last section, the fields which exist in a twisted structure are considered and compared with the twisted-field model used in the electronic

interaction calculations. A description of some experimental twisted circuits will be found in Chapter VII.

A. BEAM INTERACTION WITH A TWISTED FIELD

A linearly polarized slow-wave structure supports a field characterized by

$$E_x = E_0 e^{j(\omega t - \beta_0 z)}$$
$$E_y = 0 \quad , \tag{4.1}$$

where β_0 is the circuit propagation constant and the field is polarized in the x direction. Now consider this circuit to be twisted about its axis with a period defined by

$$P = \frac{2\pi}{\beta_t} \quad , \tag{4.2}$$

as shown in Fig. 4.1. The quantity β_t is the twist propagation constant. A first approximation for the new electric field is obtained by twisting the solution given in (4.1). Therefore, we have, for the twisted circuit,

$$E_x = E_0 \cos \beta_t z \, e^{j(\omega t - \beta_0 z)}$$
$$E_y = E_0 \sin \beta_t z \, e^{j(\omega t - \beta_0 z)} \quad . \tag{4.3}$$

While these statements are not rigorous at all, they seem intuitively satisfying; and the more rigorous discussion of Section IV.D, on the fields existing in twisted periodic structures, shows that (4.3) is the correct result for small twist rates characterized by $\beta_t/\beta_0 \ll 1$.

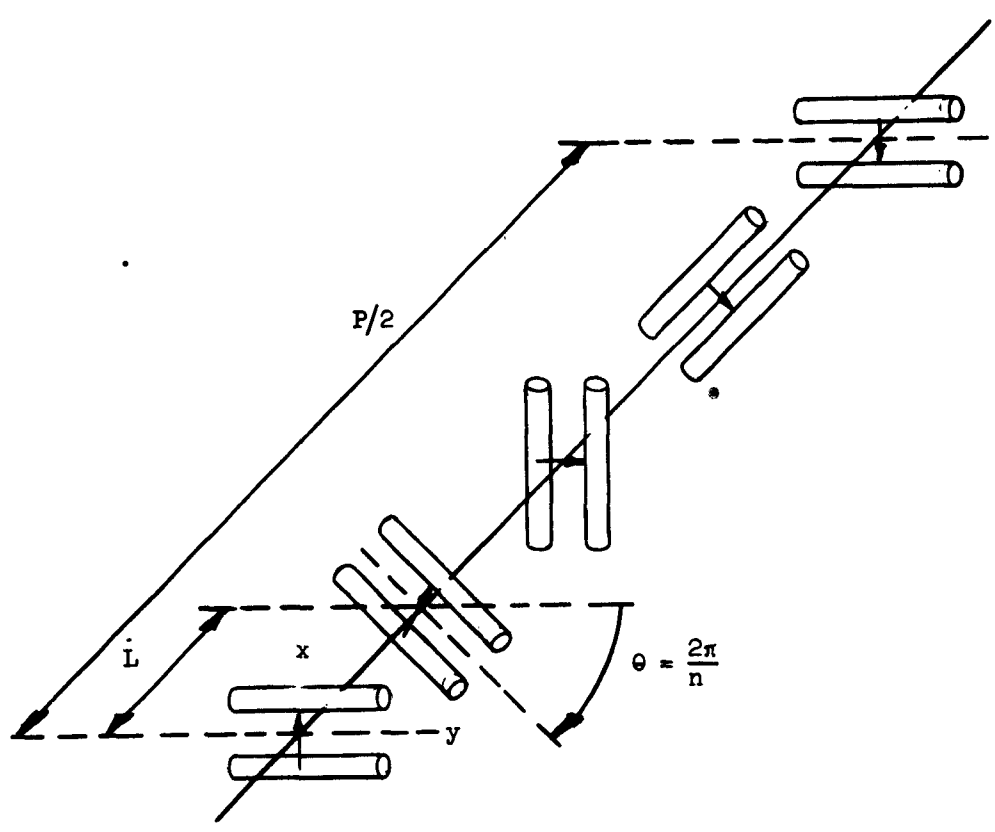

FIG. 4.1--Schematic representation of a periodic twisted coupler. The arrows represent the transverse electric field. The structure twists $2\pi/n$ radians per section or 2π radians in one period that is n sections long.

From Eqs. (2.4) the polarized field quantities are:

$$E_+ = E_0 e^{j\omega t} e^{-j(\beta_0 + \beta_t)z} \qquad (4.4)$$

$$E_- = E_0 e^{j\omega t} e^{-j(\beta_0 - \beta_t)z}$$

It can be seen that the effect of the twisting of the circuit field is to subtract β_t from the propagation constant of the field which is polarized in the direction of the twist and add β_t to the propagation constant of the oppositely polarized field.[1] These twisted field components may be used in Eqs. (2.5) to find the coupled mode equations. Everything is formally the same as in the previous case except now we obtain polarization factors which are a function of z. The circuit voltage given in Eqs. (2.9) is defined as

$$\frac{V}{D} = \sqrt{2}\, E_0 e^{+j(\omega t - \beta_0 z)} \quad , \qquad (4.5)$$

so that the polarization factors are given by

$$f_+ = \frac{1}{\sqrt{2}} e^{-j\beta_t z}$$

$$f_- = \frac{1}{\sqrt{2}} e^{+j\beta_t z} \qquad (4.6)$$

These have been normalized so that they satisfy (2.11), as required. The coupled mode equations which describe the twisted coupler are then (2.16) with the polarization factors given by (4.6). By combining these

[1] It should be noted that the definitions of the complex polarized variables given in (2.4) are based upon a left-hand coordinate system to agree with previous analyses. However, β_t has been defined in a right-hand coordinate system so that positive β_t and we are associated with the same azimuthal direction.

results, the final coupled mode equations are:

$$\frac{\partial A_1}{\partial z} + j\,\beta_1 A_1 = j\,\frac{K}{\sqrt{2}}\,A_0\,e^{-j\,\beta_t z}$$

$$\frac{\partial A_2}{\partial z} + j\,\beta_2 A_2 = j\,\frac{K}{\sqrt{2}}\,A_0\,e^{+j\,\beta_t z}$$

$$\frac{\partial A_3}{\partial z} + j\,\beta_3 A_3 = j\,\frac{K}{\sqrt{2}}\,A_0\,e^{-j\,\beta_t z}$$

$$\frac{\partial A_4}{\partial z} + j\,\beta_4 A_4 = j\,\frac{K}{\sqrt{2}}\,A_0\,e^{+j\,\beta_t z}$$

$$\frac{\partial A_0}{\partial z} + j\,\beta_0 A_0 \pm j\,\frac{K}{\sqrt{2}}\left[(A_3 - A_1)\,e^{+j\,\beta_t z} + (A_2 - A_4)\,e^{-j\,\beta_t z}\right] \quad .. (4.7)$$

The definitions of the parameters are the same as in (2.16). It is evident from Eqs. (4.7) that the synchronism conditions for strong interaction between the circuit and one of the beam waves are considerably different from those in the case of untwisted couplers. This is considered in the next section.

B. SYNCHRONISM CONDITIONS IN THE TWISTED COUPLER

The circuit phase velocity which yields strong coupling to one of the beam waves may be obtained from (4.7). The conditions which make the z variation of the right-hand side of one of the first four equations equal to the z variation of one of the normal modes on the beam is

$$\beta_0 = \beta_i \mp \beta_t \qquad . \quad (4.8)$$

The propagation constant β_i is one of those representing the transverse waves, and the upper sign is to be used when considering coupling to one of the positively polarized waves and the lower sign is for negatively polarized waves. It should be commented that the coupled mode analysis described involves a system in which the dc magnetic field is in the positive z direction. If the magnetic field is reversed, the polarization of the beam waves is reversed, although the propagation constants remain the same. A tabulation of the ratio of circuit phase velocity to dc beam velocity required to yield synchronism with a specific beam wave is given in Table I. The cyclotron frequency is a positive number in these relations.

TABLE I

SYNCHRONISM CONDITIONS FOR TWISTED COUPLERS

Circuit Synchronous with Mode	v_0/u_0	
	$+ B_0$	$- B_0$
A_1	$\left[1 + \frac{\omega_c}{\omega} - \frac{\beta_t u_0}{\omega}\right]^{-1}$	$\left[1 + \frac{\omega_c}{\omega} - \frac{\beta_t u_0}{\omega}\right]^{-1}$
A_2	$\left[1 - \frac{\omega_c}{\omega} + \frac{\beta_t u_0}{\omega}\right]^{-1}$	$\left[1 - \frac{\omega_c}{\omega} - \frac{\beta_t u_0}{\omega}\right]^{-1}$
A_3	$\left[1 - \frac{\beta_t u_0}{\omega}\right]^{-1}$	$\left[1 + \frac{\beta_t u_0}{\omega}\right]^{-1}$
A_4	$\left[1 + \frac{\beta_t u_0}{\omega}\right]^{-1}$	$\left[1 - \frac{\beta_t u_0}{\omega}\right]^{-1}$

In general, both the cyclotron frequency and the twist rate of the circuit are at our disposal so that it is possible to couple strongly to any two oppositely polarized transverse waves. It is important to note that β_t can be either positive or negative, depending on the direction of twist. For example, by making the twist rate such that

$$\beta_t = \frac{\omega_c}{\omega_0} \quad , \qquad (4.9)$$

the coupler excites both cyclotron waves equally. The circuit velocity should be equal to the dc beam velocity in this case. If the magnetic field is then reversed, the synchronism conditions are changed so that coupling to only one wave is achieved. This synchronism condition is important since the equal excitation of both cyclotron waves is the optimum situation for the dc pumped quadrupole discussed by Gordon[4] and others.[18]

In other cases, coupling to the positive or negative energy cyclotron and synchronous waves is achieved by making

$$\beta_t = \frac{1}{2}\,\frac{\omega_c}{u_0} \quad . \qquad (4.10)$$

It is also possible to achieve strong coupling to only one of the synchronous waves with a twisted, linearly polarized circuit, and to lower the magnetic field requirement for cyclotron-wave couplers. In particular it is possible to use an infinite phase velocity circuit[(1)] and a ratio of ω_c/ω less than unity to couple to the fast cyclotron wave. It is also possible to couple to the slow cyclotron wave and to the synchronous waves with an infinite phase velocity coupler by employing the proper twist rate.

Care must be taken in considering the interactions described above since, as is shown in Section IV.D, the assumed fields which lead to these results are not valid in all cases. Even so, the basic concept of the twisted circuit is important, and useful applications do arise. Some applications are considered in the next section.

---

(1) That is, a circuit which has an infinite phase velocity before it is twisted.

C. EQUAL EXCITATION OF THE CYCLOTRON WAVES

Of the various synchronism conditions that were discussed in the previous section, the condition which leads to equal excitation of both cyclotron waves appears to be of the greatest interest at present. It was noted that this importance exists because the optimum coupler for a particular type of dc quadrupole amplifier is one which excites the cyclotron waves equally. Bernstein and Feinstein[26] have noted this and described the application of a twisted coupler in this connection. Their description of the coupler was not in terms of a coupled mode formalism and it is worthwhile to note that this independent description based on coupled mode theory gives the same results. Another important reason for emphasizing this synchronism condition is that, since the waves are excited with equal amplitude, there is no beam loading in such a coupler and we are led to the consideration of a cyclotron-wave klystron completely analogous to the synchronous-wave klystron discussed in Chapter III.

In solving Eqs. (4.7) for this case, we assume that the circuit phase velocity and twist rate are such that there is strong coupling to the cyclotron waves and very little excitation of the synchronous waves. In that case the equations to be solved are:

$$\frac{\partial A_1}{\partial z} + j\,(\beta_e + \beta_c)\,A_1 = j\,\frac{K}{\sqrt{2}}\,e^{-j\,\beta_t z}\,A_0$$

$$\frac{\partial A_2}{\partial z} + j\,(\beta_e - \beta_c)\,A_2 = j\,\frac{K}{\sqrt{2}}\,e^{+j\,\beta_t z}\,A_0 \qquad (4.17)$$

$$\frac{\partial A_0}{\partial z} + j\,\beta_0 A_0 = j\,\frac{K}{\sqrt{2}}\left[A_2\,e^{-j\,\beta_t z} - A_1\,e^{+j\,\beta_t z}\right] .$$

These may be solved directly without difficulty, but it is simpler to redefine the wave amplitudes so that Eqs. (4.17) fall into a category

that we have already considered. If we now define the new waves

$$A_1' = A_1 e^{j\beta_t z}$$

$$A_2' = A_2 e^{-j\beta_t z} \quad , \qquad (4.18)$$

then the system of equations (4.17) becomes

$$\frac{\partial A_1'}{\partial z} + j(\beta_e + \Delta) A_1' = j \frac{K}{\sqrt{2}} A_0$$

$$\frac{\partial A_2'}{\partial z} + j(\beta_e - \Delta) A_2' = j \frac{K}{\sqrt{2}} A_0$$

$$\frac{\partial A_0'}{\partial z} + j\beta_0 A_0 = j \frac{K}{\sqrt{2}} (A_2' - A_1') \quad , \qquad (4.19)$$

where

$$\Delta = \beta_c - \beta_t \quad . \qquad (4.20)$$

When the twist rate or the magnetic field is adjusted to give $\Delta = 0$, Eqs. (4.19) are identical to (2.30) which describe the linearly polarized synchronous wave coupler. Thus, the solution to the present problem is exactly the same as it was for the synchronous wave coupler except that now the cyclotron wave propagation constants are different. The wave amplitude expressions given by (2.33), or (3.42) in the case of a resonant coupler, are in agreement with the results in the above reference where they are applicable.

The exact correspondence between the twisted cyclotron-wave coupler and the linearly polarized synchronous wave coupler is valid only at the condition $\beta_c = \beta_t$. Note that this does not mean that the circuit wave must be synchronous with the beam waves since β_0 need not be equal to β_e in order to have Δ vanish. Consequently, the dependence on synchronism

between the circuit and the beam that appeared in the synchronous wave equations cited above is correct here also. However, if Δ is not zero, the character of the equations changes. By comparing (4.19) with coupled mode descriptions of circuit interactions with the space-charge waves, such as are given by Louisell,[27] we see that identifying $|\Delta|$ with β_q leads to the traveling-wave tube equations when Δ is positive and to those for the backward-wave oscillator when Δ is negative. Consequently, published solutions for the propagation constants in space-charge wave devices can be used here. The correspondence between the two cases does not exist at $\Delta = 0$ ($\beta_q = 0$) because of the way in which the coupling coefficient in the space-charge wave equations depends upon β_q.

In general the solutions of (4.7) for other synchronism conditions are easily obtained by the methods which have been used to solve the coupled mode problems that have been described earlier. In particular, it will be found that a simple change of notation such as the one used above for the case of $\beta_c = \beta_t$, will lead to the formalism of the problems that have already been considered.

D. ELECTRIC FIELDS IN TWISTED CIRCUITS

In the first section of this chapter we derived the coupled mode equations describing the interaction between an electron beam and a twisted electric field. This field was taken as an approximation of the electric field that exists in a twisted circuit. The purpose of this section is to consider the electric fields which propagate on a twisted structure, and to show that the field assumed in the electronic interactions described previously is correct for small twist rates.

In general, the twisted circuit is a periodic structure in which each section is rotated about its axis with respect to the previous section as was indicated in Fig. 4.1. The field quantities associated with the circuit are, in general, periodic in both z and θ. Let L be the fundamental period of the structure before it is twisted and n be the number of these periods which must be advanced before the twisted circuit orientation repeats. That is, we are assuming that the twist angle per period of the structure is $2\pi/n$ where n is an integer. If the circuit is symmetric about its axis, and n is even, there will be a higher order symmetry, but this can be destroyed by imagining a small perturbation of one part of the circuit.

By means of Floquet's theorem,[28] the circularly polarized components of the potential in the circuit, which has a period of nL in the z direction and a θ periodicity to be defined, can be written as a sum of space-harmonics:

$$V(z\ ,\ \theta) = e^{-j\ \beta_{\pm} z}\ e^{-jp\theta} \sum_{k,\ell} A_{k,\ell}\ e^{-j\ \frac{2\pi k}{nL}\ z}\ e^{-j\ell\theta}\ , \qquad (4.21)$$

where $\beta_{\pm}$ is the phase shift per unit length of the positive or negative circularly polarized field component in the structure in a right-hand coordinate system and p is $+1$ for the positive polarized component and -1 for the negative polarized component. The coefficient $A_{k,\ell}$ contains the radial variations of the potential. The indices k and ℓ are integers which will be found to be related. If we advance on the circuit by an axial distance L and rotate by an amoung $\pm 2\pi/n$ (the $\pm$ sign gives the direction of the twist), the circuit is the same and the potential is a complex constant times the potential at the starting point, that is,

$$V(z + L\ ,\ \theta \pm \frac{2\pi}{n}) = V(z\ ,\ \theta) \cdot e^{-j\ \beta_{\pm} L}\ e^{\mp jp\ \frac{2\pi}{n}}\ . \qquad (4.22)$$

Upon using (4.21) and (4.22) we obtain an equation that is satisfied only if

$$k \pm \ell = nm\ , \qquad (4.23)$$

where m is any integer. If we allow axial symmetries of the structure which can reduce the period as mentioned above, it is found that (4.23) is still the correct restriction to be placed on k and ℓ. The general potential expression is then written

$$V(z\ ,\ \theta) = e^{-j\ \beta_{\pm} z}\ e^{-jp\theta} \sum_{\ell,m} A_{\ell,m}\ e^{-j\ \frac{2\pi}{nL}\ (nm \mp \ell)z}\ e^{-j\ell\theta}\ , \qquad (4.24)$$

where the upper sign with ℓ is to be used if the twist is in the positive sense with advancement in the positive z direction and the lower sign is for a negative twist.

We see from (4.24) that there is a multiplicity of spatial harmonics which must be combined to yield the general field configuration. There are in general n branches to the ω-β diagram as indicated in Fig. 4.2 for the positively polarized field component. For the purposes for which we are considering twisted circuits, that is, in transverse wave couplers, the value of ℓ is zero, yielding $e^{\pm j\theta}$ azimuthal variation. From the figure we see that these components all lie on one branch of the ω-β curve.

The fact that there is a number of branches to the ω-β diagram can alter the expected dispersion characteristic for a circuit considerably. While we are ordinarily not interested in the extra multipole fields which arise due to the twisting of the circuit, the intersections of the various branches can lead to stop-bands if there is any discontinuity which can couple the space harmonic components represented by the different branches.

The propagation constants that can be expected in twisted circuits can be determined from (4.24) by assuming that both field polarizations propagate with the propagation constant β_0 in the frame of reference that twists with the circuit. In that case, by denoting the variables in the twisted frame with primes, we have

$$z' = z$$

$$\theta' = \theta - \beta_t z \qquad , \qquad (4.25)$$

where β_t was given in (4.2) and it carries the sign of the direction of the twist. Then (4.24) gives

$$V' = e^{-j(\beta_\pm + p\,\beta_t)z'} \sum_{\ell,m} A_{\ell,m}\, e^{-j\frac{2m\pi}{L}z'} e^{-j\ell\theta'} \qquad , \qquad (4.26)$$

where the prime denotes the potential in the twisted frame. Clearly the quantity in front of the summation represents the propagation factor of

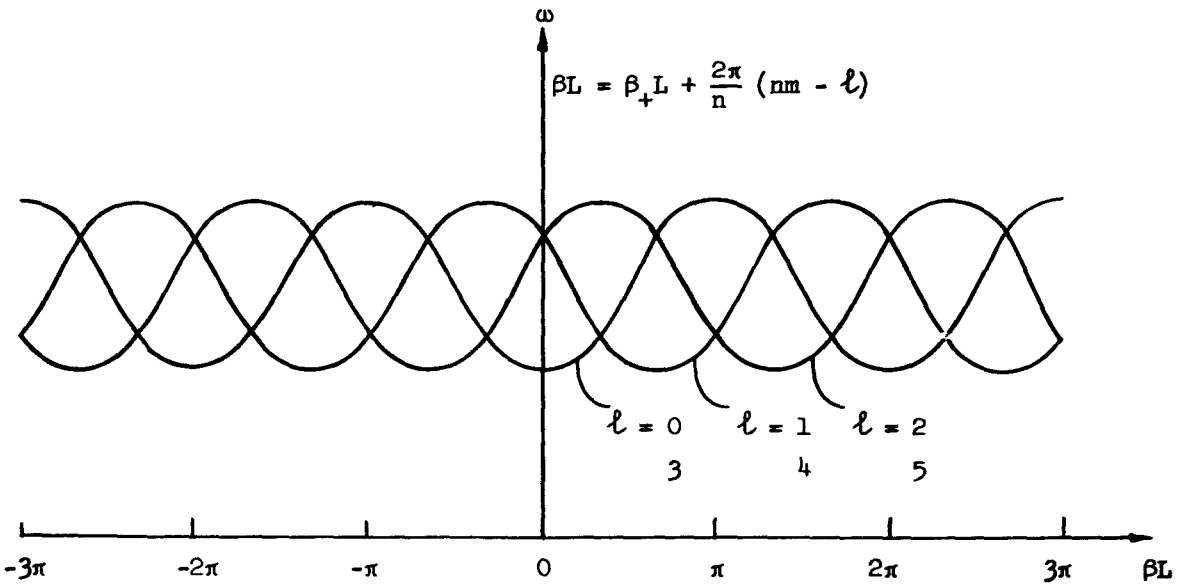

FIG. 4.2--A sketch of a typical $\omega - \beta$ diagram for a circuit that twists $2\pi/3$ radians per section, that is, $n = 3$. The circuit is twisted in the positive sense as indicated by the sign in front of ℓ .

the fundamental $(m = \ell = 0)$ field component of the periodic structure. Equating this to $\exp[-j\beta_0 z]$ gives

$$\beta_+ = \beta_0 - \beta_t$$

$$\beta_- = \beta_0 + \beta_t \qquad , \qquad (4.27)$$

where β_0 is the propagation constant observed in the twisting frame of reference. These results are in agreement with those given in Eqs. (4.4) when it is noted that E_+ and E_- are defined in a left-hand coordinate system.

While the above discussion is designed to show the nature of the dispersion characteristic in a general twisted circuit, it is not well suited for a calculation of the field components involved in a typical circuit. The field configuration will certainly be different from that of the untwisted circuit. Bernstein and Feinstein[26] have considered this question in connection with some work in a twisted coupler of the type discussed in Section IV.C. Their assumption is the one used in Section A of this chapter, where we assumed that the transverse field of the twisted circuit is simply obtained by twisting the linearly polarized field configuration that is valid for the untwisted circuit. One feels that this is a good approximation, but, as is pointed out in the reference, this does not yield a field expression which satisfies $\nabla \cdot \vec{E} = 0$. It is also true that, by estimating the nature of the field perturbations as the circuit is twisted, it can be seen that a new component of the transverse field is produced. This is in space and time quadrature to the main transverse field.

A description of the exact nature of the fields that exist in a twisted periodic circuit appears quite difficult and the discussion given here will be restricted to an approximate approach. It was shown that the potential in a general circuit obeyed (4.24). In order to obtain a description of the nature of the transverse fields in a twisted circuit, we neglect all of the space harmonics of the circuit and consider only the fundamental component for which m and ℓ are zero. The potential then consists of components with the two propagation constants given by

(4.27). The potential components are assumed to be solutions of Laplace's equation in accordance with the initial assumptions made in using (2.8) as the equations governing the circuit. In rectangular coordinates we have

$$V(x, y, z) = [a_+ \sinh (\beta_0 + \beta_t) x + b_+ \sinh (\beta_0 + \beta_t)y]\, e^{-j(\beta_0 + \beta_t)z}$$

$$+ [a_- \sinh (\beta_0 - \beta_t) x + b_- \sinh (\beta_0 - \beta_t)y]\, e^{-j(\beta_0 - \beta_t)z} \quad , \qquad (4.28)$$

where the coefficients $a_\pm$ and $b_\pm$ are to be determined by the boundary conditions. The solutions which correspond to zero transverse electric field on the axis have been omitted in the above expression since they are not important for transverse-wave interactions.

The circuit is assumed to be oriented as shown in Fig. 4.1. In order to determine the coefficients in (4.28) we impose the condition that, when the circuit has twisted through $\pi/2$ radians, the circuit potential has also rotated by $\pi/2$ radians. A statement must also be made about the potential distribution in the x-y plane. The required boundary conditions are taken as:

$$V(a, 0, 0) = V_0$$

$$V(0, a, \frac{\pi}{2\beta_t}) = V_0\, e^{-j\,\beta_0 \frac{\pi}{2\beta_t}} \qquad (4.29)$$

$$V(0, a, 0) = 0 \quad ,$$

where $2a$ is the transverse spacing between the circuit elements. The last condition in (4.29) is somewhat arbitrary, but it gives a good approximation of what the potential in a twisted circuit would be. Equations (4.29) and (4.28) are enough to obtain the four coefficients $a_\pm$ and $b_\pm$, if

we use the additional statement that Eqs. (4.29) are valid for any β_0 and β_t . The expression for the potential is then found to be

$$V = \frac{V_0}{2}\left\{\left[\frac{\sinh(\beta_0 + \beta_t)x}{\sinh(\beta_0 + \beta_t)a} + j\,\frac{\sinh(\beta_0 + \beta_t)y}{\sinh(\beta_0 + \beta_t)a}\right]e^{-j(\beta_0 + \beta_t)z}\right. \tag{4.30}$$

$$\left. + \left[\frac{\sinh(\beta_0 - \beta_t)x}{\sinh(\beta_0 - \beta_t)a} - j\,\frac{\sinh(\beta_0 - \beta_t)y}{\sinh(\beta_0 - \beta_t)a}\right]e^{-j(\beta_0 - \beta_t)z}\right\}.$$

The transverse electric fields can be computed directly from (4.30). Generally, the circuit dimensions will be such that only the first term in the expansion of the hyperbolic cosine and sine make a significant contribution to the field and in this case we obtain

$$E_x = -\frac{V_0}{\beta_0}\,\frac{1}{\beta_0 a}\,\frac{1}{1 - \left(\frac{\beta_t}{\beta_0}\right)^2}\left[\cos\beta_t z + j\,\frac{\beta_t}{\beta_0}\sin\beta_t z\right]e^{-j\,\beta_0 z} \tag{4.31}$$

$$E_y = -\frac{V_0}{\beta_0}\,\frac{1}{\beta_0 a}\,\frac{1}{1 - \left(\frac{\beta_t}{\beta_0}\right)^2}\left[\sin\beta_t z - j\,\frac{\beta_t}{\beta_0}\cos\beta_t z\right]e^{-j\,\beta_0 z}\ .$$

The first term in E_x and E_y represents a field which corresponds to twisting up the field of the linearly polarized counterpart of the twisted circuit, and is the field configuration that was assumed in the first section of this chapter. The second terms in (4.31) represent a modification of this field that arises because of the twisting. It is proportional to β_t/β_0 and in quadrature to the main field component. We cast this in a

different form by observing the fields in the twisting frame of reference. The twisted field of the linearly polarized circuit is denoted by $E_{\parallel}$ and the field perpendicular to this by $E_{\perp}$ as shown in Fig. 4.3. These fields are related to those in the laboratory frame of reference by

$$E_{\parallel} = E_x \cos \beta_t z + E_y \sin \beta_t z$$
$$E_{\parallel} = E_x \sin \beta_t z - E_y \cos \beta_t z \qquad (4.32)$$

Substituting (4.31) into (4.32) yields

$$E_{\parallel} = \frac{E_0 e^{-j \beta_0 z}}{1 - (\beta_t/\beta_0)^2}$$
$$E_{\perp} = \frac{\beta_t}{\beta_0} \frac{E_0 e^{-j \beta_0 z}}{1 - (\beta_t/\beta_0)^2} , \qquad (4.33)$$

where E_0 is a coefficient consisting of the factors in (4.31). Figure 4.3 shows the standing-wave pattern that is created when a forward and a reverse traveling-wave on the circuit are combined. Note that a simple planar short on each end of a twisted structure does not result in the ideal twisted cavity since the end conditions are not correct. However, for small twist rates the field pattern would be essentially that shown in the figure except near the shorted ends of the cavity. This is observed experimentally in Chapter VII.

In order to determine how these results affect the calculations made in the earlier part of this chapter the field of the twisted circuit is written in circularly polarized variables. We find that the fields

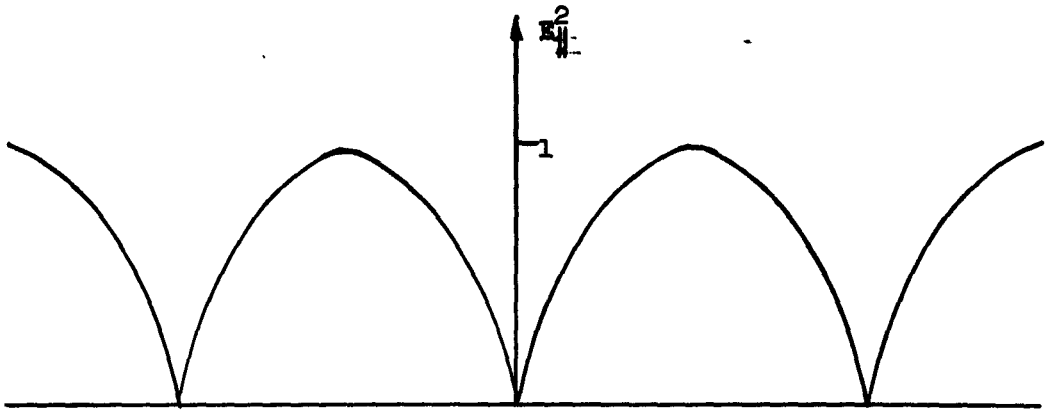

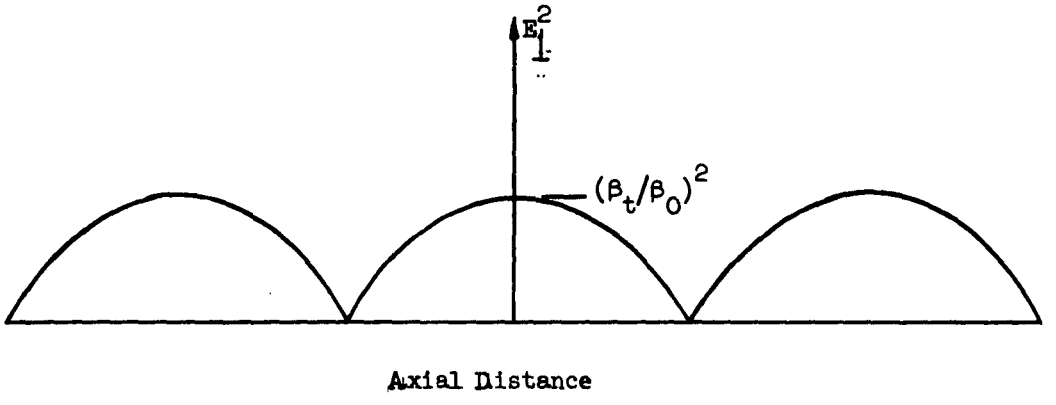

FIG. 4.3--The standing-wave patterns of the two field components on a twisted circuit due to equal forward and reverse propagating waves.

corresponding to (4.4) are given by

$$E_+ = \frac{E_0}{1 + \beta_t/\beta_0} e^{-j(\beta_0 + \beta_t)z}$$

$$E_- = \frac{E_0}{1 - \beta_t/\beta_0} e^{-j(\beta_0 - \beta_t)z} \qquad (4.34)$$

That is, the circularly polarized field components are no longer of equal amplitude. This means that f_+ and f_- in (4.6) are altered by the factor $(1 \pm \beta_t/\beta_0)^{-1}$, respectively. These new polarization factors then obey (2.11) to first order in (β_t/β_0). It is not appropriate to continue the discussion to larger twist rates because of the approximations that have been made up to this point.

As a result of the above discussion we see that the coupled mode equations and the resulting electronic interactions that were derived in the first sections of this chapter were correct for $\beta_t/\beta_0 \ll 1$. However, if the twist rate is larger than this, the amplitudes of the two circularly polarized field components become different while their propagation constants are still the same. The interaction is still described by the coupled mode equations of Chapter II, but the modified polarization factors indicated above must be used.

CHAPTER V

CYCLOTRON-WAVE FREQUENCY DOUBLERS

The use of cyclotron-wave interactions in a quadrupole type of resonant cavity to achieve frequency doubling will be discussed in this chapter. Such an interaction was reported by Ashkin,[21] who excited a fast cyclotron wave on a beam entering a quadrupole cavity and observed second harmonic power output from the quadrupole. Cuccia had observed this earlier,[20] and reported some results and proposed multipliers employing higher order multipole cavities. Lindsay and Caunter[22] have carried out a ballistic analysis for the special case of the fast cyclotron wave doubler operating at cyclotron resonance, which was the type of operation used in the experiments mentioned above. It has been noted by all of these workers that high conversion efficiencies may be expected with this type of doubler.

The above studies have all been connected with the special case in which the fundamental frequency is equal to the cyclotron frequency and the coupler and quadrupole circuits were characterized by an infinite phase velocity. It is obvious, however, that these observed frequency doubling interactions are a special case of the general situation in which periodic structures with finite phase velocity and frequencies other than the cyclotron frequency are used.

The analysis to be presented here will be based on a coupled mode approach to the problem, and will include the interactions with both the fast and slow cyclotron waves, with arbitrary combinations of these waves existing at the beam input to the quadrupole. This will make it possible to predict the operating characteristics of the general class of cyclotron-wave frequency doublers.

The study of this problem by means of coupled mode equations results in the description of the circuit fields as a superposition of traveling waves. The field in the resonant quadrupole is then given as a sum of forward and reverse propagating waves. The analysis which will be

given in this chapter neglects the interaction between the beam and the reverse propagating wave; that is, it assumes interaction with a single forward propagating circuit wave of constant amplitude. While this is generally not an acceptable assumption, as is evidenced by some of the results for resonant coupler circuits given in Chapter III, it causes no significant error here, as it applies to practical situations. This is because quadrupole interaction impedances are quite small, resulting in devices which are many wavelengths long. Consequently, it is safe to neglect interactions with the traveling waves on the circuit which are not synchronous with one of the beam waves.

A. COUPLED MODE EQUATIONS

The coupled mode equations representing interaction between a beam and coupler type transverse fields were given in Chapter II. In the present chapter we consider the case in which the beam interacts with a field having the quadrupolar symmetry shown in Fig. 5.1. Blφtekjaer and Wessel-Berg[19] have analyzed this situation and have obtained the coupled mode equations which are to be the starting point for the analysis given in this and the next chapter. In order to cast these equations in the same notation used earlier in this paper, we briefly describe the steps leading up to their final results. The material presented in this section is not new, except for various commentaries, and the equations can be found in the above reference in a different notation.

A traveling-wave field of quadrupolar symmetry which is a solution of Maxwell's equations may be represented by:

$$E_x = \frac{m}{e} R_e \left\{ (B_1 x + B_2 y)\, e^{j(\omega_q t - k_q z)} \right\}$$

$$E_y = \frac{m}{e} R_e \left\{ (B_2 x - B_1 y)\, e^{j(\omega_q t - k_q z)} \right\}$$

$$E_z = \frac{m}{e} R_e \left\{ -j \frac{k_q}{2} \left[B_1 (x^2 - y^2) + 2 B_2 x y \right] e^{j(\omega_q t - k_q z)} \right\} . \quad (5.1)$$

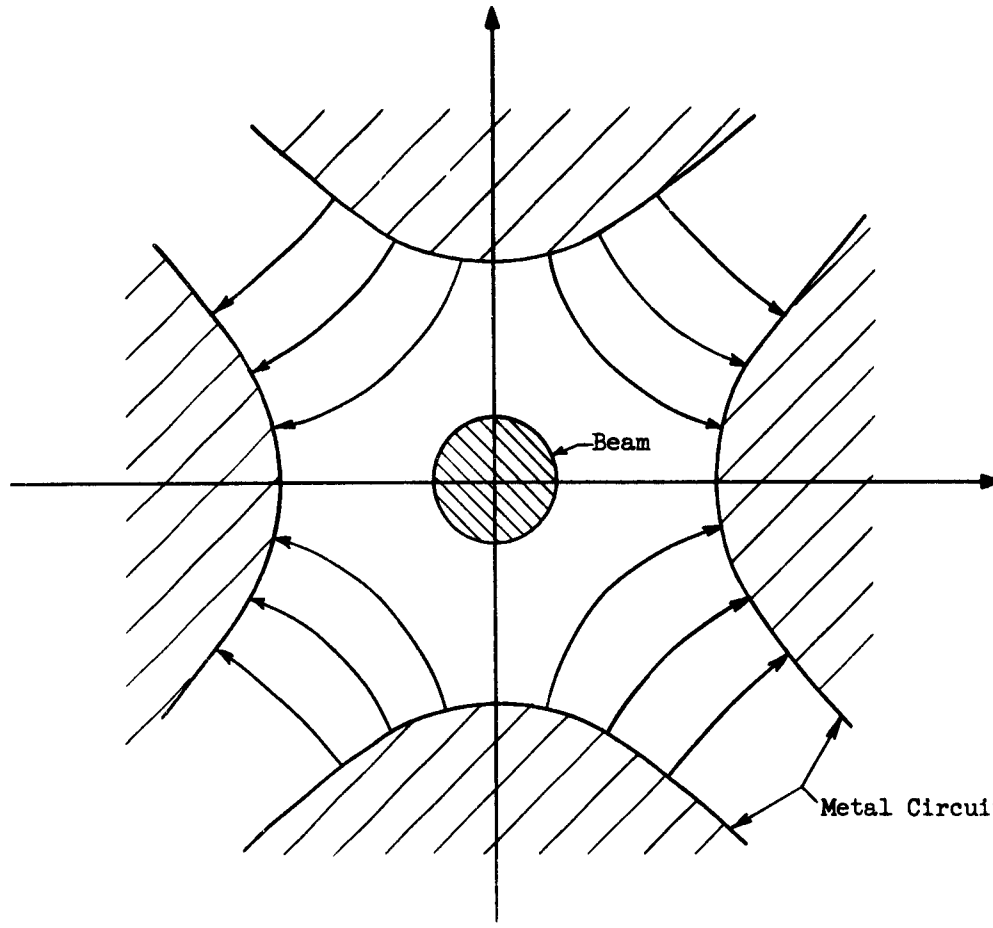

FIG. 5.1--A cross section of a structure that supports a quadrupole field. The equipotential surfaces are hyperbolas in the ideal case.

In these equations ω_q is the radian frequency, and k_q is the propagation constant of the structure supporting the quadrupole field. The terms B_1 and B_2 are arbitrary complex constants which may be selected to give fields of circular or linear polarization. Both E_x and E_y are linear in the transverse dimensions and satisfy Maxwell's equations to first order in x and y. The quadratic E_z expression results from forcing the assumed transverse fields to satisfy the field equations. The analysis here is to be a linearized one, and so E_z will not play a part in the interaction equations, but it is required to explain the energy exchange in the quadrupole.

The filamentary beam model used in Chapter II will also be used here. The use of this model may be questioned on the basis of the fact that, in a beam of finite diameter, all of the electrons in the quadrupole do not see the same transverse field to first order in the displacement. In the coupler calculations this was true and it was possible to describe the beam motion in terms of the motion of the center of mass of the beam in the complex calculations. Fortunately, the same procedure may be used here.

A real beam may be considered to be a bundle of filamentary beams. In the case of the coupler field all of these filaments experienced the same force, while in the quadrupole field the situation is somewhat different. By substituting $x_0 + x_1$ and $y_0 + y_1$, where (x_1,y_1) is measured from the individual filament position (x_0,y_0), for x and y in the first two of Eqs. (5.1), we find that filaments at different dc positions (x_0,y_0) are in exactly the same quadrupolar field. In addition, there is a coupler type field which is dependent upon the position of the filament. If the synchronization condition is correct this last field will lead to undesired beam expansion by exciting one or more of the transverse waves, which are then amplified by the quadrupole field in the same way as in an ordinary transverse wave parametric amplifier.[19] Another way of saying this is that the quadrupolar field will amplify initial zero frequency excitation on the beam filaments. Thus, in the cases to be studied in this chapter, in which the quadrupole is synchronous with the fast cyclotron wave, we should avoid having dc beam rotation at the cyclotron frequency since this represents a zero

frequency cyclotron wave. In the next chapter it will be seen to be necessary to have some dc beam rotation to avoid expansion in the quadrupole which is synchronous with the synchronous waves on the beam. The crucial point of this argument is that we may employ the filamentary beam model for finite size beams, if care is taken to avoid the zero frequency filamentary beam modes which can be amplified by the quadruple field.

The equations of motion for the filamentary beam are then obtained by substituting Eqs. (5.1) into (2.1) in Chapter II. This yields equations for the velocities and displacements which have some coefficients that are periodic in both t and z :

$$\frac{\partial v_x}{\partial t} + u_0 \frac{\partial v_x}{\partial z} + \omega_c v_y = - R_e[B_1 x + B_2 y]\, e^{j(\omega_q t - k_q z)}$$

$$\frac{\partial v_y}{\partial t} + u_0 \frac{\partial v_y}{\partial z} - \omega_c v_x = - R_e[B_2 x - B_1 y]\, e^{j(\omega_q t - k_q z)}$$

$$\frac{\partial x}{\partial t} + u_0 \frac{\partial x}{\partial z} - v_x = 0$$

$$\frac{\partial y}{\partial t} + u_0 \frac{\partial y}{\partial z} - v_y = 0 \quad . \tag{5.2}$$

Blφtekjaer and Wessel-Berg[19] show that these equations may be solved by making substitutions of the form

$$x = \sum_{n=-\infty}^{\infty} x_n e^{j\left[(\omega + n\omega_q)t - (\gamma + \beta_e + nk_q)z\right]}, \tag{5.3}$$

for each displacement and velocity. Writing the propagation constant as shown in terms of γ facilitates the solution of the system of equations. Next, we define the wave amplitudes just as in (2.13) of Chapter II. Note that the numerical subscripts here correspond to Siegman's[10] definitions

which were given in Eqs. (2.13) and are different from those used by Wessel-Berg and Blϕtekjaer:

$$A_{1,n} = \tfrac{1}{2}jk\,(v_{x,n} - jv_{y,n}) \;,\; A_{2,n} = j\tfrac{1}{2}k\,(v_{x,n} + jv_{y,n})$$

$$A_{3,n} = \tfrac{1}{2}jk\,(v_{x,n} - jv_{y,n} + \omega_c y_n + j\omega_c x_n)$$

$$A_{4,n} = \tfrac{1}{2}jk\,(v_{x,n} + jv_{y,n} + \omega_c y_n - j\omega_c x_n) \quad , \tag{5.4}$$

where

$$k = \sqrt{\tfrac{1}{2}\,\frac{\omega}{\omega_c}\,\frac{m}{e}\,I_0} \quad .$$

It is found convenient to define

$$C_+ = -\frac{1}{2\omega_c u_0}\,[B_2 + jB_1]$$

$$C_- = -\frac{1}{2\omega_c u_0}\,[B_2 - jB_1] \quad , \tag{5.5}$$

which represent the positively and negatively polarized components of the quadrupole field as may be seen by considering the complex forms of Eqs. (5.1). Finally, by combining (5.2), (5.3), (5.4) and (5.5), the coupled mode equations are obtained:

$$-j\left[\gamma - \left(\frac{\omega_c}{u_0} - n\,\frac{\omega_q}{u_0} - k_q\right)\right] a_{1,n} = C_+ a_{2,n-1} + C_+ a_{4,n-1}$$

$$+ C_-^* a_{2,n+1} + C_-^* a_{4,n+1}$$

and

$$-j\left[\gamma + \frac{\omega_c}{u_0} - n\left(\frac{\omega_q}{u_0} - k_q\right)\right]a_{2,n} = C_-a_{1,n-1} + C_-a_{3,n-1} + C_+^*a_{1,n+1} + C_+^*a_{3,n-1}$$

$$-j\left[\gamma - n\left(\frac{\omega_q}{u_0} - k_q\right)\right]a_{3,n} = C_+a_{2,n-1} + C_+a_{4,n-1} + C_-^*a_{2,n+1} + C_-^*a_{4,n+1}$$

$$-j\left[\gamma - n\left(\frac{\omega_q}{u_0} - k_q\right)\right]a_{4,n} = C_-a_{1,n-1} + C_-a_{3,n-1} + C_+^*a_{1,n+1} + C_+^*a_{3,n+1} \quad . \qquad (5.6)$$

As in Chapter II, when the exponential variation has been omitted, lower case letters are used for the amplitudes. Equations (5.6) relate the amplitudes of the waves at the frequency $\omega + n\omega_q$ to those at the frequencies $\omega + (n-1)\omega_q$ and $\omega + (n+1)\omega_q$. We shall be concerned, for the most part, with the solution of these equations for some special cases.

B. SOLUTION OF EQUATIONS

Equations (5.6), subject to the conditions specified on the beam at the entrance to the quadrupole, describe completely all small signal interactions possible between the four basic transverse waves and the assumed quadrupolar field. The solutions for the same synchronism conditions that are of interest in this chapter (synchronism with the cyclotron waves) as well as in the next chapter (synchronism with the synchronous waves) have been considered in the reference cited before. However, in that case, the goal was to use the quadrupole interaction in a parametric type of device in which there would be no phase relation

between the input beam waves and the quadrupole field. This results in the omission of a term in the final power expressions. This procedure is not allowable for the present discussion since, in the case being studied here, the beam waves will interact with the quadrupole and will establish the circuit field so that the quadrupole phase is related to the input phase of the beam wave.

As discussed by Bløtekjaer and Wessel-Berg,[19] the solution to (5.6) to first order in the quadrupole field amplitudes C_+ and C_- can be found by a simple perturbation procedure. We follow this same approach here, but keep terms which were omitted in the previous work due to the assumption of random quadrupole phase. In carrying out this small quadrupole amplitude analysis, only the frequencies represented by $n = 0, \pm 1$ are considered since other values of n represent interactions which are of second order in the small coefficients which couple the beam to the quadrupole. That is, we include the signal frequency ω and the sum and difference frequencies, $\omega_q + \omega$ and $\omega_q - \omega$, which arise in the beam as a result of the parametric type of interaction. As a result of this, a set of homogeneous equations such as (5.6) for $n = 0, \pm 1$ is obtained. The requirement that a nontrivial solution exist is that the system determinant be zero:

$$\begin{vmatrix} D_+(-1) & 0 & 0 & 0 & C_-^* & 0 \\ 0 & D_+(0) & 0 & C_+ & 0 & C_-^* \\ 0 & 0 & D_+(+1) & 0 & C_+ & 0 \\ 0 & C_+^* & 0 & D_-(-1) & 0 & 0 \\ C_- & 0 & C_+^* & 0 & D_-(0) & 0 \\ 0 & C_- & 0 & 0 & 0 & D_-(1) \end{vmatrix} = 0 \quad , \quad (5.7)$$

where

$$D_+(n) = j\left[-\gamma + \frac{\omega_c}{u_0} + n\left(\frac{\omega_q}{u_0} - k_q\right)\right]$$

$$D_-(n) = j\left[-\gamma - \frac{\omega_c}{u_0} + n\left(\frac{\omega_q}{u_0} - k_q\right)\right]. \qquad (5.8)$$

The synchronous waves have been neglected in (5.7) because the synchronism conditions which are imposed below in Eq. (5.9) result in negligible interaction with the synchronous waves if the quadrupole is just a few wavelengths long, measured at the beam velocity. Due to the small quadrupole interaction impedance which is found in practical circuits, the circuit will be much too long to allow significant cumulative interaction with the synchronous waves.

The reference shows that solutions of (5.6) which are of first order in small quantities are obtained for the synchronism conditions

$$\frac{\omega_q}{u_0} - k_q = \pm 2\frac{\omega_c}{u_0} . \qquad (5.9)$$

When $\omega_q = 2\omega$, as is the case in the frequency doubler, the upper sign leads to synchronism between the fast cyclotron wave on the beam at the entrance to the quadrupole circuit and the assumed fields, while the lower sign corresponds to synchronism with the slow cyclotron wave. This may be seen by substituting ω_q/v_q into (5.9), solving for the quadrupole phase velocity v_q, and setting $\omega_q = 2\omega$.

1. Synchronism Condition $2\omega/u_0 - k_q = +2\omega_c$.

As pointed out above, the condition given by

$$\frac{2\omega}{u_0} - k_q = +2\frac{\omega_c}{u_0} \qquad (5.10)$$

results in a quadrupole field that is synchronous with the fast cyclotron wave. It is this case, with $k_q = 0$, which has been the basis of the studies on transverse wave frequency doubling in the past, and we shall begin with it here in the general formulation of cyclotron wave doublers.

The determinant (5.7) represents a sixth order polynomial in γ . However, the approximate values of γ that are different from the unperturbed solutions are obtained by retaining only the part of the determinant in which the diagonal elements are of the order of magnitude of the small off-diagonal terms. Upon substituting (5.10) and (5.8) into (5.7) and noting from (5.3) that the unperturbed values of γ are $\pm \beta_c$ for the cyclotron waves, it is found that the significant portion of (5.7) is the fourth order determinant

$$\begin{vmatrix} D_+(-1) & 0 & C_-^* & 0 \\ 0 & D_+(0) & 0 & C_-^* \\ C_- & 0 & D_-(0) & 0 \\ 0 & C_- & 0 & D_-(1) \end{vmatrix} = 0 \quad . \tag{5.11}$$

In the case of a frequency doubler, which is the case we are concerned with here, the quadrupole frequency will be twice the signal frequency. It is then found that the four values of γ , which are different from the unperturbed solutions, are

$$\gamma = \pm j\sqrt{C_- C_-^*} \pm \beta_c \quad . \tag{5.12}$$

Upon recalling that the z-variation of the wave amplitudes is $e^{-j(\gamma + \beta_e + nk_q)}$, as indicated in Eq. (5.3), it is seen that the imaginary part of γ results in exponential growth and decay of the wave amplitudes excited on the beam.

The above calculation of the beam wave propagation constants in the quadrupole region is the first step in describing the interaction between the beam and the circuit. The next step is to substitute (5.12) into (5.6) and apply the beam entrance conditions to determine the exact nature

of the interaction. In doing this it is necessary to note the relationships which are valid for the negative frequency terms arising from the choice of $n = -1$. It can be shown that[19]

$$a_{2,-\omega,-n} = a^*_{1,\omega,n} \quad . \tag{5.13}$$

It is then found that, for the present case, in which the assumed quadrupole is exactly double the input signal frequency, the wave amplitudes in the quadrupole region are given in terms of the entrance amplitudes by

$$\begin{aligned} A_1(z) &= a_1(0) \cosh \alpha z \; e^{j[\omega t - (\beta_e + \beta_c)z]} \\ A_2(z) &= a_2(0) \cosh \alpha z \; e^{j[\omega t - (\beta_e - \beta_c)z]} \\ &\quad + \frac{c_-}{\alpha} a_2^*(0) \sinh \alpha z \; e^{j[\omega t - (\beta_e - \beta_c)z]} \\ &\quad + \sqrt{3}\,\frac{c_-}{\alpha} a_1(0) \sinh \alpha z \; e^{j[3\omega t - (3\beta_e - \beta_c)z]} \quad , \end{aligned} \tag{5.14}$$

where

$$\alpha = |c_-| \quad . \tag{5.15}$$

These expressions have been normalized so that the sum of the squares of the amplitudes of the two frequency components represents the total average power. It is in this connection that the $\sqrt{3}$ arises in the third harmonic fast cyclotron wave amplitude. The equivalent of (5.14) has been obtained by Bløtekjaer and Wessel-Berg.[29] However, due to the uncorrelated phase assumption indicated above, their published results[19] cannot be used to explain the frequency doubling interactions which are described in this chapter.

Equations (5.14) show that an initial slow cyclotron wave on the beam at the frequency ω grows in amplitude and also gives rise to a growing fast cyclotron wave at the third harmonic frequency. An initial fast

cyclotron wave continues through the quadrupole region as a fast cyclotron wave at the input frequency, but its amplitude is dependent on the phase of the quadrupole field. Since the quadrupole field is produced by the energy given up to the circuit by the beam, the quadrupole phase will be determined by the beam entrance phase and the external loading on the quadrupole.

The fact that C_+ does not appear in the above discussion shows that the interactions which are under consideration do not involve the positively polarized quadrupole field component. The presence of this field component represents wasted stored energy. Consequently, for cyclotron wave frequency doublers, the highest value for the interaction impedance will be obtained by using circularly polarized quadrupole cavities. However, practical considerations involving the ease of design and excitation of such structures may well dictate the use of linearly polarized quadrupole structures.

2. Synchronism Condition $2\omega/u_0 - k_q = -2\,\omega_c/u_0$.

The procedure for finding the perturbed propagation constants for the synchronization condition

$$\frac{2\omega}{u_0} - k_q = -2\,\frac{\omega_c}{u_0} \tag{5.16}$$

is the same as for the previous case. Substituting (5.16) into (5.8) and keeping only that portion of the system determinant (5.7) which has small diagonal terms yields

$$\begin{vmatrix} D_+(0) & 0 & C_+ & 0 \\ 0 & D_+(1) & 0 & C_+ \\ C_+^* & 0 & D_-(1) & 0 \\ 0 & C_+ & 0 & D_-(0) \end{vmatrix} = 0 \ . \tag{5.17}$$

It is then found that the four values of γ which are different from the unperturbed solutions are:

$$\gamma = \pm j\sqrt{C_+ C_+^*} \pm \beta_c \quad . \tag{5.18}$$

This result shows that the interaction is entirely with the positively polarized quadrupole field component while the previous case involved the negatively polarized field. The equations describing the wave excitation in the quadrupole region are obtained by substituting (5.18) into the amplitude equations and applying the conditions on the cyclotron waves at the quadrupole entrance. Finally, then, the results are:

$$A_1(z) = \left[a_1(0)\cosh \alpha z + \frac{C_+}{\alpha} a_1^*(0) \sinh \alpha z\right] e^{j[\omega t - (\beta_e + \beta_c)z]}$$

$$+ \sqrt{3}\,\frac{C_+}{\alpha} a_2(0) \sinh \alpha z\, e^{j[3\omega t - (3\beta_e + \beta_c)]}$$

$$A_2(z) = a_2(0)\cosh \alpha z\, e^{j[\omega t - (\beta_e - \beta_c)z]} \quad , \tag{5.19}$$

where

$$\alpha = \sqrt{C_+ C_+^*} \quad . \tag{5.20}$$

These equations are normalized so that the sum of the squares of the amplitudes of the two frequency components gives the total average power, and as a result the $\sqrt{3}$ appears in the third harmonic term.

A comparison of the above results with those given in (5.14) shows that the roles of the fast and slow cyclotron waves have been reversed. Otherwise, the discussion is the same. Bløtekjaer and Wessel-Berg[19] have discussed the present synchronization conditions for the case in which $\omega_q \neq 2\omega$ and point out that it can lead to an oscillator which requires an input. When we discuss the second harmonic power output in the next two sections, it will be seen that the present interaction

scheme can lead to more second harmonic power output than fundamental power input and that an instability will give rise to oscillations in a very unusual fashion.

C. POWER CONVERSION EFFICIENCY

We now use the results of the last section to study the efficiency characteristics of the cyclotron-wave frequency doublers. The device under consideration here consists of an input coupler that excites either or both of the cyclotron waves on a beam and is followed by a quadrupole circuit. The quadrupole has a field component that is synchronous with either the fast or the slow cyclotron wave, depending upon the type of interaction desired. The quadrupole structure is shorted at each end to make it resonant at exactly twice the input signal frequency. The beam delivers energy to the quadrupole, if it is loaded properly, and second harmonic power is available from the cavity.

The second harmonic power which has been given up by the beam to the cavity can be calculated by determining the net power decrease on the beam as a result of the interaction. This power is obtained by calculating the power carried by each frequency component in (5.14) or (5.19) and subtracting the cyclotron wave input power.

1. The Fast Cyclotron-Wave Doubler

The first synchronism condition of interest is the one in which the quadrupole has a traveling-wave field component that is synchronous with the fast cyclotron wave. In this case the power given up to the assumed second harmonic field is calculated from (5.14). It is found that

$$P_q = -2\left[\left(|a_1(0)|^2 + |a_2(0)|^2\right)\sinh^2 \alpha\ell + \sinh \alpha\ell \cosh \alpha\ell \, \mathrm{Re}\left\{a_2(0)\, a_2(0) e^{-j\phi_-}\right\}\right] , \qquad (5.21)$$

where

$$C_- = |C_-|\, e^{j\phi_-} ,$$

and ℓ is the length of the quadrupole. This may be written in terms of the entrance phase θ_0 of the fast wave by noting that

$$\mathrm{Re}\left\{|a_2(0)|\, e^{j\theta_0}\, |a_2(0)|\, e^{j\theta_0} e^{-j\phi_-}\right\} = a_2(0)\, a_2^*(0) \cos(2\theta_0 - \phi_-) \quad . (5.22)$$

The question as to the validity of the small signal power conservation statement used in obtaining (5.21) can be raised, particularly in view of the fact that several frequencies are involved. However, we observe that (5.21) is the relation obtained by applying the Manley-Rowe equations,[30] and in addition the same result is obtained below by another approach.

Since the quadrupole field which has been assumed arises from the excitation of the circuit by the input cyclotron wave, there will be a relation between the cyclotron wave phase θ_0 and the quadrupole phase ϕ_- which is determined by the nature of the load presented by the quadrupole. In order to see this more clearly, and to verify (5.21), we compute the complex power given up to the quadrupole circuit by the beam. This may be done by evaluating the rf part of the integral

$$P_c = -\frac{1}{2}\iiint \vec{E}(x,y,z).\vec{J}^*(x,y,z)\,dx\,dy\,dz \quad , \qquad (5.23)$$

where $\vec{E}$ is the field due to the quadrupole and $\vec{J}$ is the current density. Since the beam is assumed to be filamentary, the current can be represented by a delta function in the transverse plane so that

$$P_c = -\frac{1}{2}\int_0^{\ell} \vec{E}(x,y,z).\vec{I}^*(x,y,z)\,dz \quad , \qquad (5.24)$$

where

$$\vec{I} = \rho_0 \vec{v} \quad . \qquad (5.25)$$

In the current expression ρ_0 is the charge per unit length and $\vec{v}(x,y,z)$ is the total velocity of the beam. In the previous section it was observed that only the positively polarized portion of the field represented by C_-

interacted strongly with the beam. After noting that, we obtain the important contribution by considering Eqs. (5.1),(5.5) and (2.20). In doing this it is important to remember that x and y. in (5.1) are real quantities, while in (2.20) they are complex. Finally we obtain

$$E_x = - j \frac{u_0}{(e/m)k} C_- (A_1 - A_2^*) e^{j(\omega_q t - k_q z)}$$

$$E_y = - \frac{u_0}{(e/m)k} C_- (A_1 - A_2^*) e^{j(\omega_q t - k_q z)}$$

$$E_z = - \frac{u_0}{(e/m)k} C_- \frac{k_q}{2k\omega_c} (A_1 - A_2^*)^2 e^{j(\omega_q t - k_q z)} \quad . \qquad (5.26)$$

Also, from (2.4) and (2.13) we obtain the components of the beam current which contribute to the second order power expression:

$$i_z = \rho_0 v_x = - j \frac{\rho_0}{k} (A_1 + A_2)$$

$$i_y = \rho_0 v_y = \frac{\rho_0}{k} (A_1 - A_2)$$

$$i_z = i_0 = u_0 \rho_0 \quad . \qquad (5.27)$$

The complex power delivered to the quadrupole and its load is finally found by combining (5.24), (5.26) and (5.27), noting that $\omega_q = 2\omega$, to obtain

$$P_c = - 2a_2(0)\, a_2^*(0) \left[\sinh^2 \alpha\ell + \cos(2\theta_0 - \phi_-) \sinh \alpha\ell \cosh \alpha\ell\right]$$

$$- 2a_1(0)\, a_2^*(0) \sinh^2 \alpha\ell + j2(\alpha\ell)\, a_2(0)\, a_2^*(0) \sin(2\theta_0 - \phi_-) \quad . \qquad (5.28)$$

The real part of the complex power is exactly the expression (5.21) as it should be. We see from (5.28) that when the loaded quadrupole is excited at resonance, that is, when the reactive power is zero, the phase is automatically adjusted so that

$$(2\theta_0 - \phi_-) = 0 \text{ or } \pi \ . \tag{5.29}$$

The interpretation of this quantity is simple when we note that the phase of either the quadrupole field or the beam wave represents a reference time when the field goes through its maximum value. That is, we could write the time dependencies as

$$e^{j(\omega t + \theta_0)} = e^{j\omega(t - t_1)}$$

and

$$e^{j(2\omega t + \phi)} = e^{j2\omega(t - t_2)} \ .$$

Then we have

$$(2\theta_0 - \phi) = 2\omega(t_1 - t_2) \equiv 2\theta \ , \tag{5.30}$$

and we see that θ represents the phase, referred to the fundamental frequency, of the input fast cyclotron wave with respect to the quadrupole field.

Finally then, substituting (5.22) into (5.21) and using a trigonometric identity, the real power delivered to the quadrupole can be written as

$$\frac{P_q}{|a_2(0)|^2} = -2 \sinh \alpha\ell \left[1 + \frac{|a_1(0)|^2}{|a_2(0)|^2} \sinh \alpha\ell + (1 - 2 \sin^2 \theta) \cosh \alpha\ell \right] \ . \tag{5.31}$$

We see that the last term here can make P_q positive and therefore can give rise to power output from the quadrupole. It is evident that $\sin\theta = \pm 1$ represents maximum second harmonic power, while $\sin\theta = 0$ represents power delivered to the beam by the quadrupole. Two special cases of (5.31) are of interest.

First, consider the case in which we have a fast cyclotron wave entering the quadrupole. This is the case which has been studied before for $\omega = \omega_c$ as indicated at the beginning of this chapter. The power conversion efficiency, η_e, is now

$$\eta_e = \frac{P_q}{|a_2(0)|^2} = 1 - \cos^2\theta e^{2\alpha\ell} - e^{-2\alpha\ell}\sin^2\theta \quad . \tag{5.32}$$

We see that the efficiency depends upon θ (as shown above, θ is determined by the phase of the quadrupole load) and $\alpha\ell$. It is interesting to look at the conversion efficiency under several conditions.

First let us look at the maximum efficiency attainable as a function of θ. Differentiating (5.32) with respect to $\alpha\ell$ and equating the result to zero determines the optimum $\alpha\ell$ for that θ. For a given length this is the same as optimizing the quadrupole load. We obtain as the optimum condition

$$e^{4\alpha\ell} = \tan^2\theta \quad , \tag{5.33}$$

which, when substituted back into (5.32), gives

$$\eta_{e\,max} = 1 - |\sin 2\theta| \quad . \tag{5.34}$$

This is plotted in Fig. 5.2 along with a similar curve calculated, for a special case, from a ballistic analysis by Lindsay and Caunter.[22] Their calculations were for the case when the signal frequency is equal to the cyclotron frequency while the results here are for arbitrary ω. The deviation between the curves is due to the small signal assumptions inherent in the wave analysis. Complete agreement is obtained if small signal approximations are used in the ballistic analysis.

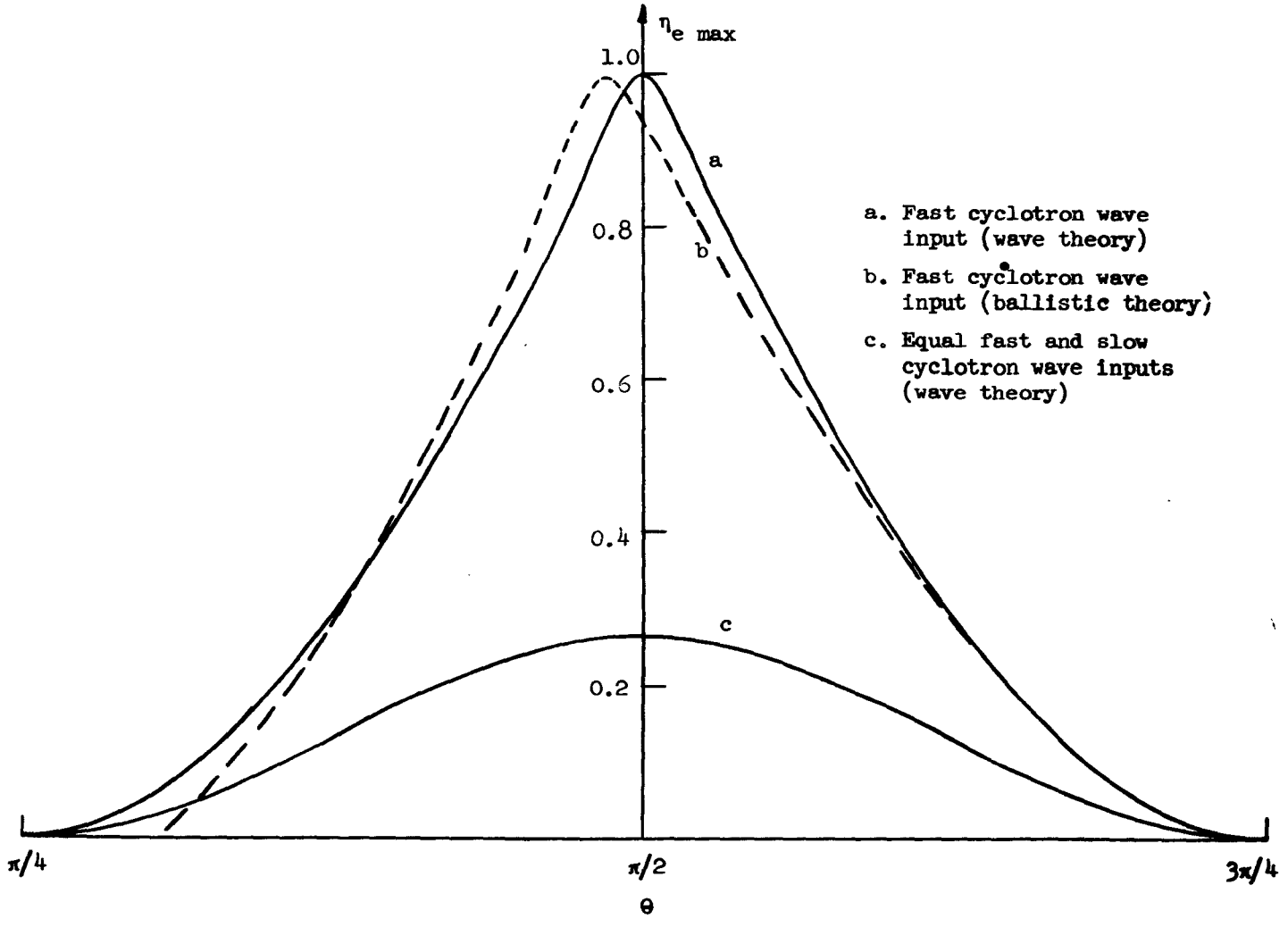

FIG. 5.2--Maximum electronic efficiency of cyclotron-wave doubler as a function of the relative input phase of the fast wave.

The optimum conditions are obviously $\theta = \pi/2$ which, we have shown, means that the quadrupole presents a purely resistive load to the beam. If the cyclotron wave excitation is not exactly at the resonance of the loaded quadrupole, then θ is different from $\pi/2$, as indicated by (5.28), with a resulting degradation of the doubler performance as shown in Fig. 5.2. Using the optimum value of θ in (5.32) yields

$$\eta_e = 1 - e^{-2\alpha\ell} \quad . \tag{5.35}$$

This is plotted in Fig. 5.3 along with the result for another case of interest. Physically, this result means that, due to the assumed quadrupole fields, the energy carried by the fast cyclotron wave is absorbed by the quadrupole exponentially. The exponential variation arises from the linear dependence of the electric field on the transverse displacement. The maximum amount of second harmonic power which could be obtained is just equal to the input fundamental power, and in that case the beam would emerge from the quadrupole with no transverse modulation. This requires an infinitely long quadrupole.

A second case of (5.21) that is of significance arises when both the fast and slow cyclotron waves have equal amplitudes at the quadrupole entrance. It was shown in Chapter IV that it is possible to excite the two cyclotron waves equally, even though they have vastly different phase velocities. Since the waves carry power of opposite sign it is possible to excite large wave amplitudes with a small expenditure of power in the coupler. This could lead to a doubler with high conversion efficiency. In this case we have in Eq. (5.21) $|a_2(0)|^2 = |a_1(0)|^2$, giving, on simplification,

$$\eta_e = 1 - e^{2\alpha\ell} + 2 \sin^2 \theta \sinh 2\alpha\ell - 2 \sinh^2 \alpha\ell \quad . \tag{5.36}$$

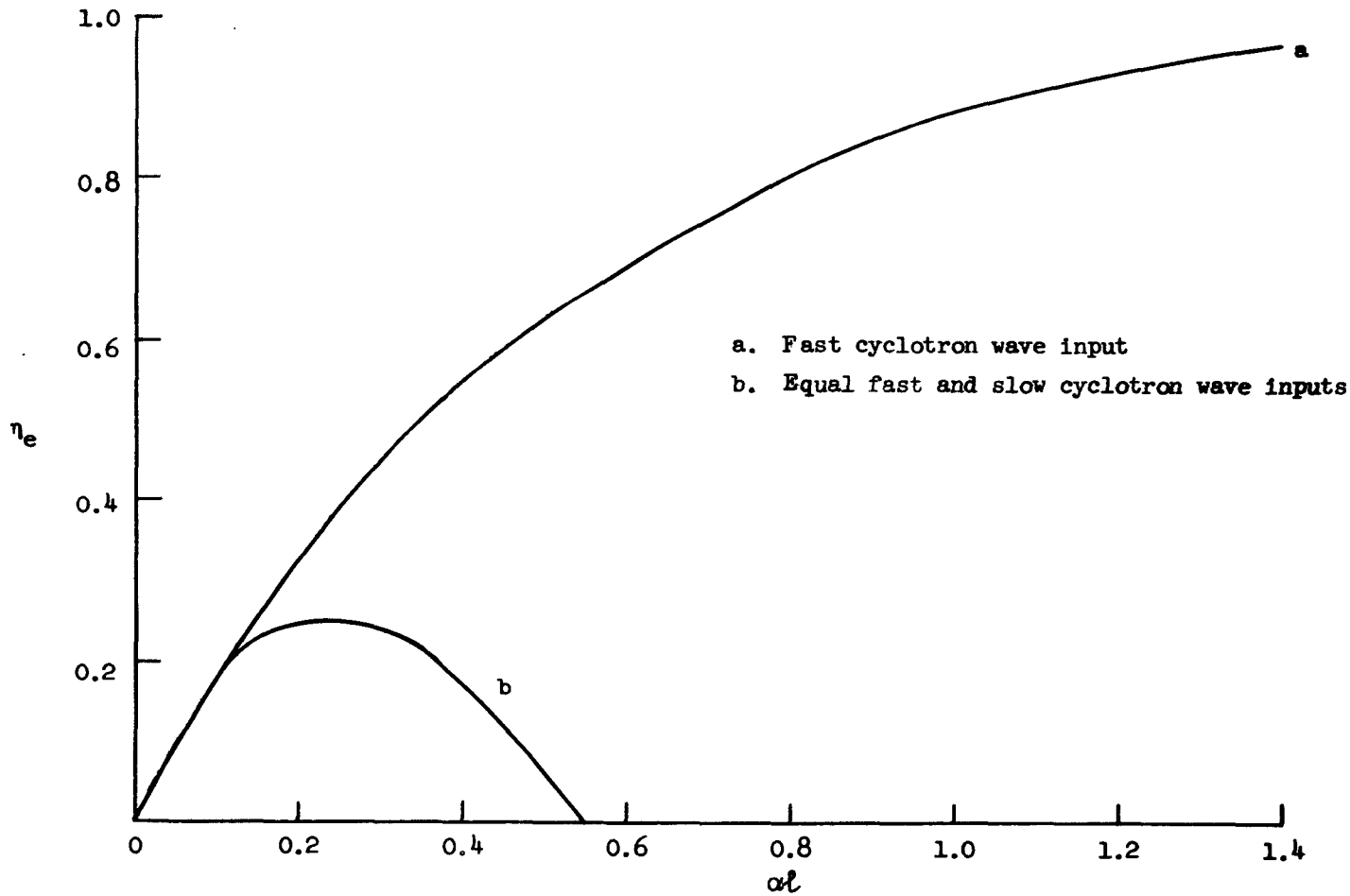

FIG. 5.3--Conversion efficiency for a quadrupole that is synchronous with the fast cyclotron wave.

We again look for the maximum efficiency for values of θ by varying $\alpha\ell$. The requirement obtained is

$$e^{2\alpha\ell} = \sqrt{\frac{2 - \cos 2\theta}{2 + \cos 2\theta}} \quad . \tag{5.37}$$

By substituting (5.37) into (5.36) and making the numerical computation, we find the dependence of the maximum efficiency on θ is that shown in Fig. 5.2. A plot of (5.31) for the optimum condition $\theta = \pi/2$ is shown in Fig. 5.3, along with the curve for the previous case. In the present case, the maximum conversion efficiency of 27% is obtained for a finite value of $\alpha\ell$.

These results can be understood from a physical viewpoint by referring to Eqs. (5.19). The fast cyclotron wave at the input delivers its power to the circuit just as in the previous example, while the slow cyclotron wave gives rise to two growing waves. One of these waves is at the input frequency and carries negative energy while the other is a third harmonic, positive energy cyclotron wave. It is this growing third harmonic wave which absorbs energy back from the quadrupole and results in the conversion efficiency reaching a maximum at 27% and then decreasing with larger values of the parameter $\alpha\ell$.

While it might be expected that just a slow cyclotron wave excitation at the quadrupole input would lead to a growth phenomenon, inspection of (5.21) shows that the beam absorbs energy from the assumed fields in the quadrupole, again as a result of the third harmonic, fast cyclotron wave. As a result, this case is of no interest when the quadrupole is synchronous with the fast cyclotron wave.

2. <u>The Slow Cyclotron-Wave Doubler</u>

The second synchronism condition of importance is the one in which the quadrupole cavity has a field component that is synchronous with the slow cyclotron wave. In this case the power given up to the assumed second harmonic field is calculated from (5.19). It is found that

$$P_q = 2\left[\left(|a_1(0)|^2 + |a_2(0)|^2\right)\sinh^2 \alpha\ell + \sinh \alpha\ell \cosh \alpha\ell \; \mathrm{Re}\left\{a_1(0)\, a_1(0) e^{-j\phi_+}\right\}\right] \quad . \tag{5.38}$$

If $a_1(0)$ and $a_2(0)$ are interchanged, this result is the negative of the power expression obtained in the case of synchronism between the fast cyclotron wave and the quadrupole field. Equation (5.38) shows that the beam delivers power to the quadrupole for any beam entrance condition. The discussion regarding the relative phase between the input slow cyclotron wave and the quadrupole is the same, except that in the present case there is no maximum efficiency for a given phase relationship. It is apparent that the optimum relationship is given by

$$\cos (2\theta_0 - \phi_\pm) = +1 \quad . \tag{5.39}$$

From (5.17), which is correct here also, if $a_1(0)$ and $a_2(0)$ are interchanged and the sign of P_c is changed, we see that this corresponds to a purely resistive quadrupole load. In this case the second harmonic power delivered to the quadrupole is given by

$$P_q = |a_1(0)|^2 (e^{2\alpha\ell} - 1) + |a_2(0)|^2 (\cosh 2\alpha\ell - 1) \quad . \tag{5.40}$$

This result is plotted in Fig. 5.4 for the cases in which only a fast wave input is supplied and in which both input waves have equal amplitude.

The characteristics of the slow cyclotron-wave doublers are distinctly different from those of the preceding case, as would be expected. Since a negative energy wave is synchronous with the circuit, the beam gives up some of its dc energy to the cavity in the form of the second harmonic power dissipated in the quadrupole. Thus this device can be viewed as a kind of driven oscillator that converts dc energy to the second harmonic frequency under the influence of the fundamental modulating signal on the beam. This interaction has been studied by others[19] for the case of unrelated beam wave and quadrupole frequencies, and it was noted that power gain was still possible in this case.

D. EFFECT OF THE LOAD IMPEDANCE

The results obtained in the previous sections show the nature of the frequency doubling interactions employing a quadrupole circuit interacting with the cyclotron waves, but they do not give a satisfactory final

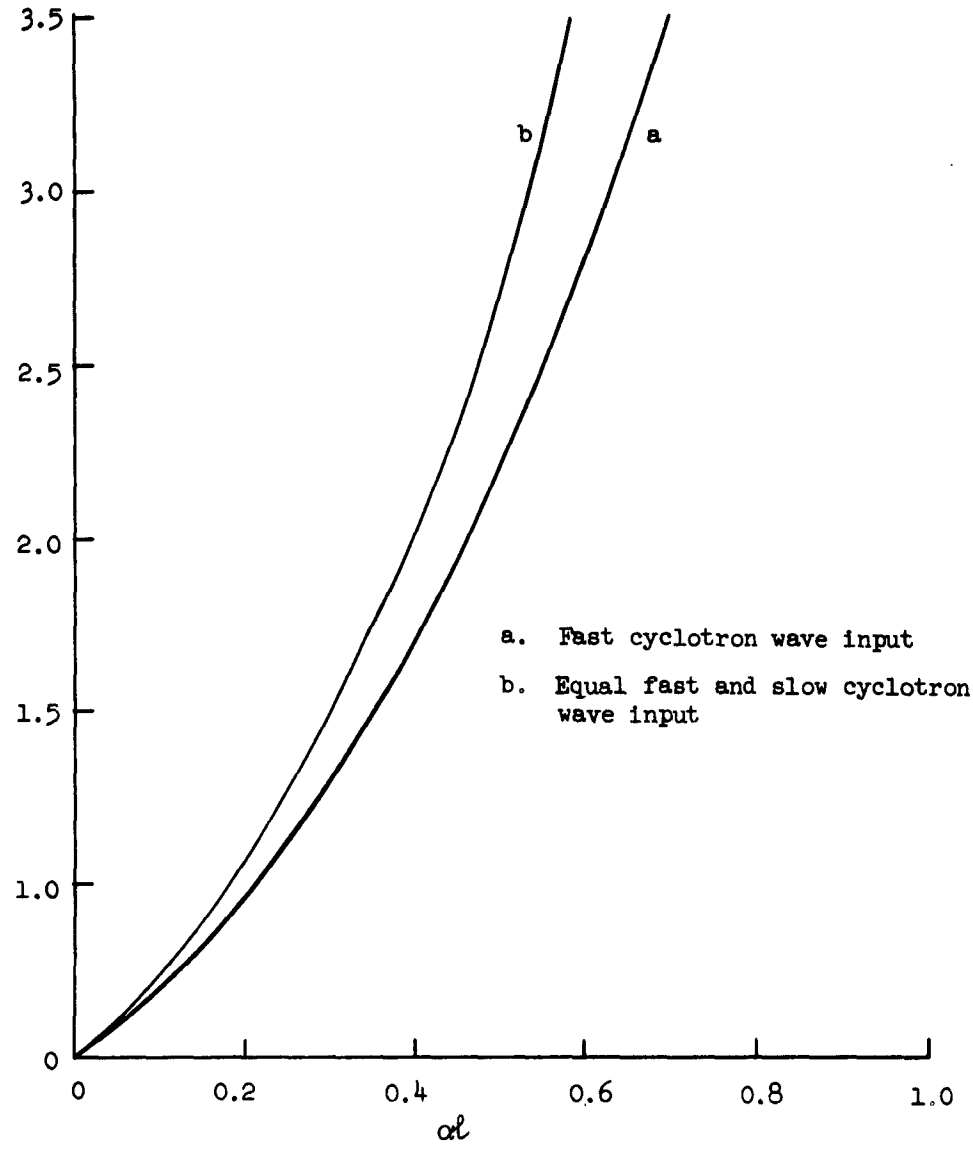

FIG. 5.4--Conversion efficiency for a quadrupole that is synchronous with the slow cyclotron wave.

formulation of the problem since the effect of the quadrupole cavity load impedance is not given explicitly in those equations.

In order to do this we require a relationship between the growth parameter α and the power being delivered to the quadrupole cavity and the external load. We define a loaded quadrupole resistance by

$$R_q = \frac{V_q^2}{2P_{2\omega}} , \tag{5.41}$$

where V_q is the potential of the quadrupole circuit, corresponding to the field that is synchronous with the beam wave, and $P_{2\omega}$ is the total second harmonic power given up to the loaded circuit by the beam. The relationship between the coefficients C_+ and C_- and the quadrupole voltage V_q can be calculated by combining (5.5) with (5.1) and integrating the electric field from the axis of the structure out to the equipotential surface that defines the quadrupole circuit. In this way it is found that, for either a linearly or a circularly polarized quadrupole, the potential is related to the polarization coefficients by

$$\sqrt{|C_+|^2 + |C_-|^2} = \sqrt{2}\,\frac{(e/m)V_q}{\omega_c u_0 a^2} . \tag{5.42}$$

Finally, using (5.41), we obtain the relation

$$\sqrt{|C_+|^2 + |C_-|^2} = \frac{2e/m}{\omega_c u_0 a^2}\sqrt{R_q P_{2\omega}} . \tag{5.43}$$

Now what is really desired, in order to make the final results exhibit the information in the most useful form, is to express (5.43) in terms of the unloaded quadrupole cavity resistance and the power which is dissipated in the external load. The load resistance is given in terms

of the unloaded value by

$$R_q = R_{q0} \frac{1}{1 + \frac{Q_0}{Q_{ext}}} , \tag{5.44}$$

while the power delivered to the external load is related to the power given up by the beam by

$$P_{2\omega L} = P_{2\omega} \frac{1}{1 + \frac{Q_{ext}}{Q_0}} . \tag{5.45}$$

Finally, by substituting (5.44) and (5.45) into (5.43), the desired results are obtained in terms of the Q of the cavity loaded by the external resistance and the power dissipated in the external load

$$\sqrt{|C_+|^2 + |C_-|^2} = \frac{2e/m}{\omega_c u_0 a^2} \sqrt{R_{q0} P_{2\omega L} \frac{Q_{ext}}{Q_0}} . \tag{5.46}$$

Thus, Eq. (5.46) can be substituted into (5.24), (5.25) and (5.40) to obtain the conversion efficiency of the cyclotron wave frequency doublers in terms of known parameters and the power on the fast cyclotron wave at the quadrupole entrance. The transcendental equations obtained in this way can be solved numerically to obtain the desired results. In plotting the efficiency and the second harmonic power output as a function of the power input, it is very convenient to form universal curves by normalizing the power so that the normalized power p is related to the actual power P by

$$p = \left[\frac{8(e/m)^2 \ell^2}{\omega_c^2 u_0^2} \frac{1}{a^4} \right] R_{q0} P . \tag{5.47}$$

Because the linearly polarized quadrupole is the most likely structure to be used, all of the calculations carried out below are for this case. However, the curves have been normalized so that, if a circularly polarized quadrupole is of interest, it is only necessary to replace R_{qo} by $2R_{qo}$ in (5.47) to make the efficiency curves valid for that situation.

1. Fast Cyclotron-Wave Doublers

The normalized second harmonic power that is delivered to the load can be expressed in terms of the power input on the fast cyclotron waves by means of (5.24), (5.25), (5.32) and (5.33). For the case in which only a fast cyclotron wave exists at the quadrupole input it is found that

$$\frac{P_{2\omega L}}{P_{\omega}} = \frac{1}{1 + \frac{Q_{ext}}{Q_0}} \left[1 - \exp\left(- \sqrt{\frac{Q_{ext}}{Q_0} P_{2\omega L}} \right) \right] . \qquad (5.48)$$

If both cyclotron waves have equal amplitude at the input the result is

$$\frac{P_{2\omega L}}{P_{\omega}} = \frac{1}{1 + \frac{Q_{ext}}{Q_0}} \left[\sinh \sqrt{\frac{Q_{ext}}{Q_0} P_{2\omega L}} \, (- \cos 2\phi) - 4 \sinh^2 \frac{1}{2} \sqrt{\frac{Q_{ext}}{Q_0} P_{2\omega L}} \right] . \qquad (5.49)$$

In these equations $P_{2\omega L}$ is the normalized second harmonic power delivered to the load and P_{ω} is the fundamental power input on the fast cyclotron-wave.

The curve showing the conversion efficiency and output power as a function of the input cyclotron wave power, when only the fast cyclotron wave is present, is curve a in Fig. 5.5. At low power levels the output power is proportional to the square of the input power as can be seen by considering (5.48) which approaches

$$P_{2\omega L} = \frac{1}{\left(1 + \frac{Q_0}{Q_{ext}} \right) \left(1 + \frac{Q_{ext}}{Q_0} \right)} P_{\omega}^2 \qquad (5.50)$$

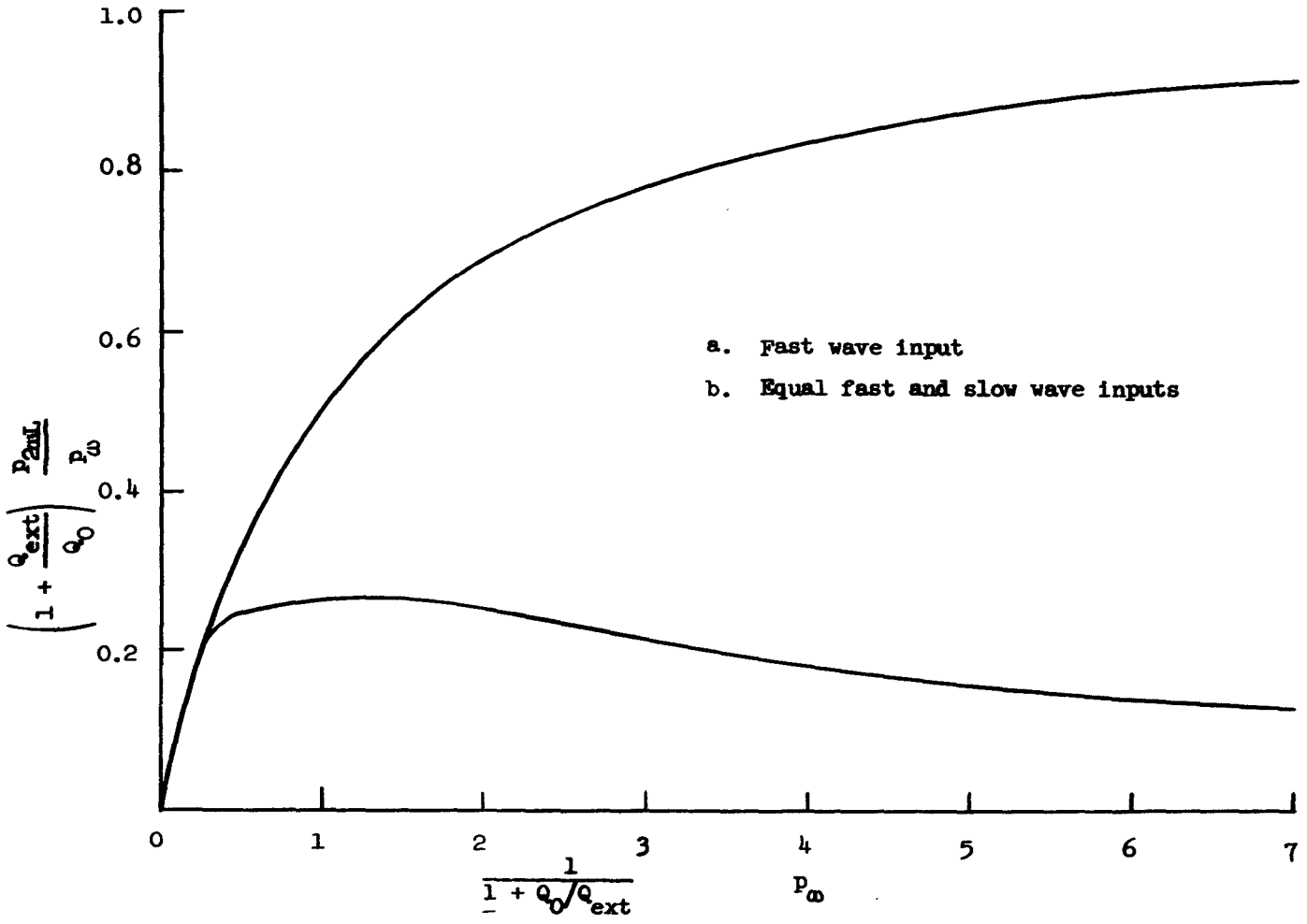

FIG. 5.5--Conversion efficiency of the fast cyclotron-wave doubler.

for output power levels such that .

$$P_{2\omega 1} \ll \frac{Q_0}{Q_{ext}} \quad .$$

The output is therefore maximum when Q_{ext}/Q_0 is unity. For large output power such that

$$P_{2\omega 1} \gg \frac{Q_0}{Q_{ext}} \quad ,$$

the conversion efficiency approaches a constant so that the output power becomes a linear function of the input power

$$P_{2\omega 1} = \frac{1}{1 + \frac{Q_{ext}}{Q_0}} P_{\omega} \quad . \tag{5.51}$$

From these results it is apparent that the optimum value of Q_{ext}/Q_0 is dependent upon the input power. For low level operation it is desirable to make Q_{ext}/Q_0 unity, while for high level operation Q_{ext}/Q_0 should be large. Generally, it is safe to assume that high conversion efficiencies are desirable and the usual operation of the frequency doubler would be in the region for which (5.51) is valid.

The characteristics of the frequency doubler when the input to the quadrupole consists of fast and slow cyclotron waves of equal amplitude is somewhat more complex than the previous case, as is evidenced by Eq. (5.49). The conversion efficiency as a function of the input power on the fast cyclotron wave is curve b in Fig. 5.5. It was pointed out in the previous section that the efficiency of a doubler operating in this way reaches a maximum and then decreases due to a growing third harmonic wave on the electron beam. This is reflected in Fig. 5.5 where

the maximum efficiency which can be attained is

$$\eta_{max} = \frac{0.27}{1 + \frac{Q_{ext}}{Q_0}} \quad . \tag{5.52}$$

The output power at maximum efficiency is

$$P_{2\omega L} = 0.25 \frac{Q_0}{Q_{ext}} \quad , \tag{5.53}$$

and the input is

$$P_{\omega} = 0.93 \left(1 + \frac{Q_0}{Q_{ext}}\right) \quad . \tag{5.54}$$

The efficiency decreases slowly with increased input power and the output power saturates at a value given by

$$P_{2\omega L_{sat}} = 1.1 \frac{Q_0}{Q_{ext}} \quad . \tag{5.55}$$

On the other hand, at low power levels the output is given by

$$P_{2\omega L} = \frac{4}{\left(1 + \frac{Q_0}{Q_{ext}}\right)\left(1 + \frac{Q_{ext}}{Q_0}\right)} P_{\omega}^2 \quad , \tag{5.56}$$

which is four times the value for the case in which there is only a fast wave entering the quadrupole. As before, the optimum value of Q_{ext}/Q_0 is dependent upon the input power, but in general the operation will be

near the maximum conversion efficiency where it is desirable to load the cavity heavily.

Although the conversion efficiency in the quadrupole is found to be small in the equal fast and slow cyclotron wave doubler, the possibility of gain in the twisted input coupler described in Chapter IV makes this device a significant competitor of the more usual fast cyclotron wave doubler. As far as overall efficiency is concerned, it would even be possible to exceed one hundred per cent conversion efficiency; that is, the second harmonic output can exceed the fundamental input.

The amount of second harmonic power that can be obtained from either of the frequency doublers described above is determined by the beam interception conditions in the quadrupole. The maximum input power for the first doubling scheme described above is that power which causes interception at the quadrupole entrance since the wave amplitude decays exponentially inside of the quadrupole. The same interception condition can usually be used in the case in which there are equal amplitude fast and slow waves at the input, since it is found that the beam expands a negligible amount when the operation is adjusted to the peak of the efficiency curve shown in Fig. 5.5.

2. Slow Cyclotron-Wave Doublers

In this case, the normalized power expressions are obtained by substituting (5.47), (5.46), and (5.45) into (5.38) or (5.40). For the optimum case with only a slow wave input we obtain

$$\frac{P_{2\omega L}}{P_{\omega}} = \frac{1}{1 + \frac{Q_{ext}}{Q_0}} \left[\left(\exp \sqrt{\frac{Q_{ext}}{Q_0} P_{2\omega L}} - 1 \right) \right], \qquad (5.57)$$

while, if both the fast and slow cyclotron waves have equal input magnitudes and the correct phase relationship so that θ in (5.38) is zero, the

efficiency is

$$\frac{P_{2\omega L}}{P_{\omega}} = \frac{1}{1 + \frac{Q_{ext}}{Q_0}} \left(\exp \sqrt{\frac{Q_{ext}}{Q_0} P_{2\omega L}} - 1 + \cosh \sqrt{\frac{Q_{ext}}{Q_0} P_{2\omega L}} - 1 \right) . \quad (5.58)$$

As before, $P_{2\omega L}$ is the second harmonic power delivered to the load and P_{ω} is the fundamental power input on the fast cyclotron wave.

The curves showing the conversion efficiency as a function of the input power are given in Fig. 5.6. It can be seen that the efficiency characteristics of the slow cyclotron-wave doublers are distinctly different from those of the fast cyclotron-wave doublers. The conversion efficiency of the quadrupole doubler that is synchronous with the slow cyclotron wave can be greater than one hundred per cent for either excitation shown in Fig. 5.6. This result simply means that some of the dc beam power is being converted to second harmonic power under the influence of the fundamental modulating signal.

We observe that the small-signal theory sets a limit on the fundamental cyclotron wave input power that yields a stable frequency doubling interaction, and if the power is increased beyond this point the quadrupole efficiency will increase until nonlinearities cause saturation. This behavior is very much like that which occurs in a monotron oscillator, except that in the present case there is no rf field at the equilibrium position of the filamentary beam. Consequently, the start oscillation condition is related to the fundamental power input, which contains both the beam current and the displacement of the beam from the axis. This phenomenon sets a limit to the conversion efficiency that can be obtained with a given value of Q_{ext}/Q_0 .

The external loading required to achieve the maximum conversion efficiency is dependent upon the operating conditions. In principle, the maximum efficiency of 390 per cent is obtained when the quadrupole is loaded heavily so that Q_{ext}/Q_0 approaches zero. However, the practical matter of beam interception modifies this picture. Figure 5.6 shows that the input power required to obtain the maximum efficiency increases with

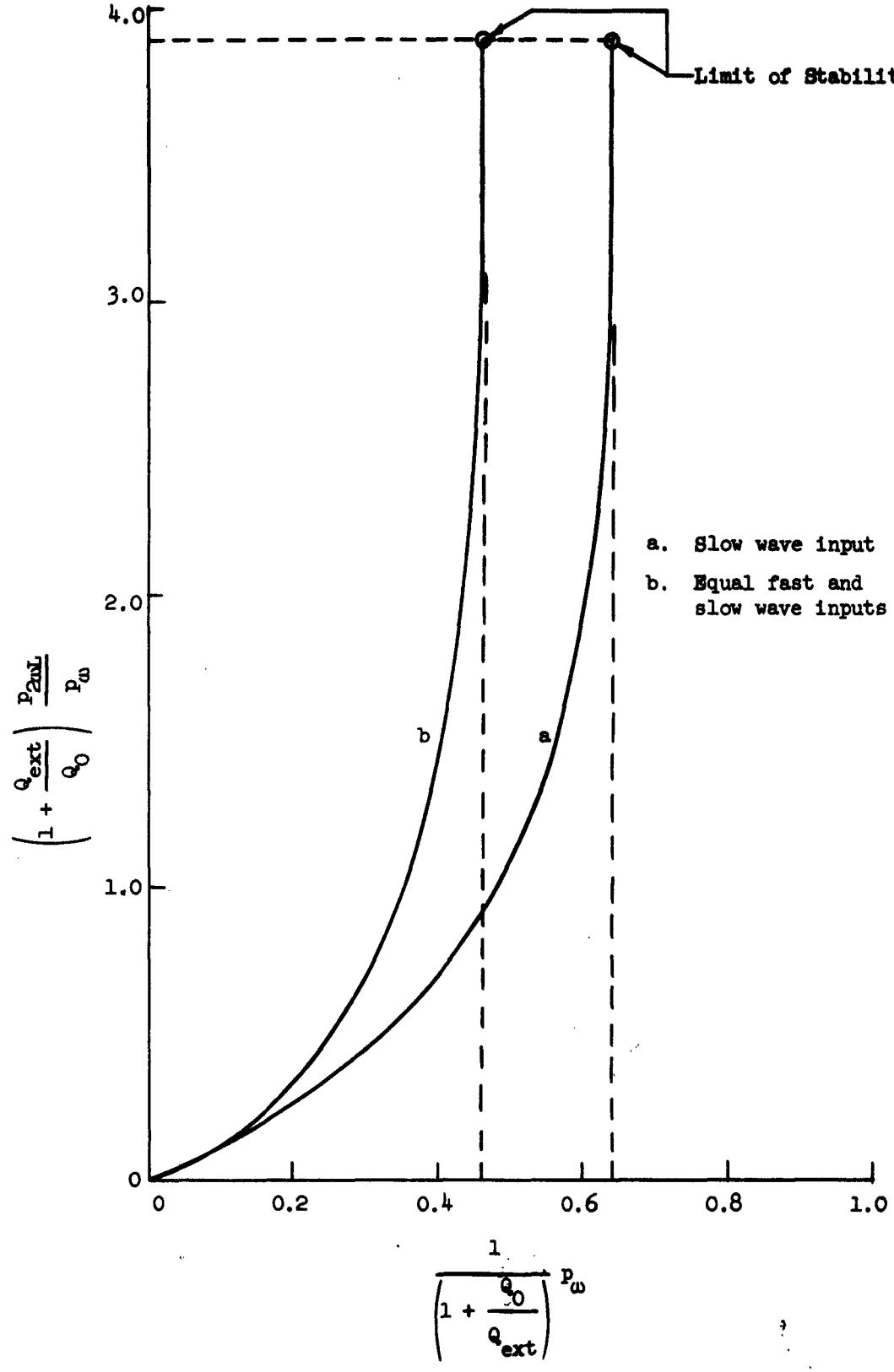

FIG. 5.6--Conversion efficiency of the slow cyclotron-wave frequency doubler.

decreasing Q_{ext}/Q_0 so that it would require an infinite input signal in order to obtain the peak efficiency. Thus, we see that the maximum efficiency will be less than 390 per cent, and that this maximum will be determined by the interception conditions in the quadrupole.

It is of interest to investigate the conditions that must be met in order to obtain the maximum efficiency from the doublers described above. In order to do this the beam excursion in the quadrupole must be calculated by substituting (5.19) into (2.20). The expression for the maximum amplitude obtained in this way can be written in terms of the normalized variables introduced in this section, and it is found that the maximum excursion is related to the second harmonic power by a simple expression. In the case of a slow wave input only we obtain

$$\frac{Q_{ext}}{Q_0} P_{2\omega L} = \left[\log \left(\frac{r_m}{r(0)} \right)^2 \right]^2 , \qquad (5.59)$$

while for equal fast and slow wave inputs

$$\frac{Q_{ext}}{Q_0} P_{2\omega L} = \left[\log \left(\frac{r_m}{r(0)} \right)^2 \left[\frac{1}{2} + \frac{1}{2} \sqrt{1 + 2 \left(\frac{r(0)}{r_m} \right)^2} \right]^2 \right]^2 , \qquad (5.60)$$

where $r(0)$ is the initial maximum excursion and r_m is the maximum excursion within the quadrupole at a load power level $P_{2\omega L}$.

These results can be combined with the efficiency characteristics shown in Fig. 5.6 to obtain the optimum operating conditions for the slow-wave doublers. The value of $\left(Q_{ext}/Q_0\right) P_{2\omega L}$ at the limit points in the figure is 2.55 for a slow wave input and 1.81 for equal inputs of the two waves. By using these values in (3.59) and (3.60), we obtain the maximum excursion in terms of the initial maximum excursion

$$r_m = 2.22\, r(0)$$

and

$$r_m = 1.70\, r(0) \quad ,$$

respectively. Then the greatest efficiency is obtained when r_m is equal to the maximum excursion allowed without beam interception, that is, the quadrupole radius minus the beam radius. Consequently, the maximum efficiency will be obtained when the input power level is adjusted so that the initial maximum excursion is related to the beam excursion that causes interception by the appropriate expression above, and then the coupling to the external circuit is adjusted so that the maximum output without interception is obtained. The actual efficiency obtained in this way is dependent upon the quadrupole parameters, but we may say that, by adjusting the length or R_{q0} of the quadrupole, large conversion efficiencies can be obtained.

E. SUMMARY OF CYCLOTRON-WAVE DOUBLERS

The analysis presented in this chapter has shown that the two basic types of cyclotron-wave frequency doublers involve a quadrupole circuit that is synchronous with either the fast or the slow cyclotron wave. The first case results in a maximum conversion efficiency of one hundred per cent, while the slow wave interactions are characterized by an efficiency that may exceed one hundred per cent. Consequently, the latter case is of considerable interest as far as high efficiency frequency doubling is concerned. However, these devices have the disadvantage of requiring circuits with much smaller phase velocities than does the fast cyclotron-wave doubler. This is detrimental because the interaction impedances of the lower phase velocity circuits are generally smaller, and because the thin beam assumption is not as good an approximation as the wavelength of the circuit wave decreases. Even so, the slow wave doublers should, with proper circuit and beam design, result in much higher efficiencies than are obtainable by means of passive interactions.

The quadrupole interactions with the synchronous waves that result in frequency doubling are considered in the next chapter. In general,

it is found that the synchronous-wave doublers are analogous to the cyclotron-wave doublers, and a more complete summary of transverse-wave frequency doublers is given at the end of that chapter. In particular we can say that the active frequency doubling mechanisms employing the synchronous waves look more attractive than those involving the cyclotron waves because of the different circuit velocity requirement.

CHAPTER VI

SYNCHRONOUS WAVE FREQUENCY DOUBLERS

The general approach to the analysis of transverse wave interactions which is offered by the Blǿtekjaer and Wessel-Berg coupled-mode theory outlined in Chapter V.A leads naturally to the discussion of synchronous wave frequency doubling interactions as well as of the cyclotron wave doubling schemes presented in Chapter V. This is a new class of frequency doubling interactions which can be expected to lead to devices that are different from those employing the cyclotron wave. This difference is a result of the identical phase velocities of the two synchronous waves, and the new role played by the negative energy beam wave. The purpose of this chapter is to develop the theory of this new class of devices and to compare their ultimate capabilities with those of the cyclotron wave doublers.

The synchronous wave frequency doubler consists of an input coupler which excites a combination of the two synchronous waves on the beam and an output quadrupole cavity in which the frequency conversion actually takes place. The coupler theory has been presented earlier, and so we are primarily concerned with the quadrupole interactions here. The analysis properly begins with Section A of Chapter V, where the basic coupled mode description of quadrupole interactions is described. The discussion will begin with the solution of Eqs. (5.6) for the synchronism conditions which lead to strong interaction between the quadrupole cavity and the synchronous waves on the beam. The assumptions involved in this chapter are the same as those described in the introductory comments and in Section A of Chapter V. Basically, these are the assumptions that the beam interacts with only one traveling-wave component of the field in the resonant cavity, and the filimentary beam assumptions. The statements which were made in Chapter V regarding the validity of these approximations are generally true in the present case also.

A. SOLUTION OF THE COUPLED MODE EQUATIONS

It has been noted that one of the synchronism conditions which lead to perturbed solutions of (5.6) is

$$\frac{\omega_q}{u_0} - k_q = 0 \quad . \tag{6.1}$$

That is, there will be a strong interaction between the synchronous waves on the beam and the quadrupole cavity when the phase velocity of a traveling-wave component of the field is equal to the beam velocity. The solutions of (5.6) which were obtained in the reference are, as in the previous case, inadequate for the discussion of frequency doublers because it was assumed that there was no correlation between the synchronous wave signal input and the quadrupole field. We therefore begin the discussion with an evaluation of the perturbation in the propagation constant perturbation γ , and the wave amplitudes for the synchronism condition (6.1).

It is reasonable to neglect the cyclotron waves in the discussion of (5.6) since there will be no cumulative interaction in a long quadrupole for the condition given in (6.1). Also, a first approximation will be to neglect all frequencies other than ω , $\omega_q + \omega$, and $\omega_q - \omega$ as was done for the cyclotron wave case. However, it will be found here that this assumption is valid only if the quadrupole is circularly polarized and that the solution for the case in which the quadrupole is linearly polarized must be obtained by a more rigorous approach which involves all frequency combinations. It will be found that, for the linearly polarized case, the three-frequency expressions are valid at low power levels, while for larger power output these solutions result in significant errors.

1. Three-Frequency Solution

On the basis of the above comments we obtain from (5.6) a set of six equations which relate the amplitudes of the synchronous waves at the frequencies represented by $n = 0 \ , \ \pm 1$. These equations are

homogeneous and the requirement that they have a nontrivial solution is that the system determinant vanish; that is,

$$\begin{vmatrix} -j\gamma & 0 & 0 & 0 & C_+^* & 0 \\ 0 & -j\gamma & 0 & C_- & 0 & C_+^* \\ 0 & 0 & -j\gamma & 0 & C_- & 0 \\ 0 & C_-^* & 0 & -j\gamma & 0 & 0 \\ C_+ & 0 & C_-^* & 0 & -j\gamma & 0 \\ 0 & C_+ & 0 & 0 & 0 & -j\gamma \end{vmatrix} = 0 \quad . \tag{6.2}$$

Evaluation of this determinant yields a sixth-order equation which can be expressed as the product of two cubic equations. The determinantal equation is then:

$$\left[\gamma^3 + \gamma \left[C_+ C_+^* + C_- C_-^*\right]\right]^2 = 0 \quad . \tag{6.3}$$

There are two unperturbed solutions

$$\gamma_1 = \gamma_2 = 0 \quad , \tag{6.4}$$

and four perturbed solutions

$$\gamma_3 = \gamma_4 = + j\sqrt{C_+ C_+^* + C_- C_-^*}$$

$$\gamma_5 = \gamma_6 = - j\sqrt{C_+ C_+^* + C_- C_-^*} \quad . \tag{6.5}$$

The substitution of (6.5) into the equations which gave (6.3) results in simple expressions for the perturbed wave amplitudes, at synchronism, and we shall restrict the discussion to that case since it reveals all

of the characteristic phenomena involved. The synchronous waves in the quadrupole are given by

$$A_3 = \left[a_3(0)\cosh \alpha z + \frac{C_+}{\alpha} a_3^*(0) \sinh \alpha z\right] e^{j(\omega t - \beta_e z)}$$

$$+ \sqrt{3}\,\frac{C_+}{\alpha} a_4(0) \sinh \alpha z\, e^{j3(\omega t - \beta_e z)} \qquad (6.6)$$

$$A_4 = \left[a_4(0)\cosh \alpha z + \frac{C_-}{\alpha} a_4^*(0) \sinh \alpha z\right] e^{j(\omega t - \beta_e z)}$$

$$+ \sqrt{3}\,\frac{C_-}{\alpha} a_3(0) \sinh \alpha z\, e^{j3(\omega t - \beta_e z)} , \qquad (6.7)$$

where α is now

$$\alpha = \sqrt{C_+ C_+^* + C_- C_-^*} \quad . \qquad (6.8)$$

These results are valid for arbitrary quadrupole polarization. In arriving at (6.6) and (6.7) it was assumed that $\omega_q = 2\omega$, which is the case in a frequency doubler. The $\sqrt{3}$ factor in the third harmonic term arises because the amplitudes are normalized so that their square gives the power carried by that wave.

Equations (6.6) and (6.7) indicate that, in general, the initial excitation of either synchronous wave results in a subsequent complex spatial variation of that wave amplitude and also a growing third harmonic synchronous of the opposite polarization. These results are very similar to (5.14) except that in the present case the form of the equation for each synchronous wave is the same, this being a manifestation of the identical phase velocities of the two waves. However, it must be pointed out that the validity of (6.6) and (6.7) is open to question in the case of a linearly polarized quadrupole because of the assumption that the finite set of equations employed in (6.3) is an accurate description of the system. It is observed that the diagonal elements of (6.3) are all

of the same order of magnitude, and that this would be true if we had employed the infinite determinant which represents all values of n. Thus, to first order in the quadrupole field amplitude, all values of n' must be retained. This was not the case in the cyclotron wave discussion given in the previous chapter. It is therefore necessary to carry out a more rigorous discussion of the solution of Eqs. (5.6) for the synchronism conditions stated in (6.1) when both C_+ and C_- are nonzero.

2. Exact Solution

The arguments stated at the beginning of this section for neglecting the cyclotron waves in the discussion of the synchronism conditions (6.1) are generally valid, and we neglect the cyclotron waves in the exact solution of (5.6). To simplify the discussion we assume (6.1) is satisfied so that the equations for the synchronous wave amplitudes can be written

$$\begin{aligned} -j\gamma a_{3,n} &= C_- a_{4,n-1} + C_+^* a_{4,n+1} \\ -j\gamma a_{4,n} &= C_+ a_{3,n-1} + C_-^* a_{3,n+1} \end{aligned} \quad . \tag{6.9}$$

The approach which will be used here to solve this set of difference equations was pointed out to the author by Blætekjaer who found the solution to a similar transverse wave problem in the same way.[31]

Equations (6.9) can be combined to yield a single difference equation relating the amplitudes of the different frequency components of each type of synchronous wave. For the positive energy wave amplitudes we obtain

$$C_+^* C_-^* a_{3,n+2} + (\gamma^2 + C_+ C_+^* + C_- C_-^*) a_{3,n} + C_+ C_- a_{3,n-2} = 0 \quad , \tag{6.10}$$

and a similar equation holds for the negative energy wave amplitudes. Now it is a legitimate step to choose the phase of the quadrupole fields and then later determine the necessary input phase for the synchronous waves with respect to the assumed quadrupole phase. Thus, since the quadrupole is assumed to be linearly polarized, we can choose

$$C_+ = C_- = C = |C| \quad . \tag{6.11}$$

As a result of this choice (6.10) becomes

$$a_{n+2} + \left(\frac{\gamma^2}{c^2} + 2\right) a_n + a_{n-2} = 0 \quad , \tag{6.12}$$

where the subscript denoting the synchronous wave involved has been dropped because the equation is applicable for both $a_{3,n}$ and $a_{4,n}$. The solution to (6.12) is obtained by assuming that the various frequency components are of the general form

$$a_n = a_0 e^{jn\theta} \quad , \tag{6.13}$$

where θ is a parameter which facilitates the mathematical solution of (6.12). Substituting (6.13) into (6.12) yields

$$\frac{\gamma}{c} = \pm j2 \cos \theta \quad . \tag{6.14}$$

By using (6.14) and (5.3), it is found that a solution for the waves described by (6.12) is

$$A = a_0(0) \sum_{|n|=0}^{\infty} e^{jn\theta} \exp j\left[(\omega + n\omega_q)t - (\pm j2C \cos \theta + \frac{n\omega_q}{u_0} + \beta_e)z\right] \quad . \tag{6.15}$$

The most general solution is obtained by summing over all possible solutions or, in this case, by integrating over all permissible values of θ . As noted in the reference cited above, the condition that only the fundamental frequency components are nonzero at $z = 0$ is sufficient to require that θ be real and that a satisfactory range of integration is $-\pi \leq \theta \leq +\pi$. As a result of the choice of signs in (6.14) two solutions are found, as

described above, and the most general solution to the problem is a linear combination of these. Finally then the general solutions for the positive and negative energy synchronous wave excitation in the quadrupole are

$$A_3 = a_{3,0}(0) \sum_{|n|=0}^{\infty} [a + (-1)^n b]\, I_n(2Cz)\, e^{j(\omega + n\omega_q)(t - z/u_0)}$$

$$A_4 = a_{4,0}(0) \sum_{|n|=0}^{\infty} [c + (-1)^n d]\, I_n(2Cz)\, e^{j(\omega + n\omega_q)(t - z/u_0)} \quad . \quad (6.16)$$

These equations were obtained as solutions to (6.12) and are quite general. We note, however, that (6.12) will generate only solutions with even n, beginning with the amplitude a_0. For this half of the solutions it is evident that

$$a + b = 1$$

$$c + d = 1 \quad . \quad (6.17)$$

The other half of the solutions is obtained by substituting (6.13) and (6.14) into (6.9) with $n = 1$ to obtain

$$a_{3,1} = \mp a_{4,0}\, e^{j\theta}$$

$$a_{4,1} = \mp a_{3,0}\, e^{j\theta} \quad . \quad (6.18)$$

By averaging over θ as before and matching the initial conditions, we obtain

$$a - b = \frac{a_{4,0}(0)}{a_{3,0}(0)}$$

and

$$c - d = \frac{a_{3,0}(0)}{a_{4,0}(0)} \quad . \tag{6.19}$$

Finally then, by noting the relation[19]

$$a_{3,-\omega,-n} = a^*_{4,\omega,n} \tag{6.20}$$

and setting $\omega_q = 2\omega$, we obtain the complete expressions for the synchronous waves in the quadrupole region:

$$A_3 = \sum_{n \geq 0} \sqrt{2n+1} \left[\begin{Bmatrix} a_{3,0}(0) \\ a_{4,0}(0) \end{Bmatrix} I_n(\sqrt{2}\,\alpha z) + \begin{Bmatrix} a^*_{3,0}(0) \\ a^*_{4,0}(0) \end{Bmatrix} I_{n+1}\left|\sqrt{2}\,\alpha z\right| \right] e^{+j(2n+1)\omega(t - z/u_0)} \tag{6.21}$$

$$A_4 = \sum_{n \geq 0} \sqrt{2n+1} \left[\begin{Bmatrix} a_{4,0}(0) \\ a_{3,0}(0) \end{Bmatrix} I_n\left|\sqrt{2}\,\alpha z\right| + \begin{Bmatrix} a^*_{4,0}(0) \\ a^*_{3,0}(0) \end{Bmatrix} I_{n+1}\left|\sqrt{2}\,\alpha z\right| \right] e^{+j(2n+1)\omega(t - z/u_0)} \quad . \tag{6.22}$$

In these equations α is given by (6.8) and the upper wave amplitude is to be used if n is even and the lower if n is odd. The factor $\sqrt{2n+1}$ has been inserted in order to normalize the amplitudes so that their square is the power carried by that wave. This is a result of the ω which appears in (2.14).

Equations (6.21) and (6.22) are to be compared with the approximate solutions given in (6.6) and (6.7). For a weak interaction, so that only the first power of αz is retained in the series expansions of sinh αz and $I_n\left|\sqrt{2}\,\alpha z\right|$, the three-frequency and the exact analyses agree as would be expected. However, for stronger interactions the exact solution shows that higher order, odd frequency harmonics on the beam become important. The only frequency component on the quadrupole is still the second harmonic, but the calculation of the power delivered to the quadrupole will be greatly modified for strong interactions as will be shown in the next section.

B. CALCULATION OF SECOND HARMONIC POWER

The second harmonic power which has been dissipated in the quadrupole and its load, in the process of establishing the beam waves described in the previous section, is obtained by calculating the power lost by the beam in the quadrupole region. In the case of a circularly polarized quadrupole, Eqs. (6.6) and (6.7) can be used for this calculation. For a linearly polarized quadrupole the three-frequency solution is not valid at high power levels and so exact wave expressions given by (6.21) and (6.22) must be used.

The power delivered to the quadrupole by the beam is found by computing the net negative power on the beam at the quadrupole exit and subtracting net negative beam power at the input end of the quadrupole cavity. Determination of this power from the three-frequency wave solutions (6.6) and (6.7) yields

$$P_{2\omega} = \left[|a_4(0)|^2\left(1 - 3\left|\frac{C_+}{\alpha}\right|^2 + \left|\frac{C_-}{\alpha}\right|^2\right) - |a_3(0)|^2\left(1 - 3\left|\frac{C_-}{\alpha}\right|^2 + \left|\frac{C_+}{\alpha}\right|^2\right)\right]\sinh^2 \alpha\ell$$

$$+ \left[\frac{C_-}{\alpha}|a_4(0)|^2 \cos 2\theta_4 - \frac{C_+}{\alpha}|a_3(0)|^2 \cos 2\theta_3\right] \sinh 2\alpha\ell \quad , \qquad (6.23)$$

where ℓ is the length of the quadrupole cavity and θ_3 and θ_4 are the respective phases of the positively and negatively polarized

synchronous waves. The phases of the quadrupole field components represented by C_+ and C_- have been chosen to be zero as described in the previous section. Both polarizations have been retained in (6.23), as it causes no difficulty to do so and it will allow a comparison between the approximate and exact solutions for the linearly polarized case.

The interpretation of the input synchronous wave phases in (6.23) can be investigated in the same way as was done for the cyclotron wave case by calculating the complex power delivered to the quadrupole cavity by the beam. If the quadrupole is circularly polarized, the discussion is exactly the same as in Chapter V.C. If the circuit is linearly polarized, the situation is altered. The complex power delivered to the quadrupole cavity can be calculated by means of (5.13) and equations corresponding to (5.15) and (5.16) involving the synchronous wave amplitudes. When this power is calculated, it is observed that a fifth harmonic term arises in the electric field expressions which corresponds to (5.15). This frequency does not appear in the wave amplitude expressions (6.6) and (6.7) and this result is an indication that the assumed three-frequency solution is not consistent with the original equations. However, since we have neglected the higher frequency terms in (6.7), there is no fifth harmonic current to go into the power calculation and the real part of the complex power calculated in this way agrees with (6.23). The reactive power absorbed by the quadrupole and load has terms proportional to

$$|a_3(0)|^2 \sin 2\theta_3$$

and

$$|a_4(0)|^2 \sin 2\theta_4 \quad , \tag{6.26}$$

which must be zero at the quadrupole resonant frequency. As a result of these considerations, and inspection of (6.23), it is concluded that the quadrupole fields will in general be set up so that the phases of the beam waves with respect to the quadrupole field of the same polarization

are given by

$$\theta_3 = \frac{\pi}{2}, \frac{3\pi}{2}$$

and

$$\theta_4 = 0, \pi \quad . \tag{6.27}$$

1. Positively Polarized Quadrupole

The basic interactions represented in (6.23) fall into three categories. The first is the case in which the quadrupole cavity has only a positively polarized field component. That is, it is polarized like the input synchronous wave which carries positive energy. The quadrupole field will be set up so that θ_3 is given by (6.27) for any angular orientation of the quadrupole cavity. The second harmonic power dissipated in the cavity and its load is obtained from (6.8) and (6.23):

$$P_{2\omega} = -2\left[|a_4(0)|^2 + |a_3(0)|^2\right] \sinh^2 \alpha\ell + |a_3(0)|^2 \sinh 2\alpha\ell \,. \tag{6.28}$$

This is exactly analagous to the result obtained in Chapter V for the case in which the quadrupole was synchronous with the fast cyclotron wave. The characteristics of the synchronous wave interactions are the same as described for the cyclotron wave case. When only the positive energy synchronous wave is excited by the input coupler, it is found that the beam wave energy is transferred to the quadrupole as indicated by curve a in Fig. 5.3. When both synchronous waves are excited with equal amplitude on the beam, as would be the case with a linearly polarized input coupler, the power output is the same as described by curve b in Fig. 5.3.

As a result of the above discussion it can be concluded that the interactions involved in a positively polarized quadrupole offer no basic advantages over the cyclotron wave doubler in which the quadrupole is synchronous with the fast cyclotron wave.

It is true that the synchronous waves offer the advantage of a synchronism condition which is independent of the magnetic field. However, this must be weighed against the reduction in circuit phase velocity, and therefore interaction impedance, which results when synchronous wave interactions are used.

2. Negatively Polarized Quadrupole

In this case the quadrupole is polarized in the same direction as the synchronous wave which carries negative power. The phase of the resonant quadrupole will again adjust itself so that θ_4 satisfies (6.27). The second harmonic power dissipated in the cavity and its load is obtained from (6.8) and (6.23):

$$P_{2\omega} = +2\left[|a_4(0)|^2 + |a_3(0)|^2\right] \sinh^2 \alpha\ell + |a_4(0)|^2 \sinh 2\alpha\ell \,. \quad (6.29)$$

This is exactly analogous to the result obtained in Chapter V for the case in which the quadrupole was synchronous with the slow cyclotron wave. As in that case, the interaction is one which can lead to appreciable gain if either synchronous wave exists on the beam at the quadrupole entrance. Curves showing the total second harmonic power as a function of the growth parameter $\alpha\ell$ are given in Fig. 5.4 for the case of one synchronous wave input, or equal amplitudes of both synchronous waves. The actual power which is delivered to the load as a function of the input synchronous wave power is discussed in the next section where the matching of the cavity to the external load is taken into consideration.

Although the negatively polarized quadrupole interacting with the synchronous waves results in the same equations as in the case involving the cyclotron waves cited above, the present situation has the advantages of allowing the use of higher phase velocity circuits and allowing the synchronism condition to be independent of the magnetic field. For these reasons the present scheme is preferable to the slow cyclotron wave interaction.

3. Linearly Polarized Quadrupole

In this case the quadrupole fields can be obtained from (5.1) and(5.5)

and are given by

$$E_x = + \frac{\omega_c u_0}{e/m} 2Cx \sin(\omega_q t - k_q z)$$

$$E_y = - \frac{\omega_c u_0}{e/m} 2Cy \sin(\omega_q t - k_q z) \quad , \tag{6.30}$$

where

$$C_+ = C_- = C \quad . \tag{6.31}$$

The quadrupole field configuration is shown in Fig. 5.1. Since the excitation of the circuit is a result of the motion of the beam along the electric field lines, it is apparent that there will, in general, be a required relationship between the angular orientation of the quadrupole cavity and the input coupler which excites the initial synchronous waves on the beam. In particular, the linearly synchronous polarized wave coupler described in Chapter III should be oriented so that the beam waves at the quadrupole entrance satisfy (6.27).

The second harmonic power which is dissipated in the cavity and its external load can be obtained from (6.8) and (6.23); in general,

$$P_{2\omega} = \frac{1}{\sqrt{2}} \left[|a_4(0)|^2 \cos 2\theta_4 - |a_3(0)|^2 \cos 2\theta_3 \right] \sinh 2\alpha\ell \quad . \tag{6.32}$$

In the case in which just one synchronous wave is excited at the quadrupole entrance, or if both have the proper phase relative to the quadrupole as indicated by (6.27), the power is given by

$$P_{2\omega} = \frac{1}{\sqrt{2}} \left[|a_4(0)|^2 + |a_3(0)|^2 \right] \sinh 2\alpha\ell \quad . \tag{6.33}$$

It was noted in Section V.A that the three-frequency solution of the linearly polarized problem is not expected to be accurate because of appreciable excitation of higher order frequency combinations in the beam. It is therefore important to calculate the second harmonic power from the exact wave amplitudes given in (6.21) and (6.22). This is done by calculating the net change in beam power as a result of the quadrupole interaction in the same way as before. Summing the squares of the amplitudes of the negative energy waves which make up A_4 and subtracting the sum of the squares of the amplitudes of the positive energy waves which make up A_3 yields the net negative power carried by the beam at the quadrupole output. Then by subtracting the net negative power at the input, we obtain, after a great deal of manipulation,

$$P_{2\omega} = \left[|a_3(0)|^2 - |a_4(0)|^2\right]\left[1 - I_0^2 - 2\sum_{n=1}^{\infty}(-1)^n I_n^2\right] \tag{6.34}$$

$$+ 2\mathrm{Re}\left[a_4^2(0) - a_3^2(0)\right]\sum_{n=0}^{\infty}(-1)^n (2n+1)\, I_n I_{n+1} \ ,$$

where the argument of the modified Bessel functions is $\sqrt{2\alpha}\ell$. By means of known series,[32] and the relations between the ordinary and modified Bessel functions, it can be shown that

$$I_0^2(z) + 2\sum_{n=1}^{\infty}(-1)^n I_n^2(z) = 1 \tag{6.35}$$

$$\sum_{n=1}^{\infty}(-1)^n (2n+1)\, I_n(z)\, I_{n+1}(z) = \frac{z}{2} \ . \tag{6.36}$$

Thus, the second harmonic power calculated from the rigorous solutions of

the coupled mode equations is obtained in a very simple form:

$$P_{2\omega} = \left[|a_4(0)|^2 \cos 2\theta_4 - |a_3(0)|^2 \cos 2\theta_3\right] \sqrt{2}\alpha\ell \quad . \quad (6.37)$$

We see that (6.37) and (6.32) agree exactly at low power levels, but that the approximate solution is over-optimistic at high power levels. A comparison of these results with the other synchronous wave interactions will be given in Section D of this chapter.

Although there is no counterpart of the type of interaction described above given in Chapter V it is apparent, from the discussion of twisted circuits which was given in Chapter IV, that a twisted quadrupole would allow a cyclotron wave interaction completely analogous to the synchronous wave interaction in a linearly polarized quadrupole. However, this would offer no advantage over the present case and the design would be much more complex.

C. EFFECT OF THE LOAD IMPEDANCE

The results obtained in the previous section indicate that the synchronous wave frequency doubler can yield high frequency conversion efficiencies for several special cases. However, the equations presented there are not in a form which exhibits the dependence of the power dissipated in the external load upon the input power, the quadrupole parameters, and the coupling coefficient Q_0/Q_{ext} . The equations of the previous section can be expressed in terms of these quantities in a manner similar to that used in Section V.D.

As pointed out in Section B of this chapter, the synchronous wave interactions involving a circularly polarized quadrupole are exactly equivalent to the cyclotron wave interactions which were discussed in Chapter V. If the quadrupole is positively polarized, α is given by (5.43) and (6.28) is identical to (5.21). Consequently, the curves in Fig. 5.5 are appropriate for this case. If the quadrupole is negatively polarized, α is still given by (5.43) and (6.29) is identical to (5.38). The curves shown in Fig. 5.6 therefore give the frequency conversion characteristics for this case. The discussion of these situations is

identical to that given in Chapter V for the analogous cyclotron wave cases. The only differences between the cyclotron wave and synchronous wave cases are the synchronization conditions.

The situation not represented in the previous chapter is the linearly polarized case given by (6.37). It is evident from (6.8) and (5.43) that the gain parameter is in this case

$$\alpha = \sqrt{|C_+|^2 + |C_-|^2} = \frac{\sqrt{2}(e/m)V_a}{\omega_c u_0 a^2} .$$

Consequently, using (5.41) and the normalization given by (5.47) in (6.37) yields

$$P_{2\omega L} = \frac{1}{\left(1 + \frac{Q_{ext}}{Q_0}\right)\left(1 + \frac{Q_0}{Q_{ext}}\right)} [P_{3,\omega} - P_{4,\omega}]^2 , \qquad (6.39)$$

where $P_{3,\omega}$ and $P_{4,\omega}$ are the respective values of the power input on the transverse waves. It should be recalled that the power input $P_{4,\omega}$ is a negative quantity. The phases θ_3 and θ_4 in (6.37) have been taken as the optimum values given in (6.27).

As pointed out previously the special case in which the input synchronous waves have equal amplitude is of a great deal of interest since gain can be achieved in the input coupler in this situation. If the power carried by the input positive energy wave is then denoted by P_ω , the output is

$$P_{2\omega L} = \frac{4}{\left(1 + \frac{Q_0}{Q_{ext}}\right)\left(1 + \frac{Q_{ext}}{Q_0}\right)} P_\omega^2 . \qquad (6.40)$$

Note that (6.40) is identical to (5.56) which describes the low level output of the cyclotron wave doubler employing both fast and slow input

cyclotron waves. The significant difference here is that the above result is valid for large signal levels while the cyclotron wave doubler saturates as indicated by (5.55).

Equation (6.39) also shows that the linearly polarized synchronous wave doubler behaves as a constant current source as the load is varied. That is, the maximum power output is obtained when Q_{ext}/Q_0 is unity for all power levels. This is unlike the other cases as can be seen in Section V.D, and is a result of the zero beam loading presented to a circuit that couples equally to both synchronous waves.

D. SUMMARY OF SYNCHRONOUS WAVE DOUBLERS

The frequency doubling interactions which have been discussed in this chapter have, with one exception, been the synchronous wave analogs of the cyclotron wave interactions described in Chapter V. Hence, most of the comments in Chapter V are applicable to the present situation. The exception is the case of the linearly polarized quadrupole which interacts equally with both synchronous waves and results in the excitation of all odd harmonic frequency components on the beam. As was pointed out previously, the cyclotron wave analog of this case can be obtained by twisting the quadrupole with a period equal to the cyclotron wavelength on the beam. Consequently, a discussion of the quadrupole interactions for the synchronous wave cases discussed in this chapter is really a discussion of all of the types of doubling interactions which can be obtained with the four transverse waves which describe the filamentary beam excitation. The details of the circuit configurations and the synchronism conditions are, of course, dependent upon the choice of cyclotron or synchronous wave interactions.

A comparison of the synchronous wave interactions can be made on the basis of the equations for the second harmonic power dissipated in the quadrupole as a function of the parameter $\alpha\ell$. The curves representing the possible interactions between one input synchronous wave and the quadrupole are shown in Fig. 6.1. Curve d represents the interaction involving only the positive energy synchronous wave and we see that the maximum second harmonic power which can be dissipated in the quadrupole is equal to the input synchronous wave power. This is the synchronous

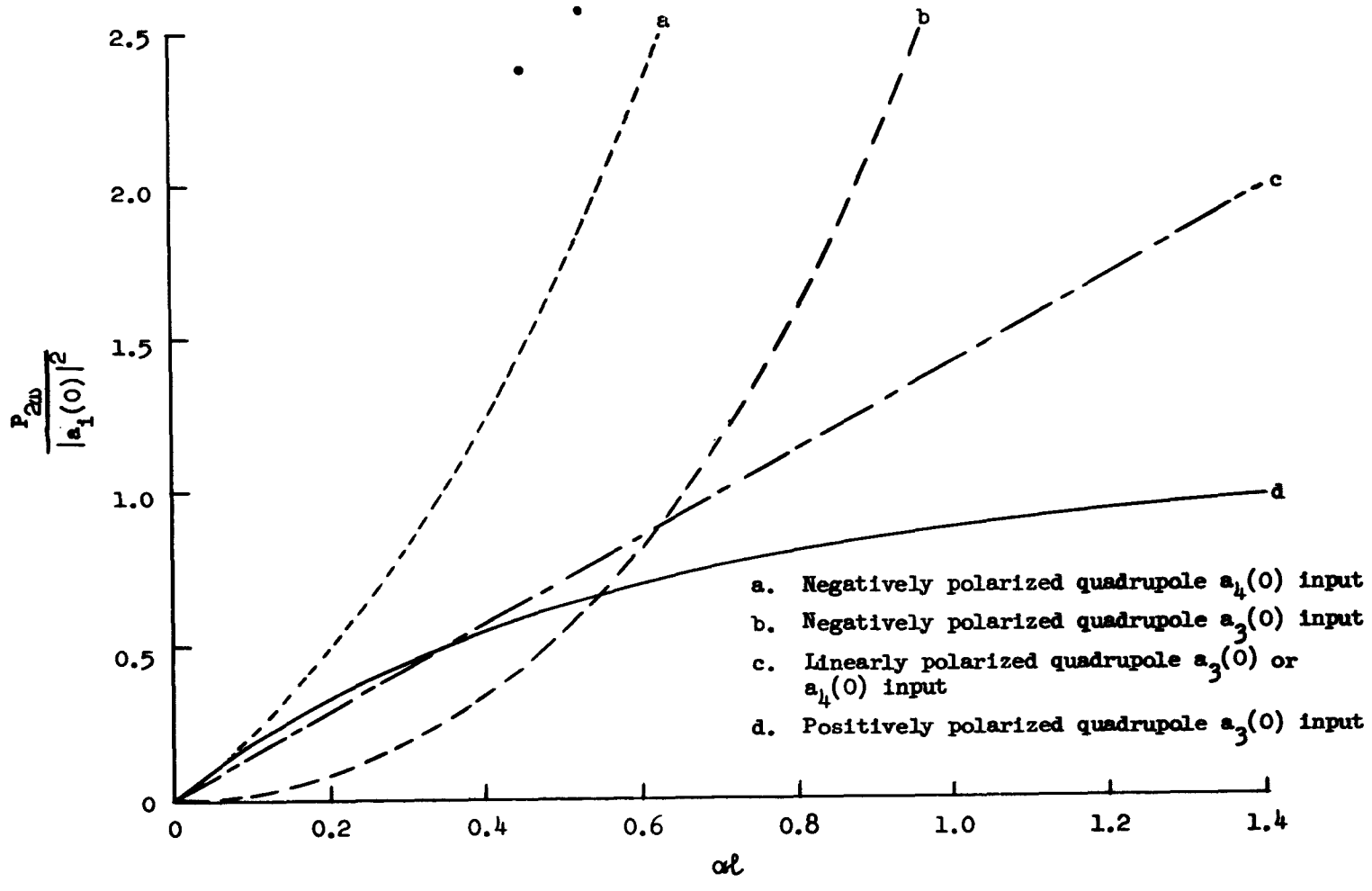

FIG. 6.1--Quadrupole conversion efficiency as a function of $\alpha\ell$ for various polarizations and one input synchronous wave.

wave counterpart of the fast cyclotron wave doubler which has been treated by others in a special case. Because no negative energy waves are involved in this case, it will be referred to as passive doubling. By setting $C_- = 0$ in (6.6) we can see that only the fundamental frequency exists on the beam and that the synchronous wave amplitude decreases exponentially within the quadrupole cavity. Consequently the factor which controls the beam interception level is the amplitude of the beam excursion at the entrance. This is calculated from Eqs.(2.20). There is no interaction if a negative energy wave is injected into a positive polarized quadrupole unless second harmonic power is supplied by an external source.

The passive interaction indicated by curve d in Fig. 6.1 is to be compared with the three basic active frequency doubling interactions shown in curves a, b, and c of the figure. Curve a represents the interaction between a negatively polarized (negative energy) synchronous wave with a negatively polarized quadrupole. This again is an interaction which involves only the fundamental frequency in the beam, but now the beam excitation grows exponentially in the quadrupole and the second harmonic power increases rapidly as either the coupling to the beam is increased (larger α) or the length is increased. As is evident from the figure, this case gives a larger conversion efficiency than any of the other cases. It is the only scheme which surpasses the passive interaction at low power levels, that is, small $\alpha\ell$. However, it is necessary to note that, due to the growing beam excursions, saturation will occur if $\alpha\ell$ is made too large. Since there is only the fundamental negative energy synchronous wave in the beam, the beam excursion for a given wave amplitude is the same as in the passive case. Consequently, in the limit as $\alpha\ell$ approaches infinity, the saturation output power of the two devices would be the same. However, the efficiency of conversion of fundamental to second harmonic power would be infinite for the active case and unity for the passive interaction.

The active interaction described above is analogous to the interaction involving the slow cyclotron wave which was discussed in Chapter V and the power characteristics given in Fig. 5.6 are applicable here. As shown in Fig. 5.6, these frequency doublers become unstable when the input power is increased beyond a critical value. This is an unusual kind of instability as is remarked in Section V.D.

An interesting input coupling scheme arises in connection with the negative energy, synchronous wave interaction described above. It was noted that the synchronous wave klystron described in Chapter III can result in purely negative energy, synchronous wave excitation on the beam at the exit of the output cavity. This klystron could then be followed by a negatively polarized quadrupole cavity, resulting in the active frequency doubling mechanism described above. Consequently, a very large overall frequency conversion efficiency could be obtained. Alternatively, the input coupler could be a circularly polarized synchronous wave monotron resulting in an oscillator which produces a fundamental and second harmonic that are phase related.

Curve b in Fig. 6.1 shows the characteristics of the interaction if the positively polarized synchronous wave serves as the input to a negatively polarized quadrupole. The conversion efficiency is now greatly reduced due to the presence of both positive and negative energy synchronous waves in the beam at the fundamental and third harmonic frequencies as indicated by (6.6) and (6.7). Also because there are both growing positive energy and negative energy waves on the beam, the net negative power carried by the beam for given beam excursion magnitudes is less than in the previous case. As a final criticism of this case, it is noted that the input is a positive energy wave, and therefore, it is not possible to take advantage of a gain mechanism in an input coupler to increase the overall conversion efficiency. Consequently, this situation is of less interest than is the previous case.

The last basic interaction scheme is represented by curve c in Fig. 5.1. In this case the quadrupole is linearly polarized and the input wave is either a positively or a negatively polarized synchronous wave. It is seen that the efficiency of the frequency conversion is about the same as that of the positively polarized quadrupole with a positively polarized synchronous wave input at small values of $\alpha\ell$, while it is distinctly improved for large $\alpha\ell$. This, coupled with the fact that the input can be a negative energy wave, makes the linearly polarized quadrupole an interesting case. The power at which beam interception occurs will be less than it is for either of the two cases which involve only one frequency on the beam, since we expect an infinite

number of frequency components here. This large frequency content results in complex beam motion and larger beam excursions than are found for the simpler cases. Even so, this is a promising scheme for a large conversion efficiency as described above.

The frequency doubling schemes described above involved a single synchronous wave input to the quadrupole. In order to take advantage of the gain which can be obtained in a linearly polarized input cavity which excites both synchronous waves equally, it is of interest to look at the situation in which the input to the quadrupole consists of both synchronous waves with the optimum phase. A plot of the ratio of the second harmonic power to the fundamental power on one of the beam waves as a function of $\alpha\ell$ is given in Fig. 6.2.

It is apparent that the negatively polarized quadrupole is again distinctly superior at large values of $\alpha\ell$. The instability at large values of $\alpha\ell$ still exists as indicated in Fig. 5.6 of Section V.D, since this case is identical to the cyclotron wave case considered there. The linearly polarized quadrupole also yields large conversion efficiencies while the positively polarized quadrupole saturates at a very low efficiency and is of no interest here. For the two interesting cases it is seen that the second harmonic power for a given input wave amplitude is distinctly larger for the two-wave input that it is for the one-wave input case.

From the above discussion it is apparent that the greatest promise for large values for the efficiency of conversion from the fundamental to the second harmonic frequency is given by the use of either a negatively polarized quadrupole or a linearly polarized quadrupole, each with both synchronous waves excited in the input coupler. Or, to cast this in a terminology which is applicable to either cyclotron or synchronous waves, the quadrupole should be synchronous with either the negative energy beam wave, or with both the positive and the negative energy waves which serve as the input. Also, the input coupler should excite both the positive and the negative energy beam waves equally. While this situation can be achieved with cyclotron wave interactions, it requires a twisted input coupler and either a quadrupole with a very slow phase velocity or a twisted quadrupole. Thus the use of cyclotron waves for these high efficiency, active doubling schemes brings on many more technical problems

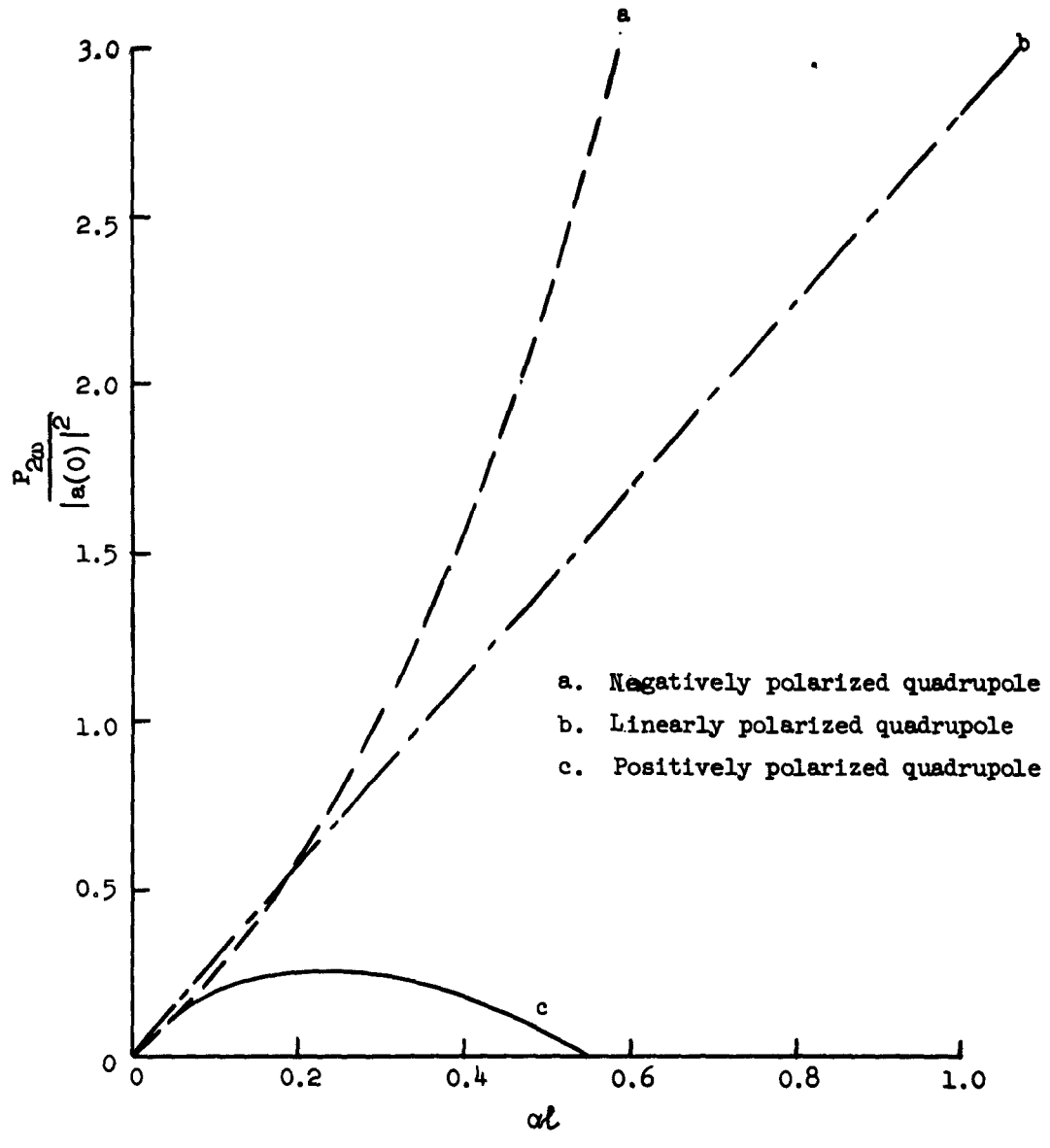

FIG. 6.2--Quadrupole conversion efficiency as a function of $\alpha\ell$ for various polarizations and equal input synchronous waves of amplitude a(0) and optimum phase.

than does the use of the synchronous waves. For these reasons it appears that the described active interactions employing the synchronous waves are the most suitable for very high efficiency frequency doubling.

CHAPTER VII

SOME TRANSVERSE-FIELD CIRCUITS

The discussion up to this point has been involved with the theory of the interaction between a beam and a transverse-field circuit. The primary purpose of this chapter is to discuss some traveling-wave structures which were investigated for use in transverse-wave devices. The material presented is not an exhaustive investigation of transverse field circuits, but represents the results of efforts to design specific devices. Even so, the basic circuits have a broad range of application and so the specific applications will not be emphasized in this chapter.

The first part of this chapter will deal with the transverse-wave couplers which were investigated during the course of the experimental program. In the second part of the chapter we will consider a quadrupole type of periodic circuit which could be used in one of the devices discussed in Chapters V and VI. Since one purpose of the experimental investigation was to show that significant transverse-wave interactions can be obtained at high power levels and high frequencies, good thermal properties as well as simple and rigid mechanical construction were important criteria in the design of all of the transverse-field circuits considered.

A. COUPLER CIRCUITS

There has been a large amount of activity in the last few years in the development of transverse-wave couplers which employ traveling-wave circuits. Johnson has described experiments using a bifilar helix as a transverse-wave coupler.[33] Other circuits which immediately come to mind are those involving meander lines and slotted ridge circuits. Honey[34] has studied the meander line in connection with another type of device, and Sorland[35] has investigated a slotted ridge circuit.

Of these circuit types, the slotted ridge is the most likely to have good thermal properties and rigidity at high frequencies. A sketch of the basic circuit is shown in Fig. 7.1a. It is evident that the stored energy in noninteracting regions (in the slots) serves to reduce the transverse impedance of the circuit and that it would be desirable to reduce the energy. The structure shown in Fig. 7.1b, proposed by Bernstein and Feinstein,[26] reduces this noninteracting energy by reducing the width of the ridge, but results in a lack of field uniformity in the interacting region. Even so, this type of circuit is easy to make, has good thermal properties, and would be quite rigid when employed at very short wavelengths. Consequently, the coupler circuit developed independently during the course of this investigation was of the type shown in Fig. 7.1c. This circuit has the advantage that it has a region of relatively uniform transverse field and, as we shall see later, it is particularly well suited for use as a synchronous-wave coupler. Variations of this basic circuit may be thought of, and one is shown in Fig. 7.1d.

1. Impedance of Idealized Circuits

Before proceeding with a discussion of the experimental coupler studies, it is worthwhile to make a general observation about traveling-wave circuits which have a transverse electric field on their axis. The particular point in question is: how large is the transverse impedance of such a circuit compared to that of a longitudinal field circuit? This is a pertinant question because the qualitative descriptions of transverse-wave and space-charge wave devices are very similar, and consequently the two types of interaction must be considered competitive in some cases.

While the impedance of a traveling-wave circuit depends upon the details of the structure, it is possible to set an upper bound on the impedance which can be attained. This is done by assuming an idealized slow-wave circuit which has only the transverse components of the electric field which are important in the interaction and the associated magnetic fields required to satisfy Maxwell's equations. It is then possible to calculate the energy stored in the circuit and thus to calculate interaction impedance. Pierce[36] has done this for the longitudinal field case and the problem is solved in Appendix A for the transverse field case. The curves in Fig. 7.2 give a comparison of the impedances of the

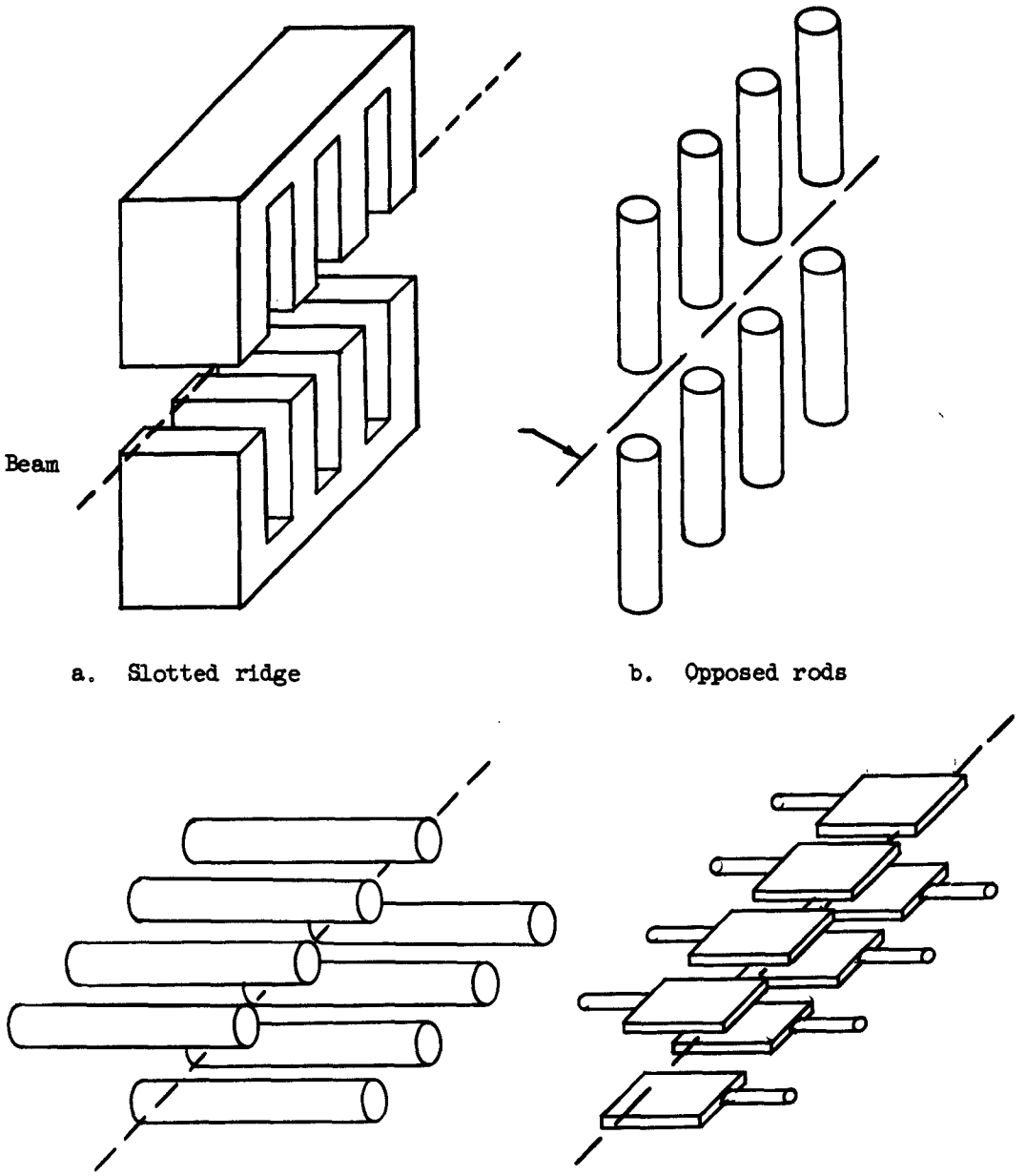

a. Slotted ridge

b. Opposed rods

c. Overlapped rods

d. Overlapped paddles

FIG. 7.1--Some basic transverse-field circuit structures. The metallic side walls that would be used in a microwave circuit have not been shown, for the purpose of clarity.

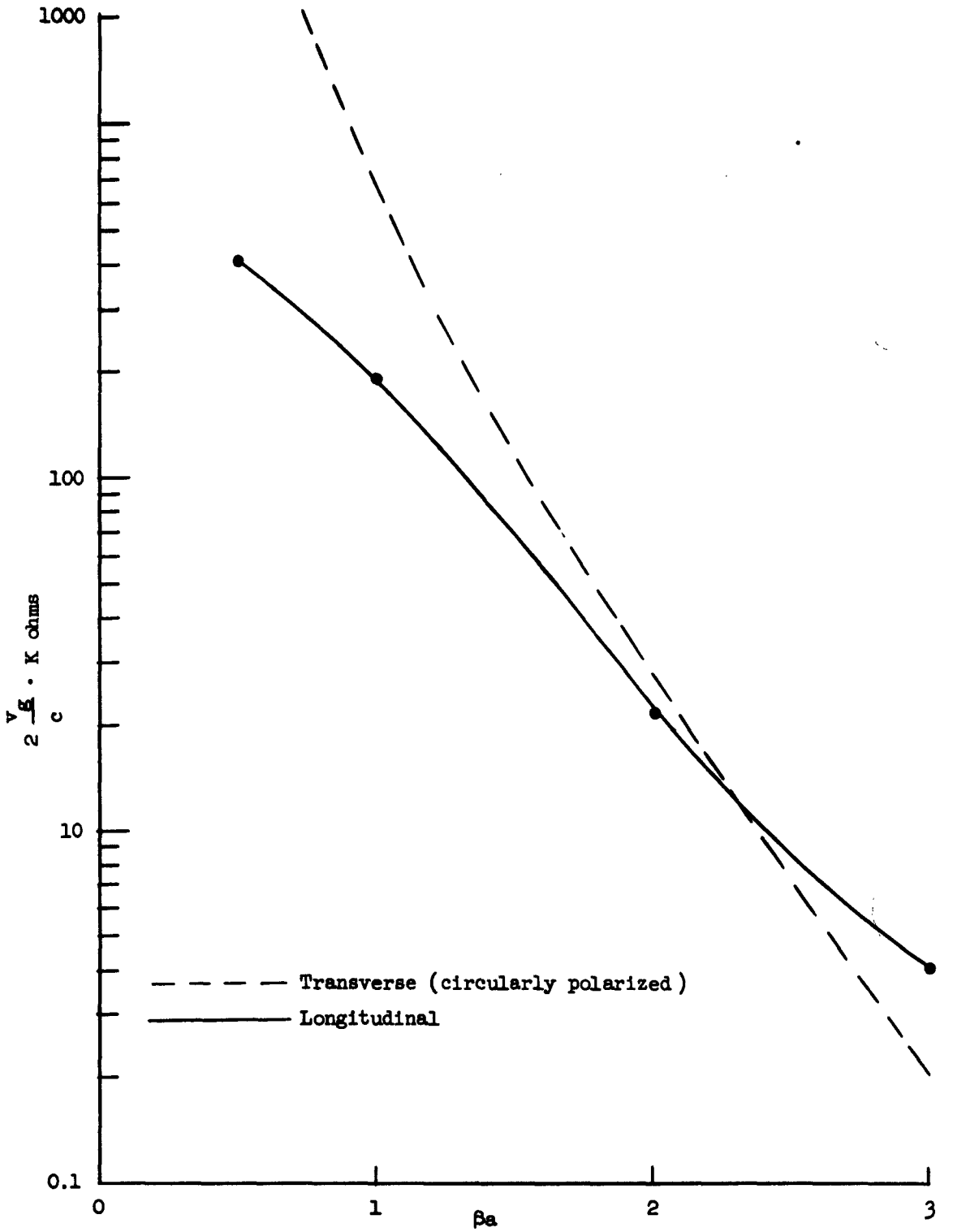

FIG. 7.2--The impedance of the idealized transverse-field and longitudinal-field circuits as a function of βa. It has been assumed that the circuit phase velocity is small compared to the velocity of light. The beam aperture in the circuit has a diameter of 2a.

idealized circularly polarized transverse-field circuit with the idealized longitudinal field circuit. The definition of impedance used here is different from that used by Pierce, as noted in Appendix A. Figure 7.2 shows that, in the region $\beta a < 2.3$, the idealized transverse field circuit has a higher impedance than does the idealized longitudinal field circuit. At smaller values of βa , the difference becomes quite significant. While these results do not say what kind of impedance values can be obtained in actual circuits, they do indicate that we can expect to find circuit configurations which yield transverse impedances that are greater than those which can be obtained in longitudinal field circuits with the same beam diameter. Alternatively, a transverse-wave coupler will allow the use of a larger beam than will pass through a longitudinal field structure which has the same impedance.

2. Experimental Linearly Polarized Circuits

Although the ideal coupler for the excitation of one of the transverse waves would be circularly polarized, the simplicity of the design and excitation of the linearly polarized structure makes it a case of particular interest. In addition there are interactions in which a linearly polarized coupler is required. In fact, linearly polarized couplers were required in the experimental tube described in the next chapter.

The goal of the experiments described here was to develop a slow wave circuit which could be used as either a cyclotron-wave or a synchronous-wave coupler at a frequency of about 3.0 kMc with a beam voltage of a few thousand volts. These structures could then be used either as a traveling-wave coupler or as a resonant periodic coupler in a high-power transverse-wave device. The basic circuit that was studied is the pin-loaded cylinder indicated in Fig. 7.1c.

The characteristics of the circuits were determined by the usual procedure of resonating a section of the structure which is an integral number of periods long and observing the characteristics of the resonant modes of the resulting cavity. One of the test cavities was made with a rectangular cross section as shown in Fig. 7.3. The basic difference between this and a circularly cylindrical cross section is insignificant. The dimensions of the test cavity could be varied so that their effect could be determined.

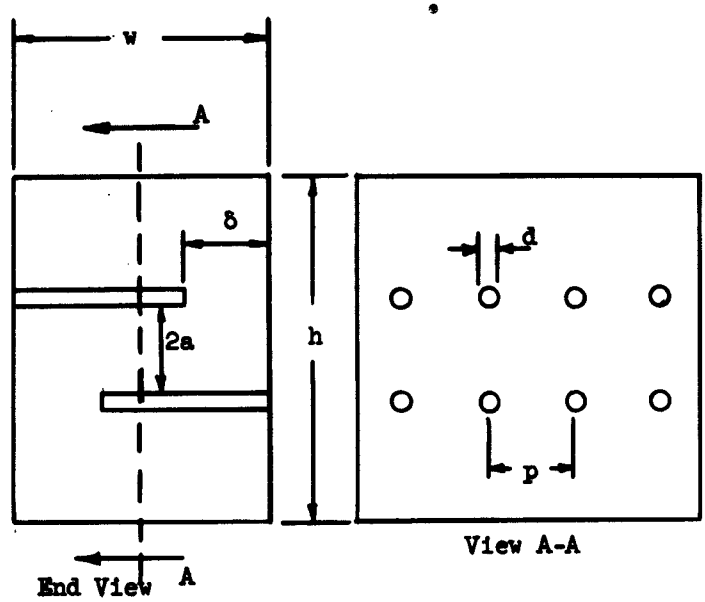

FIG. 7.3--An experimental test structure enclosed in a box. The important dimensions that are referred to in the description of the characteristics of this circuit are shown.

Some of the results of the cold tests of circuits with the dimensions given in Table VII.1 are shown in Figs. 7.4 through 7.6. A typical ω-β diagram is shown in Fig. 7.4. The structure is a closed, simply connected region so that it exhibits both an upper and a lower cutoff.

TABLE VII.1

DIMENSIONS OF TEST CIRCUITS IN INDEX

1.	2.	3.
w = 1.00	w = 1.00	w = 1.25
h = 3.00	h = 1.62	h = 1.625
2a = 0.375	2a = 0.315	2a = 0.250
δ = 0.313	δ = 0.325	δ = 0.375
d = 0.125	d = 0.063	d = 0.031
p = 0.375	p = 0.187	p = 0.100

The lower cutoff frequency is determined by the transverse dimensions of the circuit and is associated with strong transverse electric fields between the upper and lower rods in Figs. 7.1c and 7.3. Consequently, the transverse interaction impedance can be expected to be quite large near the lower cutoff frequency. The upper cutoff frequency is associated with the resonance that occurs when the rods are approximately one-quarter of a wavelength long so that one rod and its neighbor form a quarter wavelength TEM transmission line which is shorted at one end and open-circuited at the other. However, due to end effects, this resonance will occur at a frequency slightly lower than that predicted on the basis of the above model. The electric fields near the upper cutoff frequency are predominantly longitudinal, and consequently the amount of coupling to the transverse beam waves can be expected to be small in this region.

The circuit represented by Fig. 7.4 was designed to serve as a fast cyclotron wave coupler and the dispersion characteristic for the fast cyclotron wave is also shown in the figure. Since the phase velocity of the circuit and the beam are essentially the same over a large portion of the ω-β diagram, the coupler should have a large bandwidth. In order to determine the bandwidth of a co-directional coupler, it is necessary

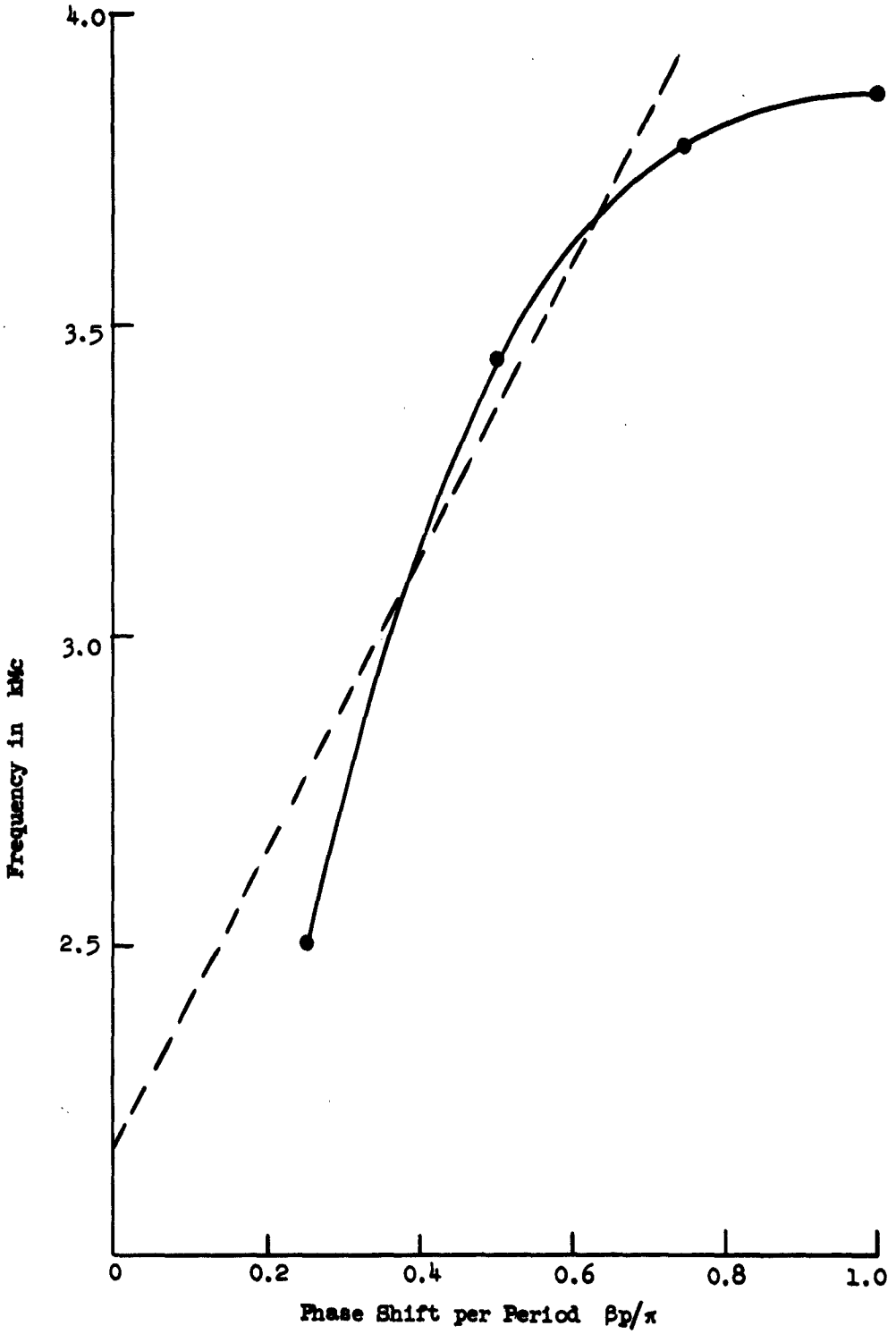

FIG. 7.4--Experimental ω-β diagram for the circuit shown in Fig. 7.3. with the dimensions given in Table VII.1 as set no.1. The dotted line represents the fast cyclotron wave on a beam which has $u_o/c = 0.14$ and a magnetic field of 715 gauss.

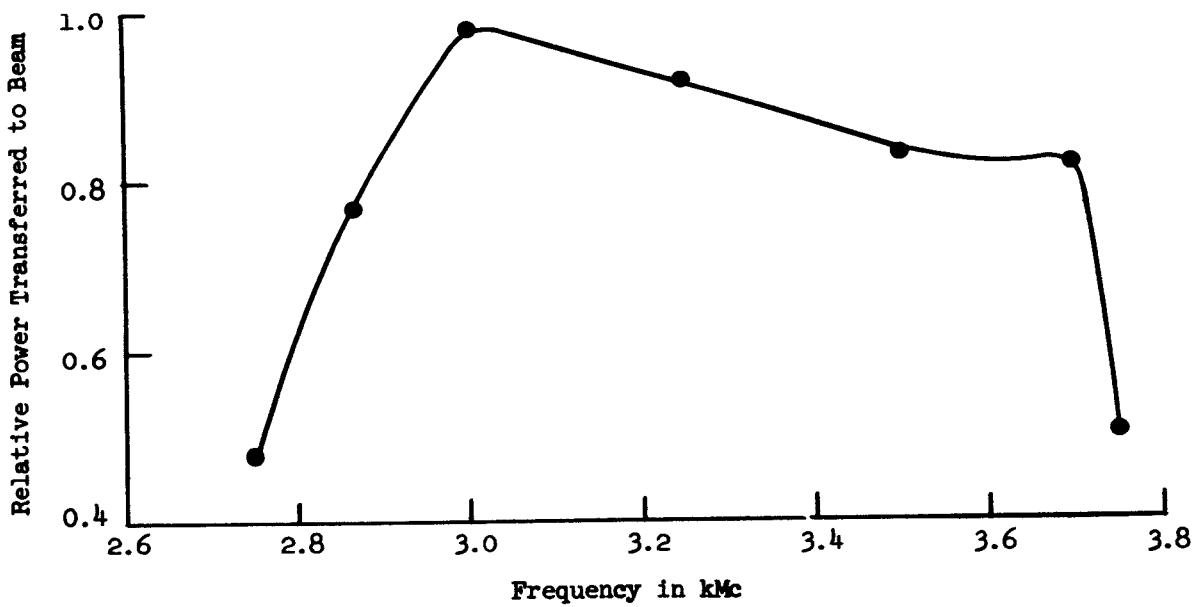

FIG. 7.5--The frequency response of a fast cyclotron wave coupler. The circuit dispersion characteristic was shown in Fig. 7.4. The circuit is taken to be 16 periods (6 in.) long and the bean voltage and current are 5000 volts and 0.5 Amperes, respectively.

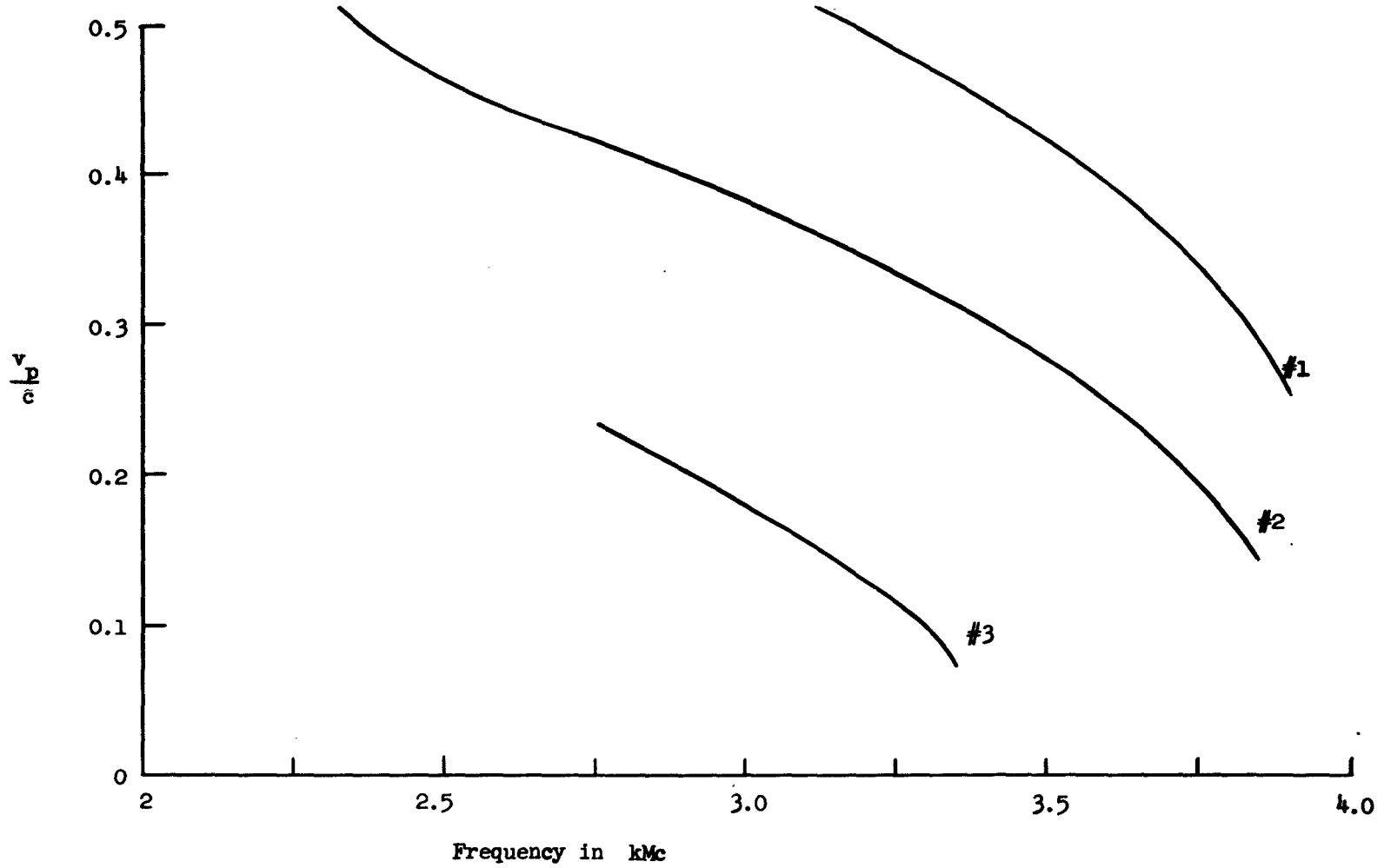

FIG. 7-6--The phase velocity of several transverse field circuits of the type shown in Fig. 7.3. The dimensions are given in Table VII.1.

to compute the dependence of the coupling coefficient upon the frequency. The impedance of the circuit was determined by the perturbation procedure described in Appendix B, and from this the coupling coefficient may be calculated by means of (2.17). Finally, the response of a co-directional type of coupler can be calculated by means of (2.23). The result of these calculations is shown in Fig. 7.5. This shows the efficiency of transfer of power from the circuit to the beam as a function of frequency. It is apparent that an overall bandwidth of 25 per cent is easily obtained in a parametric amplifier which consists of two of these couplers and a frequency-insensitive pumping section.

A comparison of the measured impedance of the above circuit with the impedance of the idealized circuits described previously is summarized in the table below. The values of the idealized impedances are half those

βa	Experimental $K_t\ v_g/c$	$\frac{1}{2}$ Idealized $K_t\ v_g/c$	$\frac{1}{2}$ Idealized $K_\ell\ v_g/c$
0.39	81	300	11
0.79	14	38	7
1.08	0.6	11	3

shown in Fig. 7.2 to account for linear polarization. We see that this circuit has yielded impedances which are greater than those of the idealized longitudinal field circuit, and that much more improvement should be possible before the upper bound imposed by the idealized transverse field circuit becomes a limitation. An experimental circuit to be described later has a smaller ratio $2a/p$, which results in impedances much closer to the theoretical limit.

Some dispersion characteristics for several different circuit dimensions are shown in Fig. 7.6. The primary factor in changing the phase velocity of the circuit is the period p. In fact, if we compare circuits at the same phase shift per period, the phase velocity is directly proportional to the period.

The circuits represented by the data in Fig. 7.6 were designed to couple to the fast cyclotron wave and consequently the variation of the

phase velocity with frequency is desirable. In order to obtain broad-band excitation of the synchronous waves, the structures should be modified to obtain a phase velocity which is essentially constant over a wide frequency range. One way of accomplishing this is to lower the lower cutoff frequency of the circuit. It would probably be necessary to reduce the period of the circuit at the same time in order to lower the phase velocity of reasonable values for the beam velocity.

A device which utilized linearly polarized synchronous-wave couplers to excite both synchronous waves will be described in the next chapter. The particular requirements call for a resonated rather than a traveling-wave circuit. It was decided to employ interaction with a space harmonic in a circuit rather than the fundamental in order to avoid the small periodicities which would be involved in obtaining a fundamental field component with a phase velocity of approximately one-tenth of the velocity of light. It will be recalled that the phase velocities of the space harmonic field components are given by

$$\frac{v_{pn}}{v_{p0}} = \frac{1}{1 + \frac{2n\pi}{\beta_0 L}} \quad , \tag{7.1}$$

where

v_{pn} = phase velocity of n^{th} space harmonic,

v_{p0} = phase velocity of fundamental component,

n = order of the space harmonic, and

$\beta_0 L$ = phase shift per period for the fundamental component.

The dimensions and the ω-β diagram for this structure are shown in Fig. 7.7. The figure also shows the ω-β curves for the transverse waves on a 3,000 volt beam. It is evident that, unless a very long coupler is used, both the $n = +1$ and the $n = -1$ space harmonics will interact with the synchronous waves. This was in fact the case in the

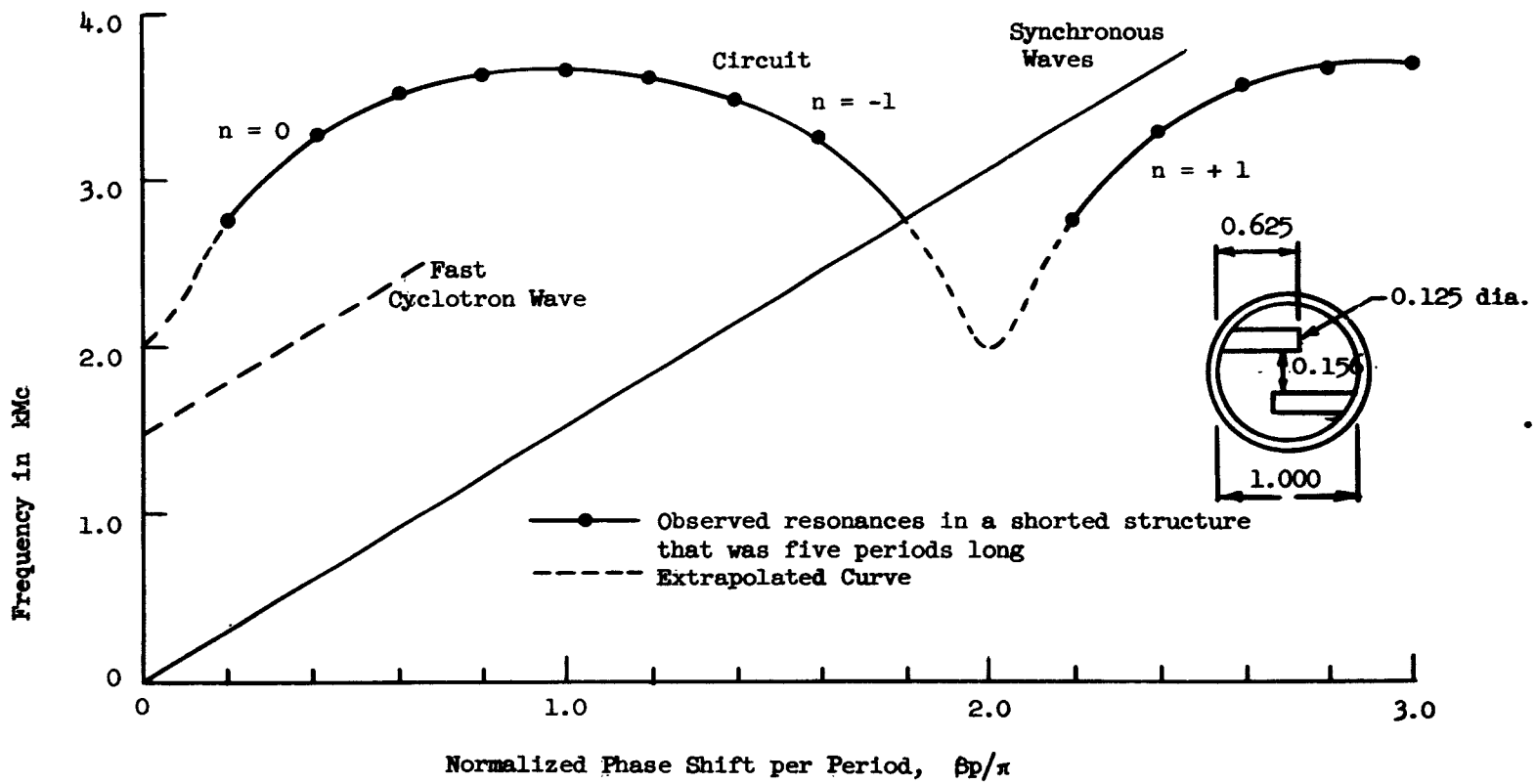

FIG. 7.7--The $\omega - \beta$ diagram for a space-harmonic synchronous wave coupler. The straight line represents the synchronous waves on a 3000 volt beam. The significant dimensions of the circuit are also shown.

experiments, and is desirable since it means that the effective interaction impedance of the circuit will be larger than it would be if only one space harmonic interacted strongly with the beam. The figure also shows that it is necessary to choose the magnetic field so that the fast cyclotron wave does not couple strongly to the fundamental field component of the circuit.

The synchronous wave coupler based on the above circuit was a resonant cavity made by placing shorting planes at each end of a structure which was five periods long. The transverse electric field amplitude on the axis of the cavity was measured by means of a perturbing needle and the results are shown in Fig. 7.8 for the mode in which there is $\pi/5$ radians phase shift per period. This mode was used because of the strong transverse fields near the lower cutoff of the circuit. It is found that only the first few space harmonics have large amplitudes and the field pattern can be matched quite well with the fundamental and two space harmonic components of the field. The dashed curve in Fig. 7.8 shows the result of this procedure. It is seen that the space harmonics corresponding to $n = \pm 1$ in (7.1) are of approximately equal amplitude. This can be altered by changing the ratio of the pin diameter to the period. However, this was not done here since, as will be seen in Chapter VIII, both space harmonics take part in the interaction for which the coupler had been designed. A summary of the characteristics of these resonant synchronous wave couplers, operating in the $\pi/5$ mode, is given below.

TABLE VII.2

SUMMARY OF SYNCHRONOUS-WAVE COUPLER CHARACTERISTICS

Mode of Operation (Phase Shift Per Period)	$\pi/5$ Radians/Period
Frequency	3.00 kMc
Group velocity	0.256c
Phase velocity	
fundamental	0.995c
- 1 space harmonic	0.110c
+ 1 space harmonic	0.090c
Impedance	
fundamental	1700 ohms
- 1 space harmonic	3.4
+ 1 space harmonic	2.5

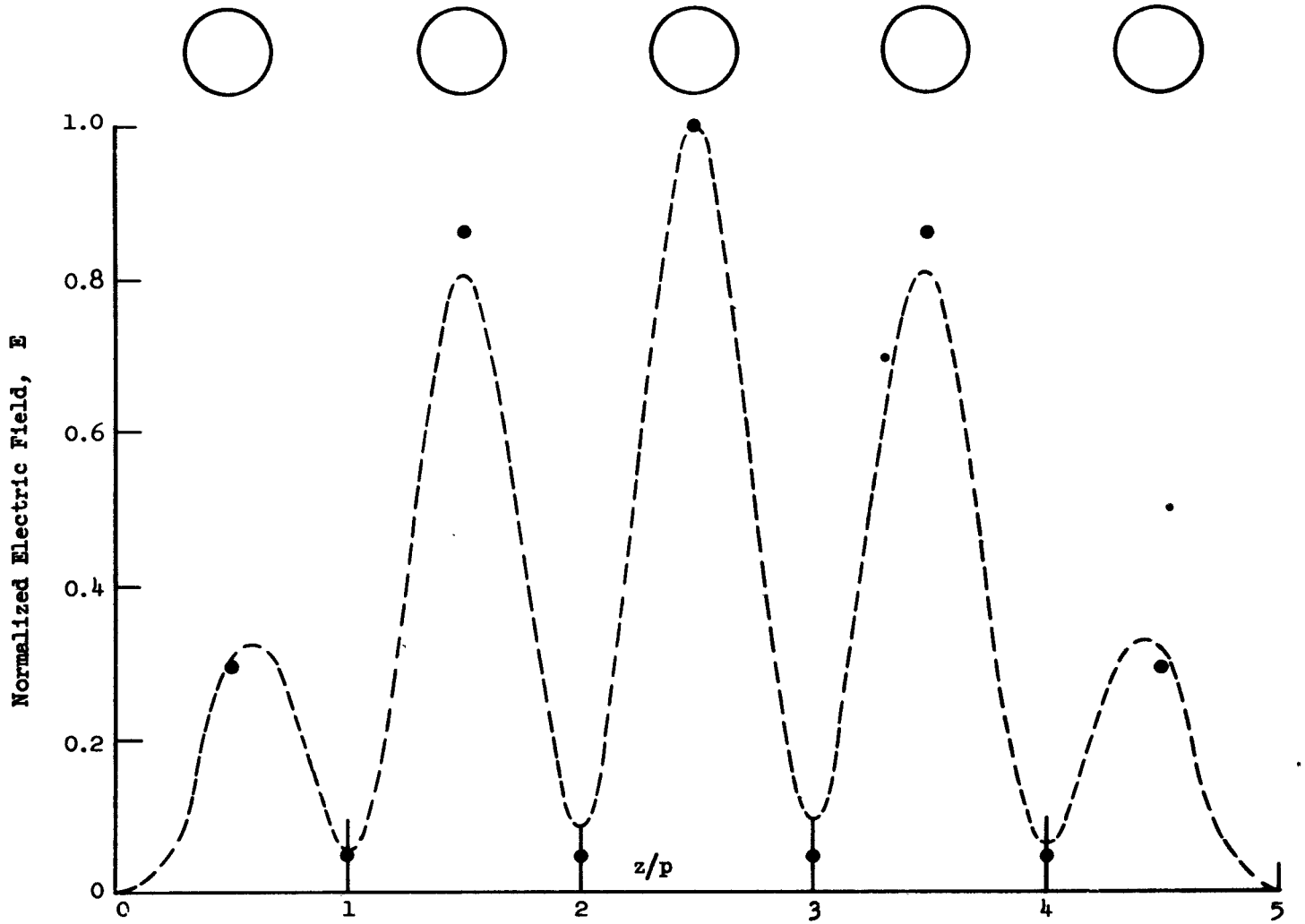

FIG. 7.8--The transverse electric field distribution for the $\beta p = \pi/5$ mode in the coupler shown in Fig. 7.7. The small circles are experimental points and the curve is calculated from the normalized space-harmonic representation $E = [0.55 \sin \pi/5\ z/p + 0.22 \sin 9\pi/5\ z/p - 0.23 \sin 11\ \pi/5\ z/p]$. The vertical lines on the experimental minima indicate the possible error in this region. The large circles show the positions of the rods which make up the circuit.

Note that the experimental value of $K_t v_g/c$ for the fundamental component of this mode is approximately 435 as compared to a value of about 700 for one-half of the idealized value for a circularly polarized circuit that is obtained by extrapolating the curve in Fig. 7.2.

In the design of a space harmonic coupler it is desirable to adjust the shape of the transverse field amplitude so that the interaction impedance for that space harmonic is made as large as possible. A good estimate of the optimum dimensions for the type of circuit under consideration here can be made, and it is shown in Appendix C that the proper relation between the pin diameter and the period is approximately

$$d = p \quad \text{if} \quad \beta_k p < 2.33$$

$$\beta_k d = 2.33 \quad \text{if} \quad \beta_k p \geq 2.33 \ ,$$

where

d = pin diameter ,

p = circuit period , and

β_k = space harmonic propagation constant .

It has been assumed here that the transverse field gap between the pins, $2a$, is small so that $(\beta_k a)^2 << 1$. This will usually be the case so that the above results offer a satisfactory guide to the design of circuits in which space harmonic interaction is desired.

3. Twisted Circuits

A discussion of beam interactions with circuits which were twisted about their axis was given in Chapter IV, and it was noted that twisted couplers could be of considerable interest. Some experimental studies of twisted slow-wave structures were carried out in an effort to determine the effect of the twisting on the originally linearly polarized slow-wave structure. Some investigation of twisted periodic circuits

has been carried out by Bernstein and Feinstein,[26] but the twist rates under consideration here are much greater than in their case. The experimental twisted circuits were based on the pin-in-cylinder design described in the previous portion of this chapter. However, in the case of the twisted circuit, each pair of pins is rotated with respect to the previous pair.

The characteristics of the twisted circuits were determined by observing the resonant frequencies and associated field configurations in a structure an integral number of periods long which was terminated at each end by transverse shorting planes. Since the image in the shorting plane is not a continuation of the original circuit, this procedure results in erroneous results unless the twist per period is small. We are instead measuring the characteristics of a resonated twist circuit rather than of an infinitely long structure. Even so, the experiments described give an insight into the nature of the fields in a twisted slow-wave circuit.

It has been noted by others[26] that the primary effect of a gradual twist on the ω-β diagram of the circuit is to lower the frequency for which there is π radians phase shift per period. This was the general trend in the experiments described here. However, if the twist rate is too great, the circuit fields cease to be twisted versions of the fields of the untwisted circuits and a comparison with the untwisted circuit characteristics becomes meaningless.

An example of the field configurations in an experimental twisted circuit is shown in Fig. 7.9. The structure consists of ten sets of pins, each set being rotated by $\pi/8$ radians with respect to the previous set, and is shorted at the two ends to produce a resonant cavity. The field patterns shown would be identified as the ones with 0.2π and 0.3π radians phase shift per period in the case of an untwisted circuit. The field components, which are defined in the figure, were determined by means of a perturbing needle in the transverse plane. By placing such a needle on the axis of the circuit, it is possible to determine both the relative amplitude and the orientation of the electric field. The simple view that the field is simply a twisted version of the field of a linearly polarized circuit would result in $E_\perp = 0$. It was pointed out in Chapter IV that this picture is not correct and that we should expect a

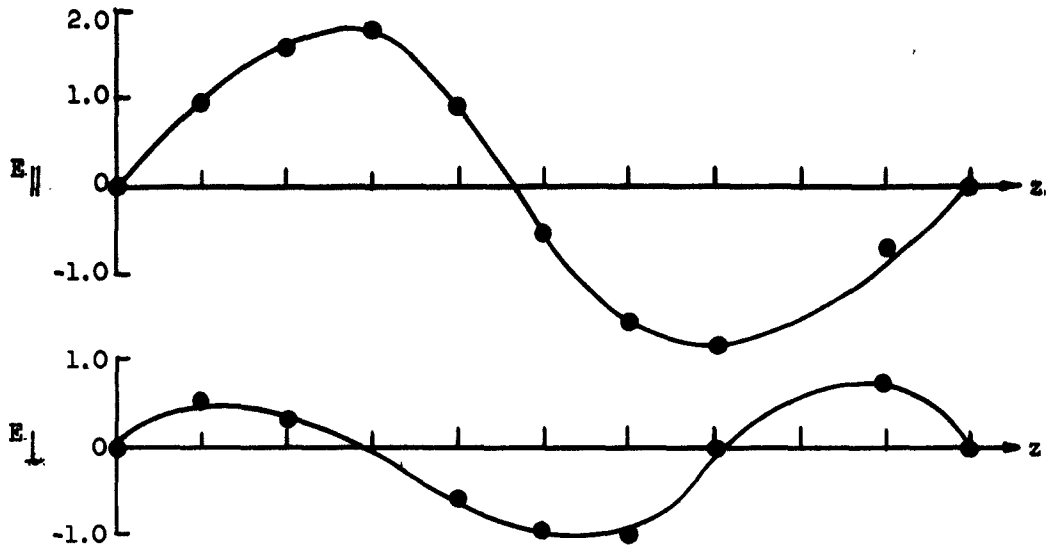

(a) $\beta p = 0.2\pi$ Mode

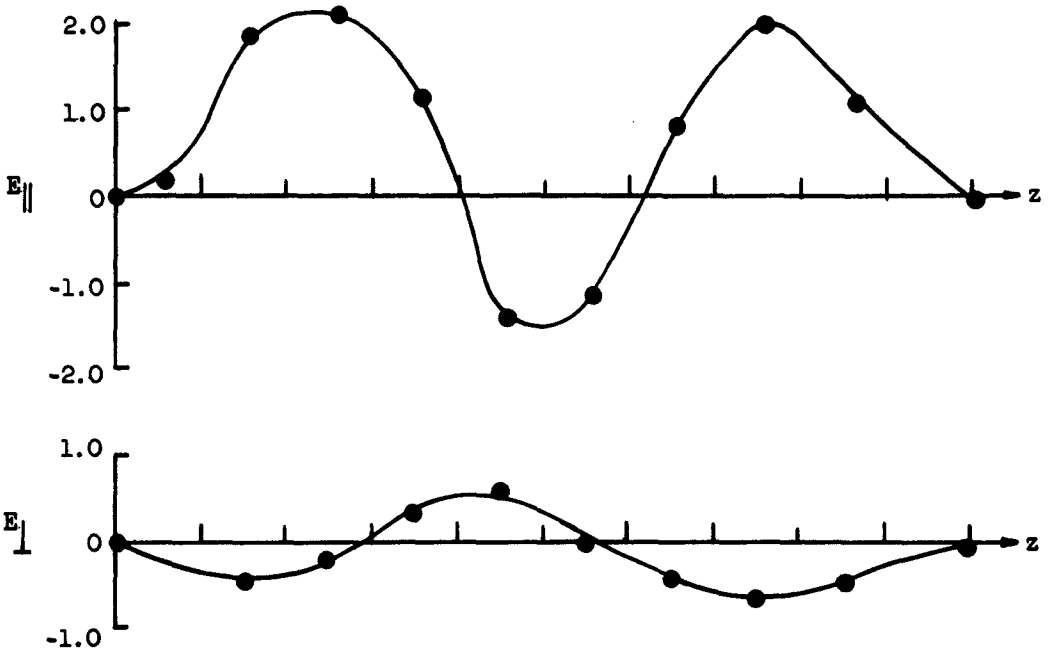

(b) $\beta p = 0.3\pi$ Mode

FIG. 7.9--Experimentally determined field distribution plots for two values of phase shift per period in a twisted resonant circuit, the cavity was ten periods long and the twist per period was π/β radians. The $E_{\|}$ was defined in Chapter IV and corresponds to the twisted field of a linearly polarized structure. The $E_{\perp}$ field is a new field, perpendicular to $E_{\|}$, which arises due to the twisting of the circuit.

new field component ($E_\perp$) to arise, and that the magnitude of this field would be approximately β_t/β_0 times the magnitude of the main field component $E_\parallel$. A comparison between some experimental measurements and the theoretical predictions for the above circuits is given below.

Mode	Theoretical $\frac{E_\perp}{E_\parallel}$	Experimental $\frac{E_\perp}{E_\parallel}$
0.2π	0.62	0.55
0.3π	0.42	0.31

The difference between the experimental and theoretical results may well be due to the fact that these measurements were made in a cavity produced by shorting the twisted structure with transverse planes. The results of Chapter IV do not give a complete picture of what the fields are in this case because the twisted circuit does not have reflection symmetry and consequently the shorting planes give rise to other modes in the cavity. If the cavity is very long or if a nonresonant traveling-wave structure is used, this problem does not arise.

The result of the experimental work described above is that we have verified that the twisting of the slow-wave structure gives rise to the additional field component which is perpendicular to the field expected on the basis of the simple model of the twisted circuit. Consequently, we can say that great care should be taken in using the simple field picture to obtain a description of the interaction as was done in the first sections of Chapter IV, although at small values of β_t/β_0 this model is quite satisfactory.

B. A QUADRUPOLE CIRCUIT

The frequency doublers described in Chapters V and VI require a quadrupole circuit which is, in general, a periodic structure. A circuit which supports a transverse electric field that approximates the required quadrupole configuration is shown in Fig. 7.10 . This circuit is very simply constructed by inserting rods into a cylindrical pipe and

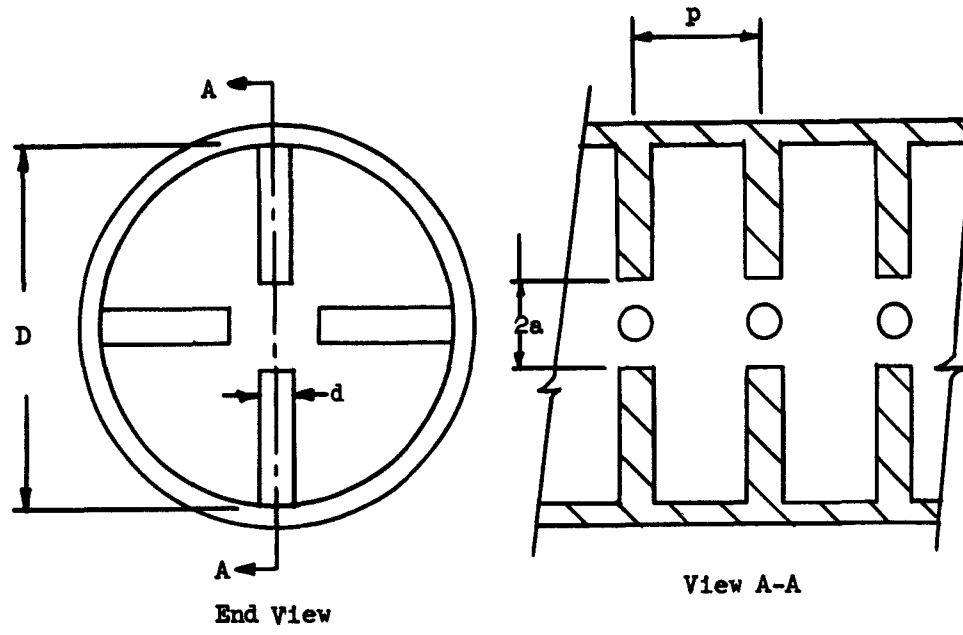

FIG. 7.10--A quadrupole circuit made by inserting rods into a cylinder. The field near the axis approximates the quadrupole field configuration shown in Fig. 5.1. The dimensions of the particular circuit that is characterized by the parameters listed in Table VII.3 are: D = 0.906 , d = 0.094 , p = 0.206 , and 2a = 0.230 .

has good thermal properties and mechanical rigidity. A section of this structure, an integral number of periods long, can be terminated with shorting planes to make the resonant quadrupole cavity assumed in the theoretical discussion of the transverse-wave frequency doublers.

In order to be used in conjunction with the couplers described previously, the quadrupole shown in Fig. 7.10 was designed to propagate in the frequency range around 6.0 kMc . The ω-β diagram for a typical quadrupole circuit is much the same shape as the one shown in Fig. 7.7. The upper cutoff frequency occurs when the rods are approximately one-quarter of a wavelength long just as in the case of the coupler circuits. The longitudinal electric fields are strong in this case, since each rod is π radians out of phase with its neighbors, and this results in weak transverse wave interaction near the upper cutoff frequency. On the other hand, there are no longitudinal fields at the lower cutoff frequency since the phase shift per period is zero. Consequently the extraneous stored energy is a minimum near the lower cutoff frequency and the transverse-wave interaction is strongest in this region.

The cavity under consideration was designed to be used in a synchronous-wave frequency doubler and consequently the phase velocity of a component of the field should be equal to the beam velocity. In order to avoid small periodicities the circuit was designed to employ space harmonic interaction. The amplitude of the quadrupolar field was determined by means of a transverse perturbing needle, and the field configuration of the $\pi/5$ mode of the circuit shown in Fig. 7.10 is given in Fig. 7.11. This mode was chosen for the doubler experiments because it has appreciable space-harmonic content and has a relatively large interaction impedance since it is near the lower frequency cutoff of the circuit. The impedance of the quadrupole is determined from the frequency perturbation data in the manner described in Appendix B. The results of the space harmonic analysis and impedance calculations for the $\pi/5$ mode of this quadrupole cavity are summarized in the table below.

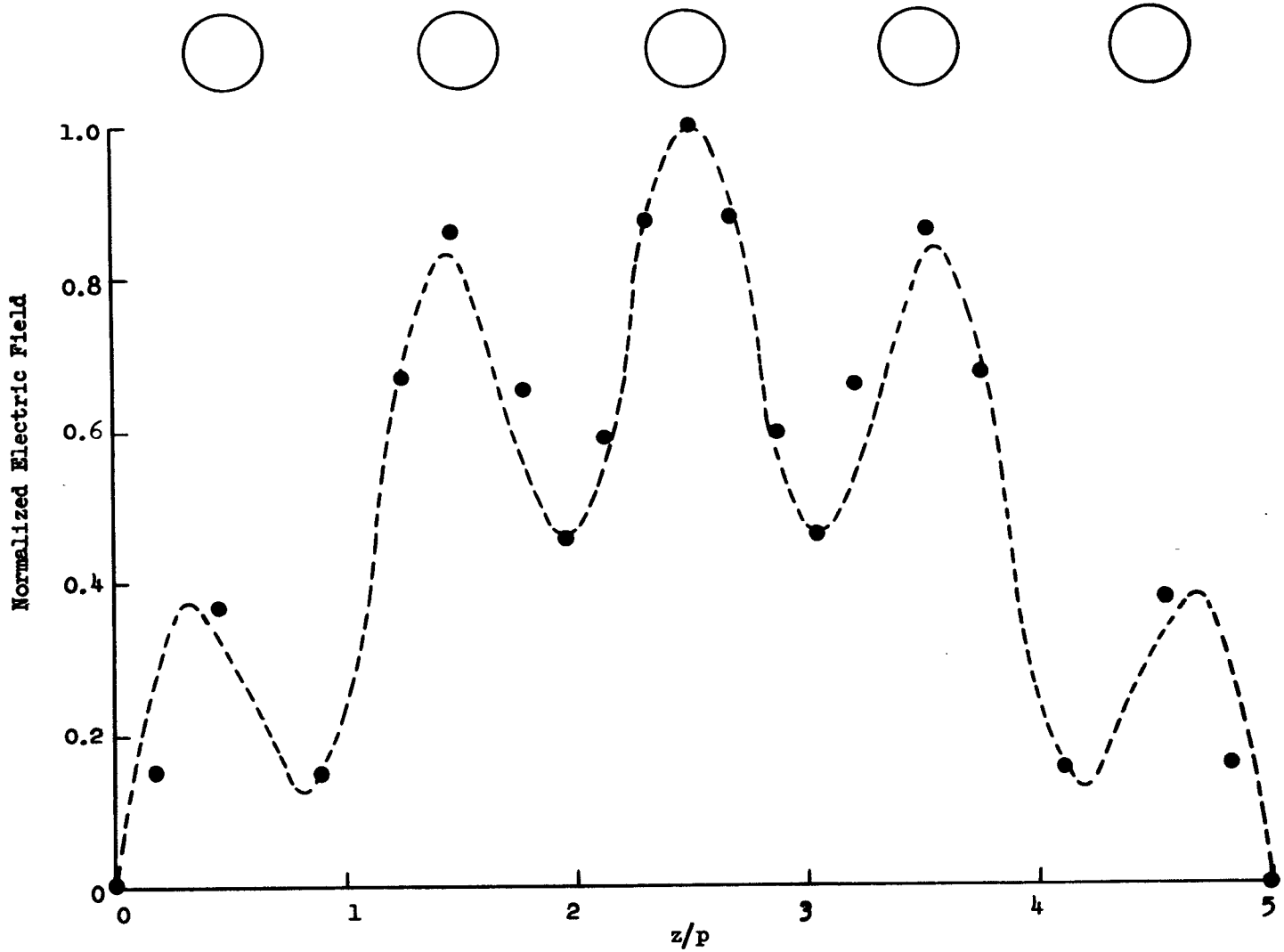

FIG. 7.11--The transverse electric field distribution for the $\beta p = \pi/5$ mode in the quadrupole cavity shown in Fig. 7.10. The small circles are experimental points and the curve is calculated from the normalized space-harmonic representation $E = [0.75 \sin \pi/5\ z/p + 0.25 \sin 9\pi/5\ z/p]$. The large circles show the positions of the rods that make up the circuit.

TABLE VII.3

SUMMARY OF QUADRUPOLE CHARACTERISTICS

Mode (Phase Shift Per Period)	$\pi/5$
Frequency	5.70 kMc
Phase Velocity	
fundamental	0.940c
- 1 space harmonic	0.105c
Quadrupole Resistance (15 Periods Long)	
fundamental	1080 ohms
- 1 space harmonic	120 ohms

CHAPTER VIII

AN EXPERIMENTAL TRANSVERSE-WAVE DEVICE

Several of the transverse-wave interactions which have been considered in the earlier part of this report are quite interesting, and the purpose of this chapter is to describe some experimental studies of these cases. One group of devices which promises to have some useful applications are those employing the active frequency doubling schemes described in Chapters V and VI. These are of particular interest since the efficiency of the frequency conversion may be large, and can in fact exceed one hundred per cent. A second device that is of importance is the synchronous wave klystron described in Chapter III. As was noted there, this amplifier has the advantages of the usual extended interaction klystron, but does not have some of the same limitations.

Thus, a single device that would allow the investigation of both the synchronous-wave klystron and one of the active frequency doubling schemes would be quite interesting. This may be done simply by employing two resonant synchronous-wave couplers followed by a quadrupole cavity. An experimental tube that was designed in this way is described in Section A below. Then the experimental results of a study of both the synchronous-wave klystron and a synchronous-wave frequency doubler are presented. In addition, the fast cyclotron-wave doubling interaction was observed and the experimental ω-β characteristic for the fast cyclotron wave was measured. Finally, the observation of oscillations in both the quadrupole and coupler cavities, for particular focusing conditions, is reported.

A. DESCRIPTION OF THE DEVICE

It was pointed out above that it is possible to design a composite transverse-wave tube, consisting of two synchronous-wave couplers and a quadrupole cavity, which will allow the investigation of both the synchronous-wave klystron and the synchronous-wave frequency doubler. A

schematic diagram of the composite transverse-wave tube is shown in Fig. 8.1. The first section of the tube is a synchronous-wave klystron which consists of two resonant synchronous wave couplers that are oriented so that their planes of polarization are perpendicular to each other. It was shown in Chapter III that this is the requirement for maximum gain. The couplers are followed by a linearly polarized quadrupole cavity that couples to both synchronous waves. This is a synchronous-wave frequency doubler of the type described in Section B.3 of Chapter VI. The quadrupole cavity is oriented as shown in the figure so that the synchronous waves excited by the couplers will have the proper input phase to yield maximum doubler conversion efficiency.

The synchronous wave couplers that were used in the device described above are the resonant transverse-field cavities described in Chapter VII and the important characteristics are given in Table VII.2. The coupling to the cavities consisted of an external transmission line as shown in Fig. 8.2. The transition between the coaxial line and the strip transmission line yielded a standing-wave ratio of less than 1.1 over the frequency range of interest when the strip-line was terminated in its characteristic impedance. The iris dimensions were adjusted so that the cavity was critically coupled to the external circuit in the cold tests. Unfortunately an error was made in these tests and the cavity was actually overcoupled. It is desirable to have the cavity critically coupled since, as was shown in Chapter III, the beam loading is zero in a linearly polarized synchronous-wave coupler. The improper coupling indicated above can be corrected by means of external tuning, but even so, the extra energy associated with the mismatch results in a reduction of the interaction impedance. For example, the interaction impedance of an exact replica of the couplers in the tube was 570 ohms for the fundamental field component in the $\pi/5$ mode as compared to 1700 ohms shown in Table VII.2.

Since three resonant cavities are involved in the tube, it was necessary to make two of them tunable so that all three would be resonant at the same frequency. The coupler cavities are identical in design so that it was most efficient to put the tuning mechanisms in these cavities. The resonant frequency of the coupler was varied by means of a tuning plunger. In this way the resonant frequency could be varied between 2.80

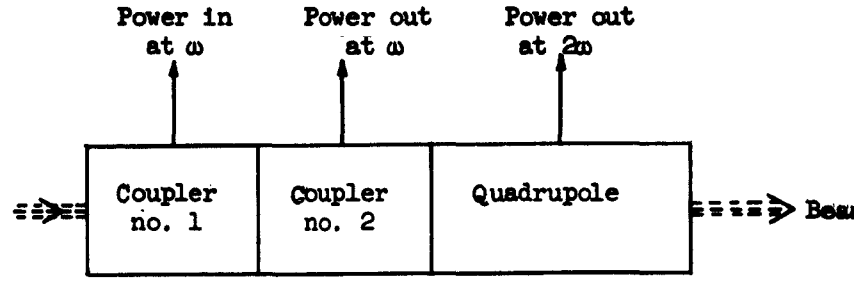

(a)

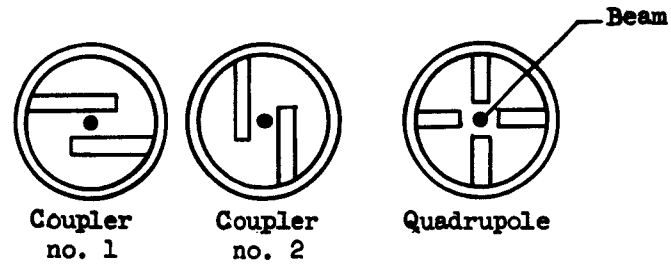

(b)

FIG. 8.1--(a) a schematic diagram of the device used to investigate some of the transverse wave interactions; (b) a cross section of each of the cavities so that the relative orientation of the periodic structures may be seen.

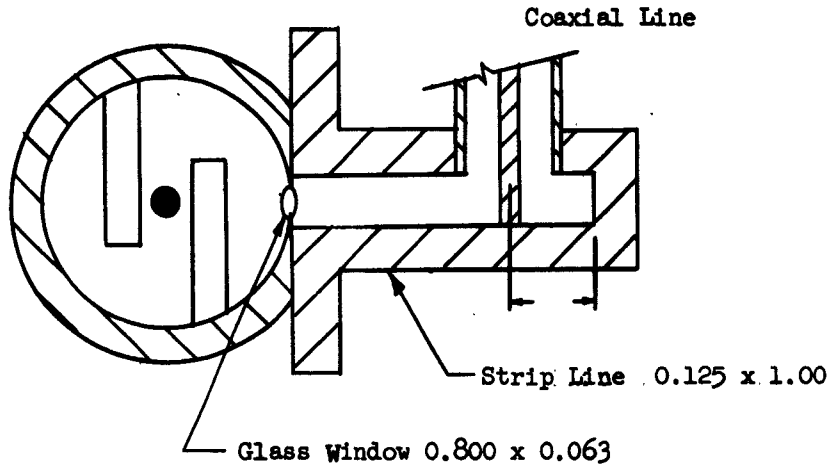

FIG. 8.2--The coupler cavities were coupled to the external circuit by means of the glass window and strip line shown. The distance d was adjusted to give the best transition from the coaxial line to the strip line.

and 3.00 kMc without appreciably affecting the interaction impedance. A photograph of an assembled coupler is shown in Fig. 8.3 and the tuning plunger can be seen clearly. The shorting plates which cover the ends of the cavity are omitted in the photograph.

The quadrupole cavity that was used in the tube is based on the circuit described in Section B of Chapter VII and the important characteristics for the resonant mode used in the interaction are given in Table VII.3. The actual quadrupole was fifteen periods long, or twenty-seven half-wavelengths long for the space harmonic component of the field, and was resonant at 5.69 kMc in the $\pi/5$ mode. The cavity was coupled to the external circuit by means of the same windows used for the coupler cavities, but in this case the external transmission line was a waveguide. The cavity was critically coupled to the external circuit in order to achieve maximum second harmonic power output. Equation (6.40) shows that this is the optimum condition. A photograph of two quadrupole cavities without the shorting end plates is shown in Fig. 8.4.

The electron gun employed in this tube provided a Brillouin flow beam. The use of this kind of focusing is generally desirable in synchronous wave devices which employ parametric interaction since, as was pointed out at the beginning of Chapter II, such a beam has no initial zero frequency synchronous wave excitation. To avoid dissipation problems the beam voltage was pulsed. Typical operating characteristics for the beam were:

Beam voltage	3000 volts
Beam current	0.230 Ampere
Beam diameter	0.070 in.
Theoretical Brillouin flow field	600 Gauss

The focusing conditions were not found to be critical and it was possible to vary either the voltage or the magnetic field in order to observe the characteristics of the various interactions without giving rise to current interception in a beam tunnel about 0.160 in. in diameter and eight in. long.

A photograph of the assembled tube is shown in Fig. 8.5. The tube was assembled by brazing the three cavities together and, therefore,

FIG. 8.3 -- A photograph of an assembled coupler cavity showing the tuning mechanism. The end plates, which have a beam aperture, have been omitted for clarity.

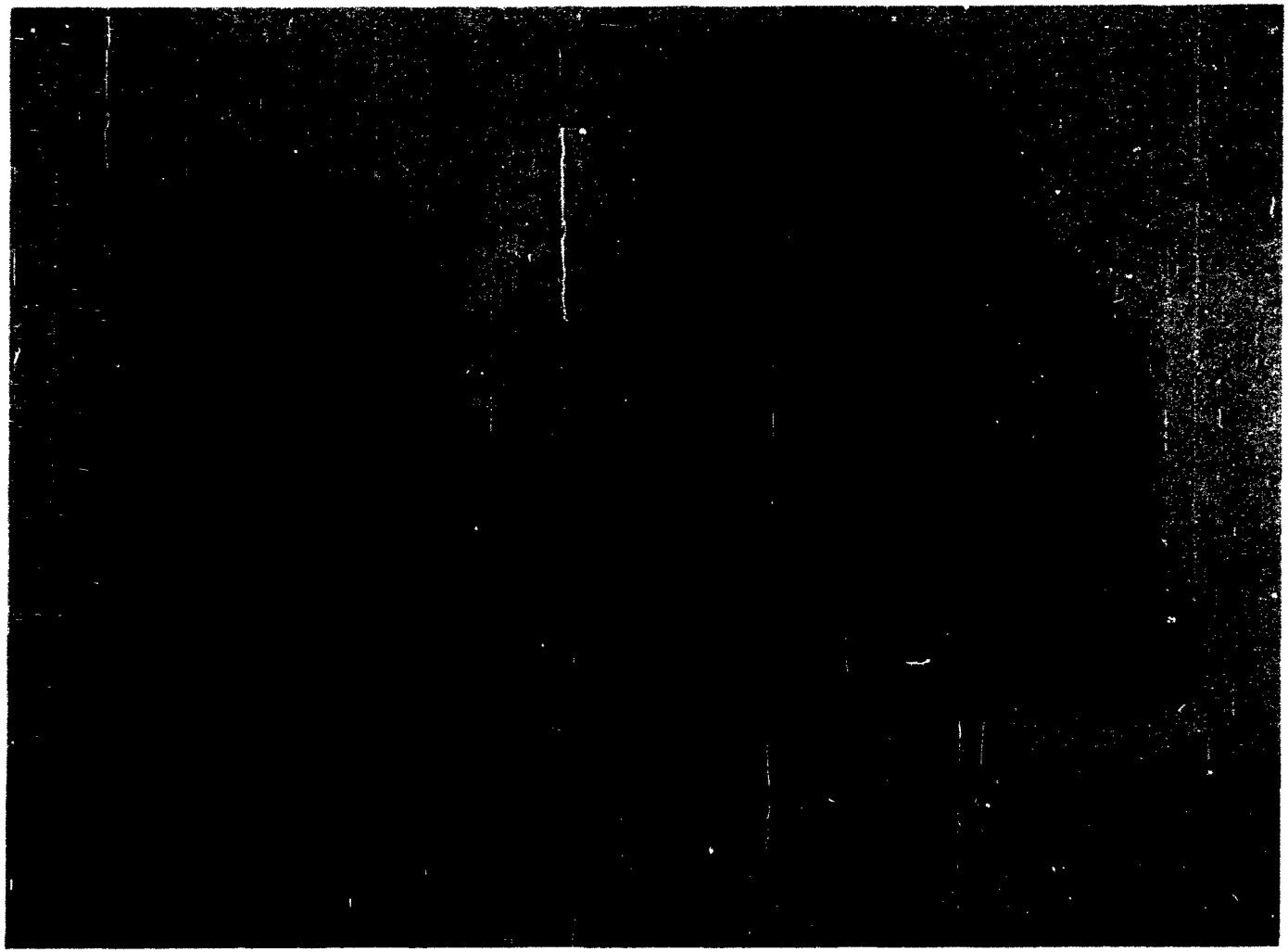

FIG. 8.4 -- A photograph of two quadrupole cavities. The window assembly and waveguide adapter are shown in the cavity on the right. The dark area in the iris region is some excess glass on cavity. The end plates have been omitted for clarity.

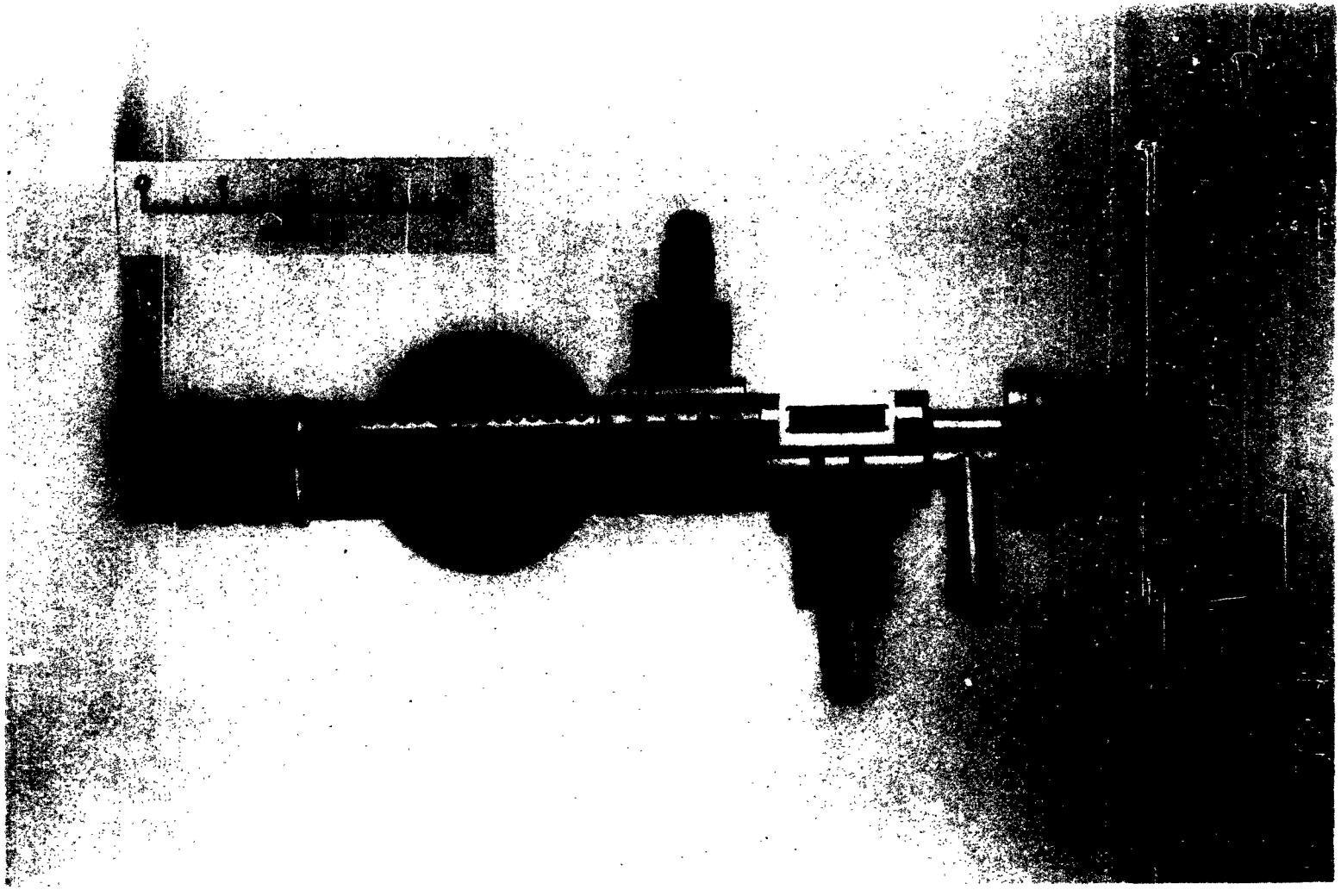

FIG. 8.5 -- A photograph of the assembled tube before evacuation. The external tuning assemblies and the coupling iris in the coupler cavities can be seen clearly.

there was no dc isolation between the cavities and the gun anode. However, the collector was isolated so that beam transmission through the rf portion of the tube can be determined.

B. AMPLIFICATION BY MEANS OF SYNCHRONOUS WAVES

As mentioned previously, the two coupler cavities of the device described above form a synchronous-wave klystron. The experimental observation of amplification in this device is reported in this section and a comparison with the theoretical characteristics is made.

The expected gain of the synchronous-wave klystron can be calculated from Eqs. (3.48) and (3.52). Since several space harmonics are involved in the interaction it is necessary to replace KM_3 in this expression with the sum of these terms due to each space harmonic as indicated in Section A of Chapter III. The important coupler parameters that are used in calculating the gain were given in Table VII.2. However, as noted above, the impedance in the table must be multiplied by 0.33 in order to obtain the tube cavity impedance due to the window design error. The calculated gain of the tube is found to be 13 db at the optimum synchronization condition. The frequency of operation is immaterial as long as it is within the tuning range of the cavities. Unfortunately, the tuning mechanism in the second coupler cavity became jammed after a few tuning adjustments, and after this the resonant frequency of the cavity had to be varied by means of an external tuner. This has no effect on the klystron experiment under discussion here, but does present difficulties in the frequency doubling experiments to be described in the next sections.

The gain characteristics of the synchronous-wave klystron are shown in Fig. 8.6. The power has been corrected for coaxial line loss and insertion loss due to a slight mismatch at the input cavity. Therefore the input and output power represent the actual power entering and leaving the terminals of the strip-line adaptors on the cavities. The peak rf power was measured by means of calibrated crystal and attenuators. The gain of the tube at small signal levels is seen from Fig. 8.6 to be 7.9 db. We have shown above that the expected gain is about 13 db. The discrepancy is probably due to the fact that the beam is of finite diamter and that the circuit fields are not uniform across the beam. The error

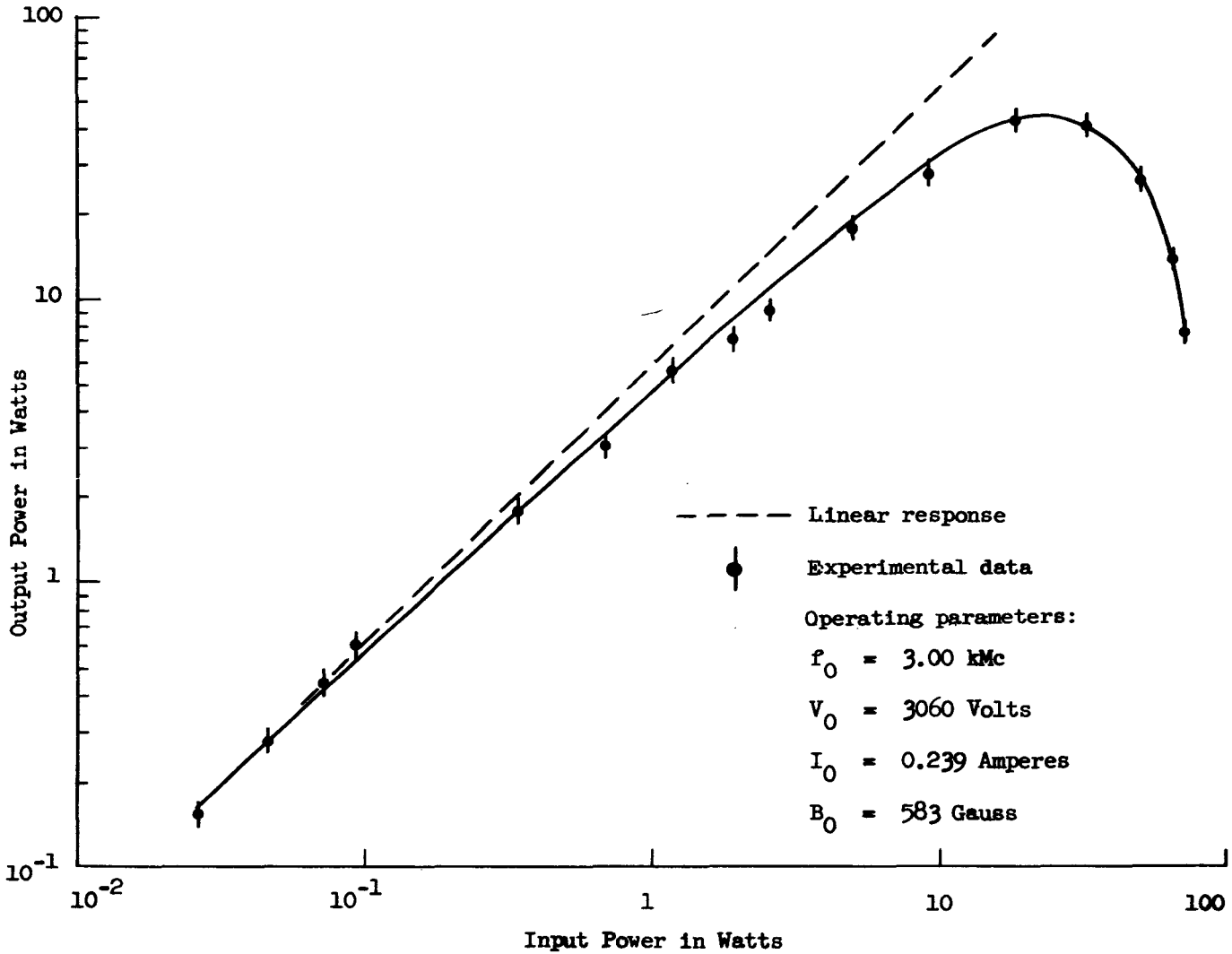

FIG. 8.6--A plot of the output power of the synchronous-wave klystron as a function of the input power. The operating parameters are shown in the table in the figure.

here is rather large and is an indication that the solution of the thick beam problem should yield some significant changes in the quantitative description of transverse-wave devices.

It is evident from the experimental data that the amplifier gain becomes dependent upon the input power at a lower level than might be expected. The fraction of the current that is intercepted on the cavity structure is shown in Fig. 8.7. It is apparent that the gradual decrease in gain which occurs below about ten watts is not a result of current interception. The small-signal theory presented in Chapter III predicts a constant gain. It is rather certain that the effect observed here can be explained in terms of a beam model which is more realistic than the filamentary beam description. That is, the large signal gain characteristics are determined by the beam diameter and the nature of the variation of the circuit fields which act on the beam as it makes large excursions.

The rapid reduction of the gain which occurs above about ten watts of input power is due to beam interception. The expected power level at which current interception will begin can be computed from Eqs. (2.20). The beam, which has both synchronous waves excited on it in the input coupler, will begin to strike the output coupler circuit when the maximum excursion exceeds 0.043 in. This is the radius of the circuit beam hole minus the radius of the beam. On this basis, the maximum power which can be carried by each synchronous wave without interception is 32 watts. Since both the input and output couplers are identical, we see from (3.48) and (3.52) that the input coupler gain is one-fourth of the square root of the total gain when the output coupler is critically coupled to the external circuit as it is here. By using the actual gain curve, we calculate that the interception shown in Fig. 8.7 begins at a power of about 4.5 watts on each synchronous wave. This is considerably less than the 32 watts calculated above, and may be due to inaccurate knowledge of the beam diameter. Some of the discrepancy may also be a consequence of violations of the filamentary beam model.

The dependence of the gain of the synchronous-wave klystron on the various parameters of the system was also investigated. The beam current could be varied over a small range by changing the control electrode on the gun. A plot of the observed power output as a function of the beam

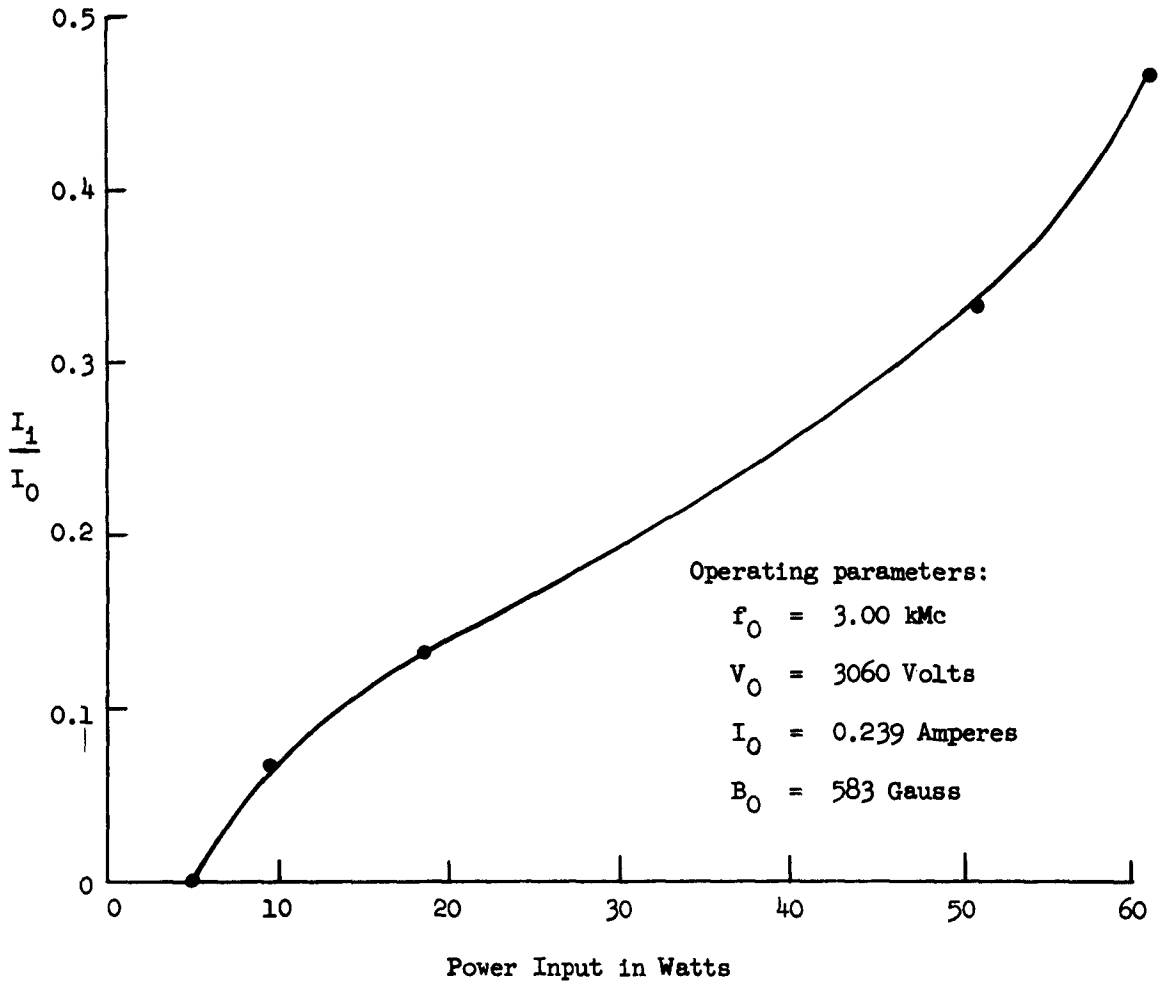

FIG. 8.7--Intercepted current as a function of the input power for the synchronous wave klystron. The operating parameters are shown in the table in the figure.

current is shown in Fig. 8.8. The input power was constant in this experiment. Equations (3.48) and (3.52) show that the output should be proportional to the square of the beam current and the curve drawn in the figure shows that the experimental data have this same behavior. We also see that the output power should be inversely proportional to the square of the magnetic field. The experimental data shown in Fig. 8.9 verify that this is approximately true. The rather large discrepancy between some of the data points and the inverse square law trend may well be due to the changing dc beam configuration as the magnetic field is varied.

The variation of the gain of the amplifier with the beam velocity is of interest also. Figure 8.10 shows a photograph of the power output of the second coupler as the beam voltage is swept through the value for synchronism. The amplitude of the lower trace is proportional to the output power while the height of the second trace above the base line is proportional to the input power. No correction for external transmission line loss has been included here so that the apparent gain is smaller than the actual tube gain. A detailed discussion of the shape of this response is given in the next paragraph. The voltage was varied by adjusting the peak beam voltage so that the synchronous-wave interaction took place during the decaying portion of the voltage pulse. The transient phenomenon at the right hand end of the traces is due to the trigger pulse which initiates the beam voltage pulse and is not associated with the electronic behavior of the tube. The third trace from the bottom represents on the same power scale as before, the power reflected from the input coupler. The upper trace represents this same reflected power which has been amplified to show more detail. The coupler is matched to the external circuit with the beam turned off and so the trace to the right of the trigger disturbance represents zero reflected power. There is a reflection as soon as the beam voltage is turned on and this is due to the interaction between the fast cyclotron wave and the fundamental component of the coupler field. The magnetic field has been adjusted so that the real part of the beam admittance, due to the fast cyclotron wave, is zero, and therefore we do not observe any transmission through the tube due to this interaction. We see that there is no significant reflection from the input

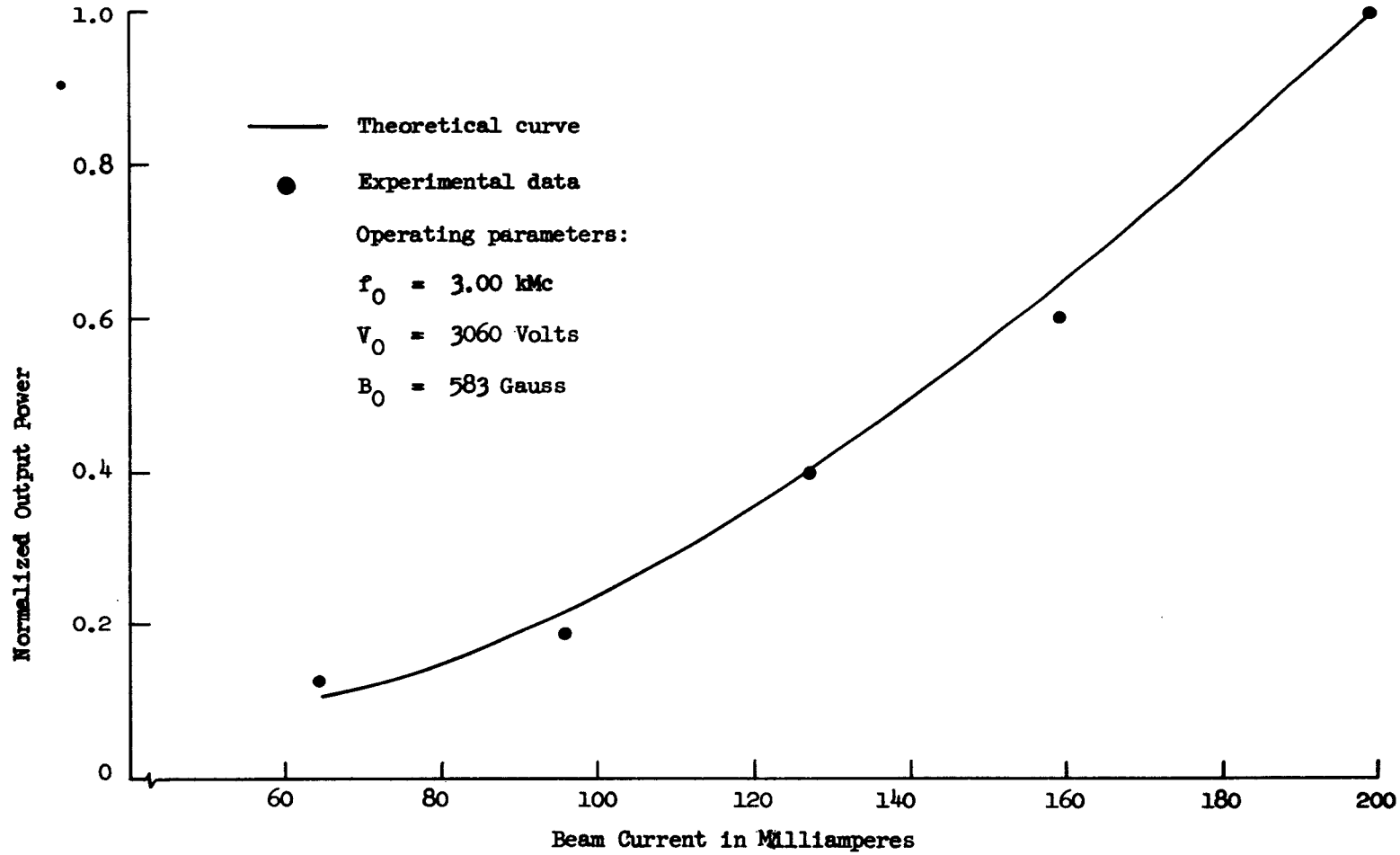

FIG. 8.8--The normalized power output of the synchronous-wave klystron as a function of the beam current for a fixed power input. The theoretical curve has been normalized to pass through the experimental point at 199 ma.

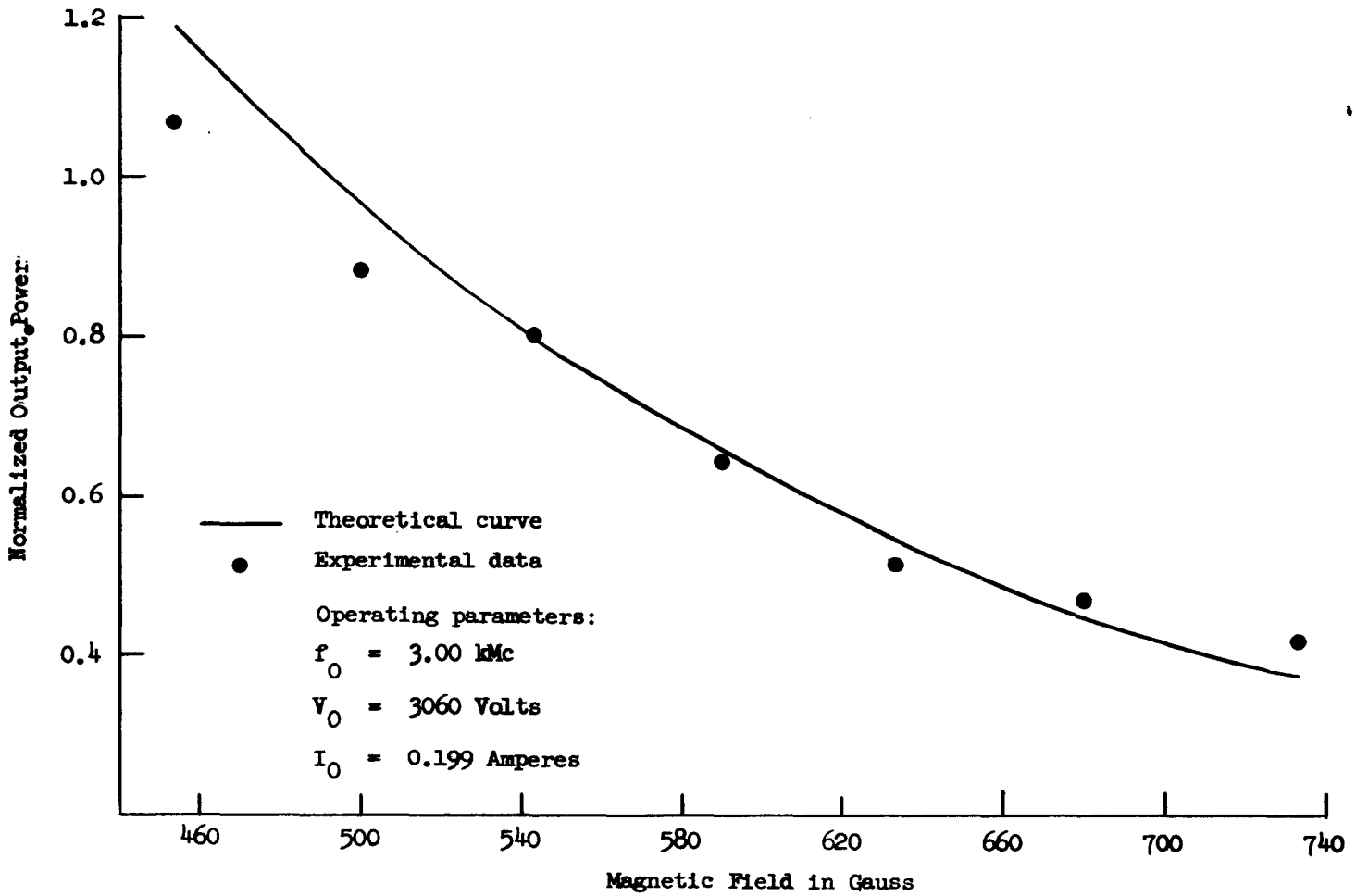

FIG. 8.9--The normalized power output of the synchronous-wave klystron as a function of the magnetic field for a fixed power input. The theoretical curve has been normalized to pass through the experimental point at 583 Gauss.

FIG. 8.10 -- A photograph of a series of oscilloscope traces showing some of the synchronism characteristics of the synchronous-wave klystron. The traces, lettered from the bottom, represent: (a) output power, (b) input power, (c) reflected power from input coupler, and (d) the reflected power amplified. The apparent gain is less than the actual net gain due to external circuit losses.

coupler which can be associated with the synchronous wave gain shown in the lower trace. This verifies that the two synchronous waves do indeed have very nearly the same phase velocity since, if this were not the case, there would be some observable beam loading. It is true that we can see some fluctuation of the reflected power in the amplified trace and this is evidence that the synchronous waves may not have exactly the same phase velocity. A more thorough investigation of this point is not feasible with this device since the nature of the beam motion is not well known, nor can the voltage and current be controlled independently over a very wide range due to the electron optics in the gun region. It should be noted that the small bump on the left side of the synchronous wave interaction is due to the interaction between the fast cyclotron wave and the space-harmonic fields of the coupler.

A detailed study of the dependency of the gain upon the beam velocity was made so that the gain curve could be compared with the theoretical predictions. The gain as a function of the beam voltage was measured carefully. It was not feasible to keep the beam current constant during this experiment due to the defocusing effect of the focusing electrode when it was used as a grid. Figure 8.11 shows the normalized gain as a function of the beam velocity. The beam velocity plotted here does not include the space-charge reduction. However, the theoretical gain curve has been shifted to include space charge by means of the standard expressions relating the beam voltage and velocity such as are given by Chodorow and Susskind.[37] The data have been corrected so that they represent a beam of constant dc resistance. This is for convenience in the calculations, and the correction is done by assuming that the experimental dependence on the beam resistance is the same as the theoretical dependence. It is seen that the agreement between the theoretical and experimental results is quite good. The fact that the experimental curve is slightly broader than the theoretical prediction may well be due to a small separation in the phase velocities of the two synchronous waves, or perhaps to a velocity distribution of the electrons in the beam.

The experimental results which have been described above show that the synchronous-wave klystron is indeed a realistic device and that a good qualitative description of its characteristics is given in terms

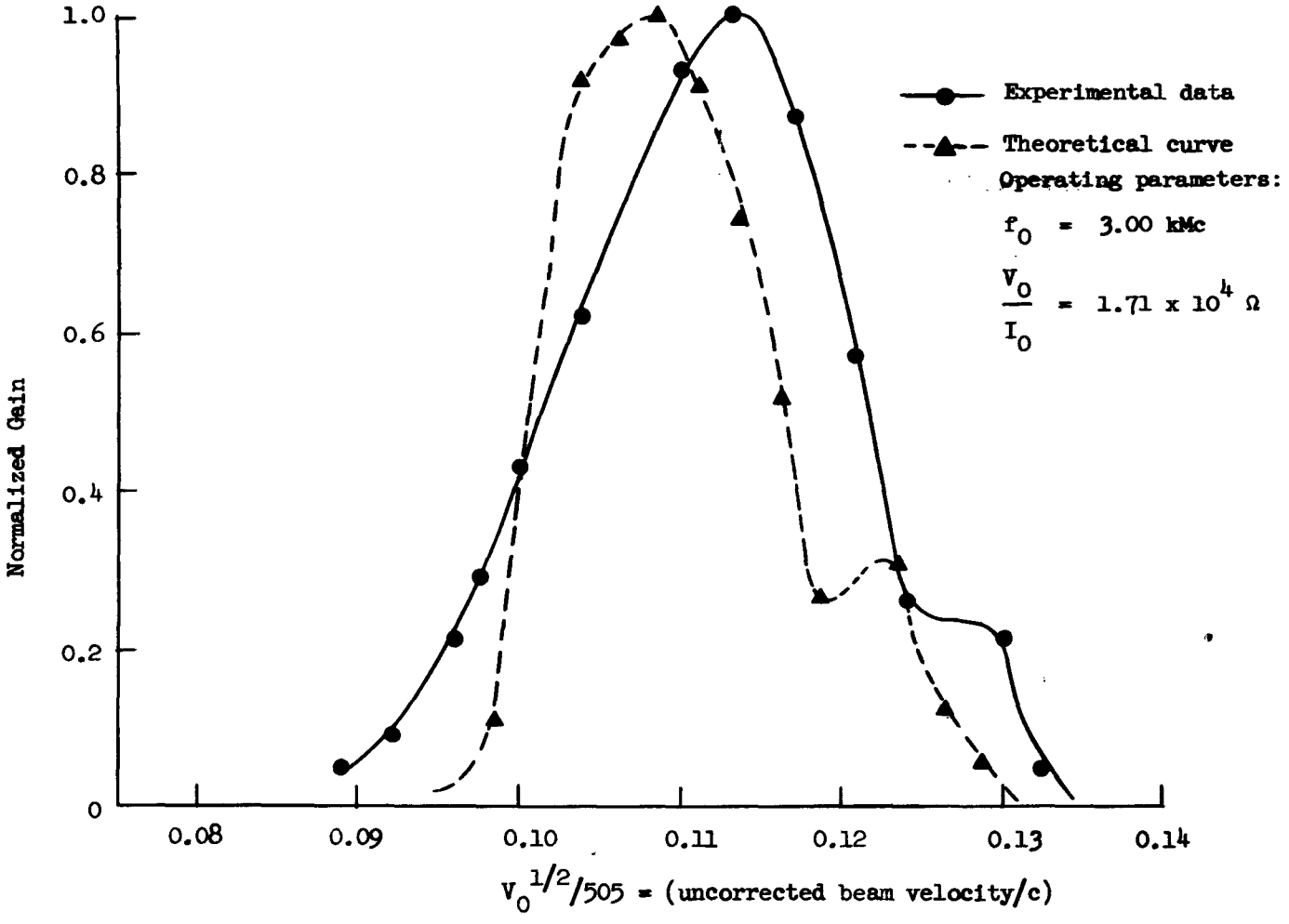

FIG. 8.11--The normalized gain of the synchronous-wave klystron as a function of the square root of the beam voltage. Both curves are for a constant beam resistance and the theoretical curve has been shifted to include the space-charge reduction of the beam velocity.

of the filamentary beam theory which has been described. It was found, however, that the experimentally observed gain was about 5 db less than the calculated value, and it was pointed out that this is probably due to the violation of the filamentary beam assumptions. Finally it should be pointed out that, although the observed gain was only 8 db, the interaction impedance had been reduced as a result of an error in the window design. If the value of the interaction impedance which was observed in cold test cavities is used, we predict that the experimental gain reported above should be increased by about 10 db. This is a net gain of 18 db which is of significance. By simply making the cavities longer, a very large gain could be achieved.

C. FREQUENCY DOUBLING WITH THE SYNCHRONOUS WAVES

The frequency doubling interaction described in Chapter VI can be observed with the tube described in Section A of this chapter by using one of the synchronous wave-couplers as the input and the quadrupole cavity as the second harmonic output. The purpose of this section is to report the results of an experimental investigation of this interaction and to compare them with the theoretical predictions.

The overall theoretical conversion efficiency of the synchronous-wave frequency doubler is calculated by considering the gain in both the input coupler and the quadrupole cavity. The coupler gain is given by (3.43) while the quadrupole gain is obtained from (6.40). The data for the quadrupole calculations are given in Table VII.3 of Chapter VII. The magnetic flux density used in the experiment was 583 gauss, as it was in the klystron experiment reported in the previous section. We then calculate the normalization constant of Eq. (5.33) and obtain the normalized power p in terms of the actual power P :

$$p = 1.66 \times 10^{-2} P \quad .$$

Consequently, we have, from (6.40),

$$P_{2\omega L} = 1.66 \times 10^{-2} P_{\omega}^{2} \quad ,$$

where $P_{2\omega L}$ is the second harmonic power delivered to the load and P_{ω} is the power on each of the synchronous waves at the quadrupole input. In order to isolate the deviations from the theory which occur in the quadrupole section of the doubler, we use the experimentally observed gain of the coupler to calculate the relation between the input and output power. For essentially the same beam conditions as here, the small-signal gain of one input coupler is approximately 1.2. Thus, we would expect the small-signal frequency doubler characteristics to be given by

$$P_{2\omega L} = 2.5 \times 10^{-2} P_{in}^{2} ,$$

where P_{in} is the input power at the fundamental frequency. This result will be compared with the experimental findings given below.

The input coupler resonant frequency should be exactly half of the frequency of the quadrupole cavity resonance in order to have optimum operation. As was noted in the previous section, the tuning mechanism of the coupler closest to the quadrupole was defective and consequently it was necessary to use the first coupler and the quadrupole for the frequency doubling experiments. The optimum orientation between the coupler and the quadrupole is preserved; however, the beam must now pass through the detuned coupler cavity before entering the quadrupole. This should have no significant effect on the small signal operation of the device and indeed there was a signal of negligible amplitude detected at the second coupler during the course of the experiments. However, there is an alteration of the saturation power due to a reduction in the dimension of the aperture through which the beam must pass. The effective aperture is now 0.156 in., rather than the 0.225 in. dimension that would have been valid if the second coupler could have been used to excite the synchronous waves. This results in a reduction of the maximum wave amplitudes that can be excited in the coupler, and consequently the conversion efficiency will be reduced since this is a square-law device, as shown in (6.40).

The experimentally observed second harmonic power is plotted as a function of the input power in Fig. 8.12. The data have been corrected for the insertion loss of all external transmission lines so that the

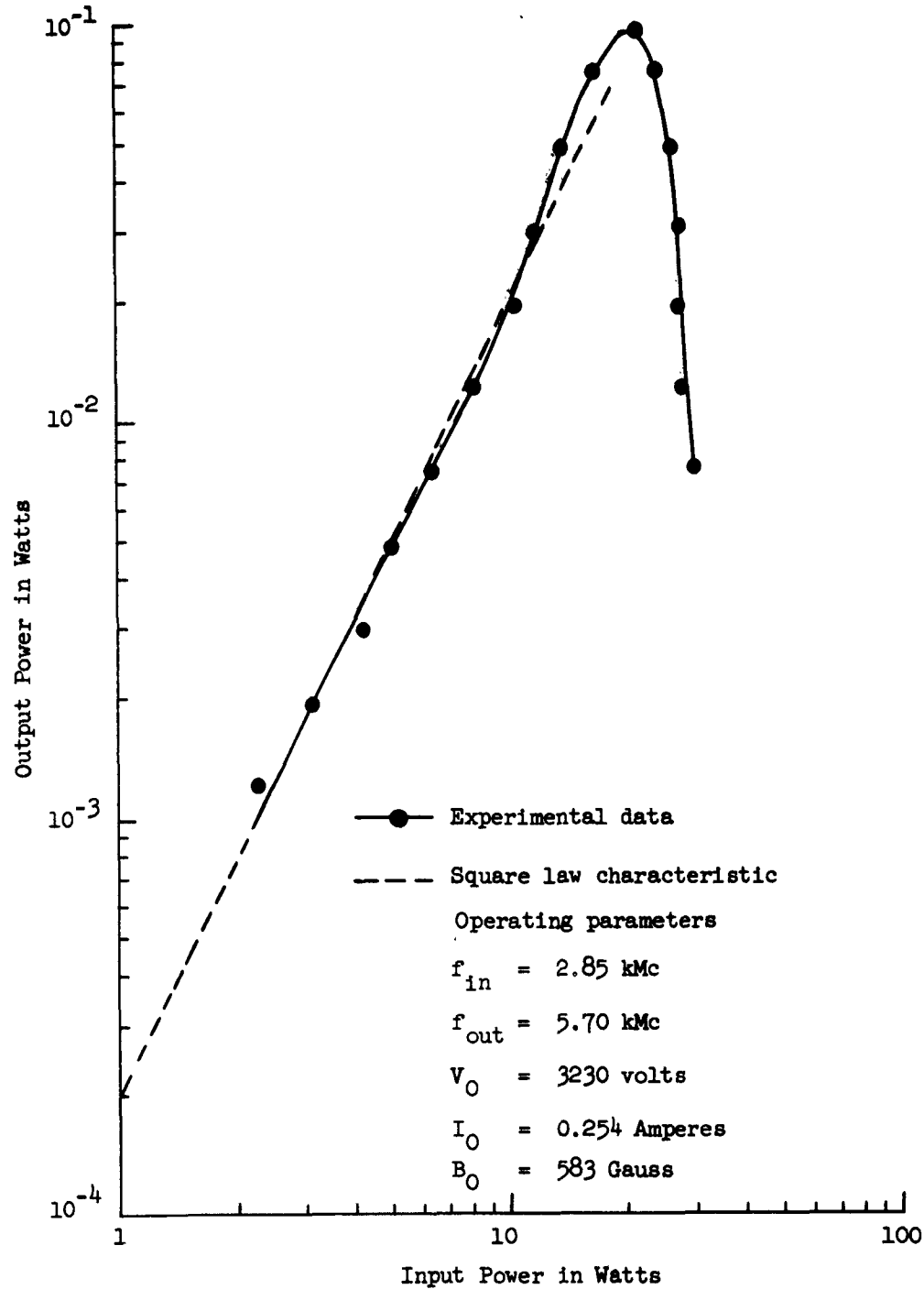

FIG. 8.12--The output power of the synchronous-wave frequency doubler as a function of the input power.

power indicated is that which exists at the input and output terminals of the tube. The square-law characteristic which gives a good fit to this data at low power levels is

$$P_{2\omega L} = 2.0 \times 10^{-4} P_{in}^{2} \quad .$$

The corresponding coefficient calculated above was 2.5×10^{-2} . This discrepancy between experimental and theoretical results by a factor of one hundred certainly indicates that the filamentary beam theory fails in this case as far as quantitative predictions are concerned. In the next section it will be shown that the filamentary beam theory gives much closer agreement with the experimental results for the cyclotron wave interaction in the quadrupole cavity. In that case the quantity βb , where b is the beam radius and β is the wave propagation constant, is approximately 0.05 while for the synchronous wave interaction βb is about 0.5 . We would therefore expect thick beam effects to be much more significant in the synchronous wave case, and the experimental evidence seems to bear this out. It should be noted that the theoretical predictions came much closer to the experimental results in the case of the synchronous wave interaction in a coupler field, treated in the previous section, than in the case of the quadrupole interaction studied here. This indicates that thick beam effects are much more significant in quadrupolar fields than in coupler fields.

The large-signal character of the data shown in Fig. 8.12 is very interesting and shows a qualitative deviation from the theoretical results. The change from the second power dependence of the output power on the input power is quite apparent and was observed in all of the synchronous-wave doubler experiments. That this is an effect which takes place in the quadrupole is verified by the fact that it was not observed in the synchronous-wave klystron experiments reported in Section B of this chapter. This result cannot be explained in terms of the interactions described in Chapter VI, in which the power characteristic was an exponential curve, because the second harmonic power observed in this experiment is not great enough to give rise to a deviation from the low-level square-law characteristic. It is difficult to speculate on the exact nature of

this phenomenon because the true character of the beam is unkown. Perhaps a satisfactory explanation can be made in terms of the space-charge wave interactions which give rise to the oscillations described in Section F of this chapter. However, a more thorough investigation, with a device in which the beam is well defined and current interception does not occur at such low power levels, would be required.

In general, the results of the experimental investigation of the synchronous-wave frequency doubler employing a linearly polarized quadrupole cavity indicate that the assumptions of the filamentary beam theory developed in Chapter VI have been violated in a crucial way. The frequency doubling that is predicted is observed, but the experimentally determined efficiency is two orders of magnitude less than predicted. It was also seen that some phenomenon, in addition to the synchronous-wave doubling interaction, was taking place. Consequently, while the predicted effect was observed, there is both a refinement of theory and more experimental work required in order to make this interaction competitive with other frequency doubling schemes.

D. FREQUENCY DOUBLING WITH THE FAST CYCLOTRON WAVE

The experiments described in the last two sections involve coupling between the synchronous waves and a space harmonic of the circuit field. It was also possible to adjust the beam voltage and the magnetic field so that there was strong coupling between the fast cyclotron wave and the fundamental component of the circuit field in both the couplers and the quadrupole. Consequently, we should observe the passive frequency doubling described in Chapter V. The expected efficiency of this interaction will be calculated and compared to the experimental results.

The theoretical conversion efficiency of the cyclotron-wave frequency doubler is computed by considering the gain in both the coupler and the quadrupole cavity. The cavity gain is given by (3.29) and the quadrupole gain is obtained from (5.34). By using the data in Table VII.3 of Chapter VII, we calculate the normalization constant given in (5.33). The magnetic field intensity of 815 gauss and the voltage of 4080 which were used in the experiment were less than the optimum values for synchronism, but larger values could not be obtained due to equipment

limitations. We obtain the normalized power given by (5.33) as

$$p = 5.8\, P \quad ,$$

and at small signal levels (5.34) gives

$$\frac{P_{2\omega}}{P_{\omega}} = \frac{5.8}{1 + \frac{Q_{ext}}{Q_0}} P_{\omega}$$

Now this result was derived under the assumption that the fast cyclotron wave was synchronous with one component of the circuit field and did not interact with any other traveling-wave components. Neither assumption is valid here because of the error in beam velocity and the shortness of the quadrupole. However, it was noted in Chapter V that, for very low power levels, the modification of the results due to other field components, and to errors in synchronism, is exactly the same as in coupler circuits. That is, we should multiply the above efficiency by the coefficient $|M_3|^2$ shown in Fig. 3.1. The value of the synchronism error ϵ calculated from (3.7) is, in this case,

$$\epsilon = -0.56 \quad ,$$

and from Fig. 3.1 we obtain for a cavity three wavelengths long,

$$|M_3(-0.56)|^2 = 0.03 \quad .$$

Only the fundamental components of the resonant field need be considered here since the space harmonics are far from synchronism. The theoretical value of the conversion efficiency in the quadrupole is found to be

$$\frac{P_{2\omega}}{P_{\omega}} = 0.087\, P_{\omega} \quad ,$$

where Q_{ext}/Q_0 has been set equal to unity. Of course, as the power level is increased the conversion efficiency of the quadrupole will not remain a linear function of the input power, but will saturate at fifty per cent as shown in Fig. 5.5.

It was necessary to use the first coupler to provide the input to the quadrupole as a result of the tuning mechanism difficulty mentioned in Section B of this chapter. It is not expected that this will cause any difficulty in the present case since the second coupler cavity is detuned. Unlike the synchronous-wave case, the saturation characteristics should not be altered because at least in theory, the beam motion in the transverse plane is circular and the dimensions of both couplers are the same.

The experimental data showing the second harmonic power output as a function of the fundamental coupler power input are plotted in Fig. 8.13. This represents the overall power characteristic of the tube and we see that a conversion efficiency of 6.7 per cent is achieved. The gain in the input coupler was observed by measuring the reflection coefficient of the coupler cavity with and without the beam in the cavity. These results give the ratio of the cold cavity Q and the Q of the cavity loaded by the beam. We obtain

$$\frac{Q_b}{Q_0} = 3.0 \quad .$$

The coupler gain, given by (3.29), is

$$G_{in} = 0.25 \quad .$$

The low level (square-law) portion of the curve in Fig. 8.13 is matched very closely by

$$\frac{P_{2\omega}}{P_{\omega}} = 0.064\, P_{\omega} \quad ,$$

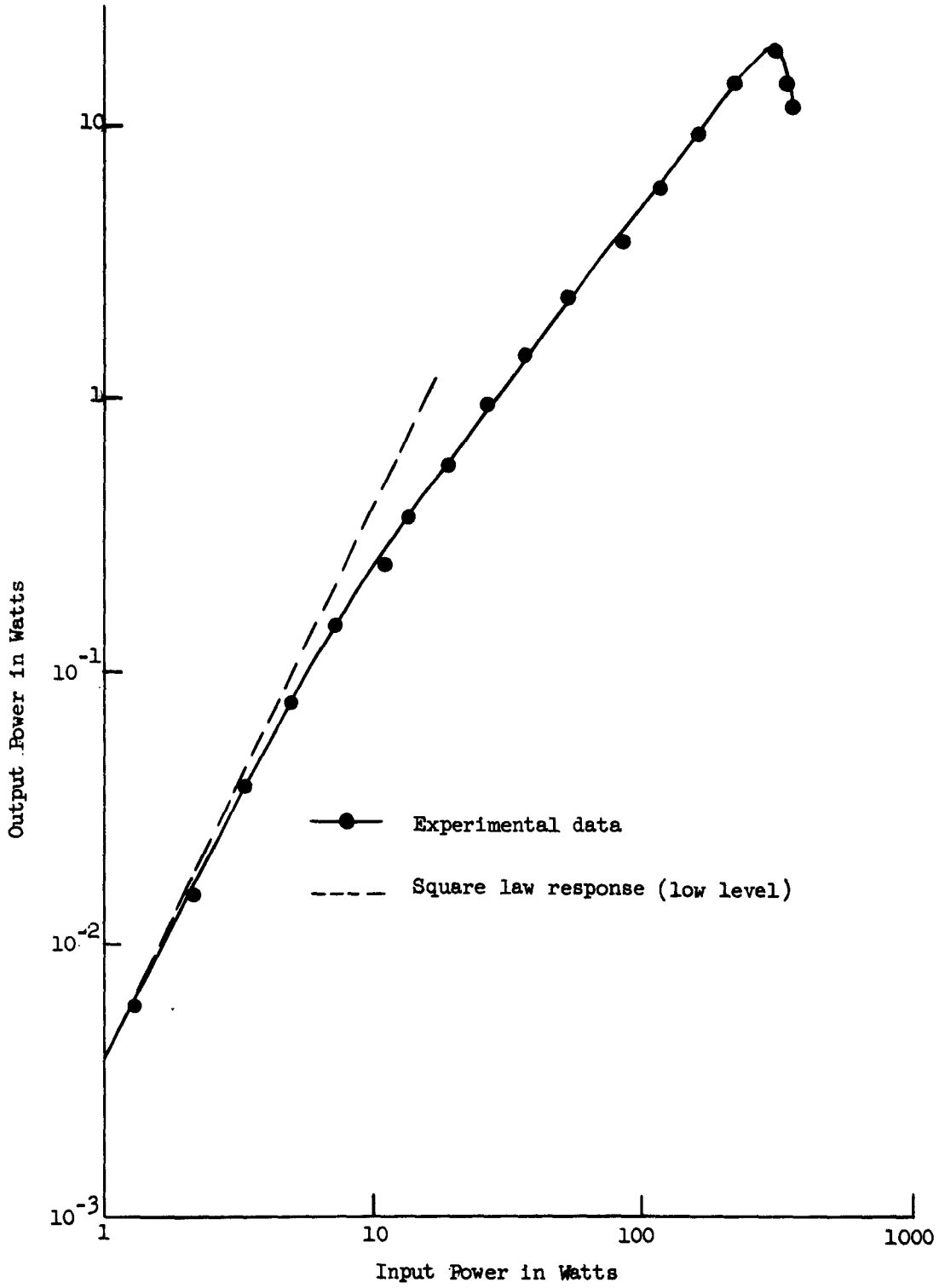

FIG. 8.13--The output power of the cyclotron-wave frequency doubler as a function of the input power.

where P_ω is the cyclotron wave power at the quadrupole entrance. This result agrees very well with the theoretical low-level power expression calculated above. Since the coupler gain is 0.25 here, we see from the figure that an experimental overall conversion efficiency of about 25 per cent would have been obtained if the coupler cavity window had been designed properly. This result is approximately the same as observed by Ashkin with infinite phase velocity structures, and there is no reason why the efficiency cannot be pushed much closer to one hundred per cent.

A plot of the fraction of the beam current which is intercepted in the input coupler is shown in Fig. 8.14. Calculations show that the current interception begins much below the value predicted by the filamentary beam theory, and it is also observed that the sharp decrease in power output observed in Fig. 8.13 does not occur until the input power reaches about twice the value at which interception was first observed. On the basis of this, one is led to believe that the beam is expanding more than the filamentary beam theory would predict, and that not all of the beam is playing a significant role in the coupling interaction in the input cavity since the abrupt loss of signal transmission through the tube is not related to the initial current interception. This may be related to beam scalloping as a result of improper focusing conditions, or it can be a result which is to be expected for any thick Brillouin flow beam. Again, it is apparent that the filamentary beam model fails in many respects. This simple theory has, however, provided a very useful guide to a qualitative description of the transverse-wave interactions that have been observed.

In summarizing the results of the experimental investigation of the fast cyclotron-wave doubler, it is to be noted that exceptionally good agreement between the theoretical and experimental results is obtained. The overall efficiency of seven per cent that was observed at saturation was low as a result of the error in window design in the input coupler. The quadrupole frequency doubling efficiency was in excess of 25 per cent. The good agreement with the theory can probably be attributed to the small value of beam diameter measured in the wavelengths of the fast cyclotron wave. The one distinct disagreement with the theoretical predictions was the power level at which beam interception occurs. In

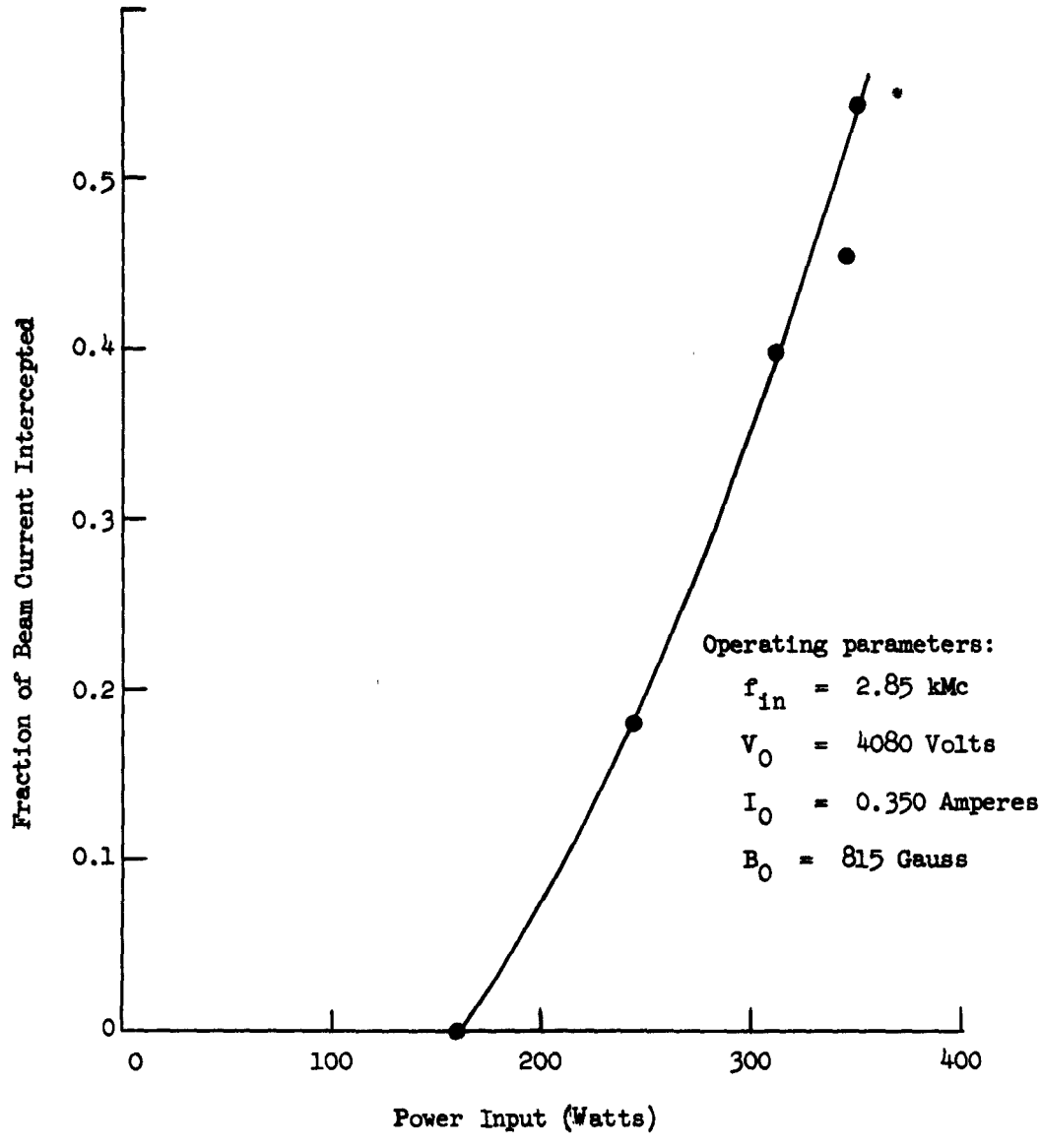

FIG. 8.14--A plot of the fraction of the beam current that is intercepted as a function of the input power for the fast cyclotron-wave doubler.

all of the experiments we have observed current interception at much lower values of the input power than would be expected. It is believed that this is a result of a thick beam phenomenon, and probably dc scalloping of the beam as well.

E. DISPERSION OF THE FAST CYCLOTRON WAVE

The question as to whether the propagation constants of the transverse waves on the Brillouin focused beam are the same as on a filamentary beam naturally arises in connection with the experiments presented here. Wessel-Berg[14] has done some theoretical work on wave propagation on thick Brillouin focused beams and arrives at the conclusion that, while additional waves do arise, there is no significant change in the propagation constants of the equivalent of the filamentary beam transverse waves that are associated with a Brillouin beam. The experiment described below was carried out in order to verify these results.

It was possible to observe transmission through the two couplers as a result of the fast cyclotron wave coupling to the space harmonic field components by properly adjusting the magnetic field and the voltage. The shape of the transmission response curve shown in Fig. 8.11 is valid for the cyclotron wave coupling also and it is apparent that the velocity of the cyclotron wave can be defined very well by observing the maximum coupling through the two couplers. Although it was not possible to change the phase velocity of the couplers, the combinations of magnetic field and beam voltage which yield a cyclotron wave phase velocity that gives maximum transmission can be observed. It is then possible to normalize this data so that an ω-β diagram for the fast cyclotron wave is obtained. The data were taken by changing the magnetic field in discrete steps and observing the beam voltage that yielded maximum coupling. This insures that the cyclotron wave has the same phase velocity at each point. The beam current was varied at each point to verify that the optimum voltage was independent of the current. This was to be expected in this experiment since the beam voltage, and therefore the current, was quite small. The normalized data taken in this way are plotted in Fig. 8.15. The agreement between the curve based on the filamentary beam model and the experimental data is excellent. There is a slight deviation at frequencies

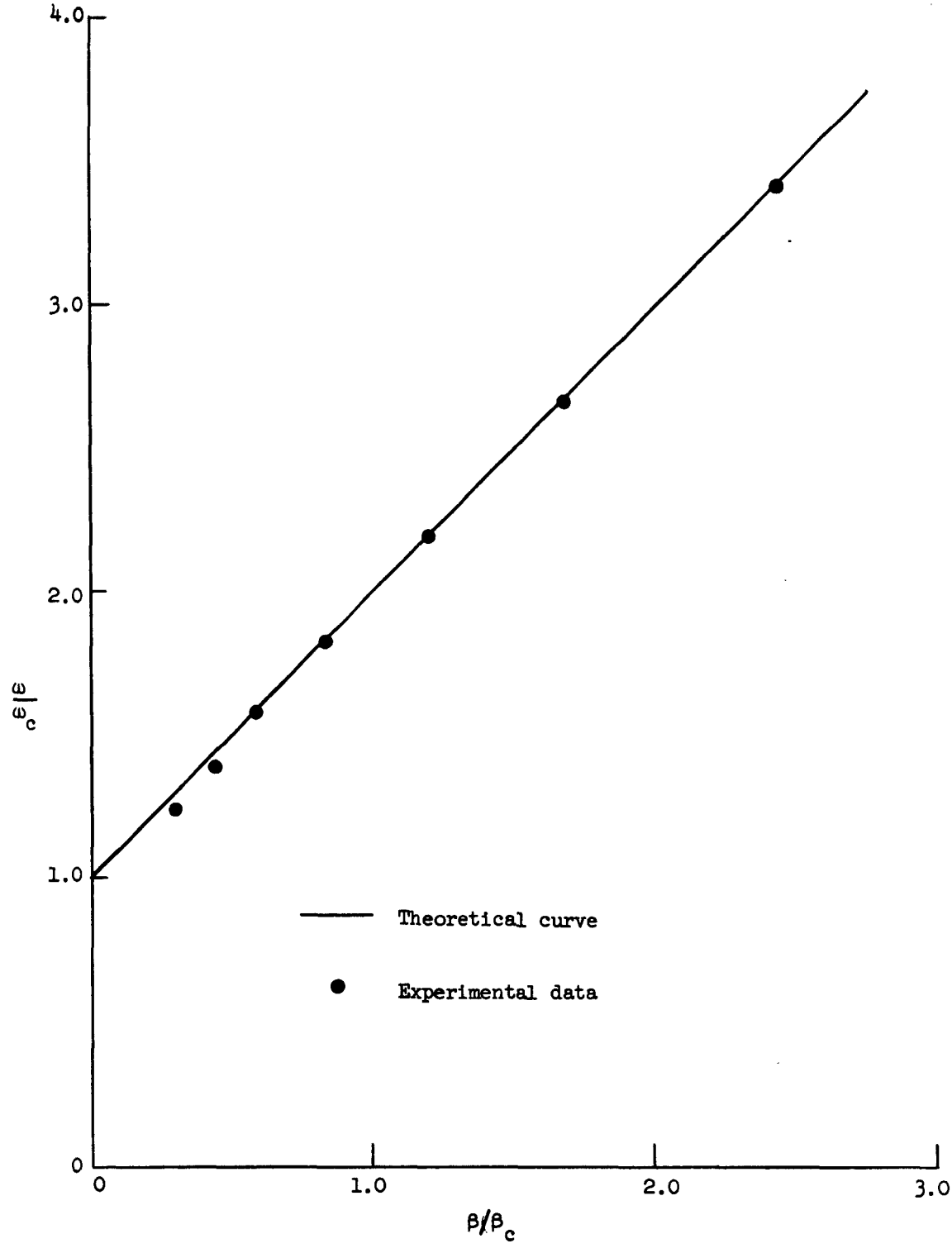

FIG. 8.15--The ω-β characteristic of the fast cyclotron wave.

near the cyclotron frequency which is of the same nature as the deviation predicted by Van Hoven and Wessel-Berg.[38] Because of the way that these data were taken, it is not possible to make a numerical comparison with the results in the reference cited above. For example, it is almost certain that the beam diameter varied in this experiment. These results do indicate that the propagation constant of the fast cyclotron wave is essentially the same as that predicted by the filamentary beam theory.

F. MONOTRON OSCILLATIONS

No mention of oscillations was made in the descriptions of the various experiments reported above. Special care was taken to look for instabilities at all stages of the investigation and none were associated with the above experiments. However, oscillations were observed in both the coupler and quadrupole cavities when the axial magnetic field was perturbed in a particular way.

It was observed that, for particular synchronism conditions, it was possible to cause oscillations in the quadrupole cavity by placing a steel rod, one-quarter inch in diameter, near the quadrupole and parallel to it. The peak output power obtained in this way was 22.0 watts at 5.70 kMc, with a peak dc beam power of 1500 watts. It is apparent that this is not an insignificant process. Similar oscillations were observed in the coupler cavities. In all cases the oscillations were accompanied by beam interception. The position of the perturbing rod that yielded oscillations was one in which the beam would be deflected toward a set of pins in the slow wave structure. For example, the optimum perturbing rod position in the case of the quadrupole oscillations was in the plane of any one of the four sets of pins that make up the quadrupole structure.

Several explanations for these results might be plausible. One explanation could be that secondary electrons due to the beam striking the slow-wave structure could be giving rise to the oscillations. However, by varying the external load on the cavities it was determined that the beam interception was due to an rf phenomenon and was not due to the perturbed dc trajectory of the beam. A second explanation could be based upon a parametric interaction between the circuit and a dc "pump" wave which was excited on the beam by the magnetic field perturbation.

This would have been an attractive solution because it might have offered evidence of the existence of some of the new transverse waves described by Wessel-Berg.[14] However, no combination of the transverse waves could be found that would explain the oscillations in this way.

Finally, the answer that immediately suggests itself is the one that fits the data. The proper explanation is that the beam is shifted off of the tube axis by the perturbing rod so that the symmetry of the fields acting on the beam is destroyed. The beam is now in a region where it observes transverse fields with a superimposed longitudinal field, and it is the coupling of the slow space-charge wave to this longitudinal field that results in the oscillations. For example, strong oscillations were observed in both the quadrupole and the coupler-cavities for the conditions

$$V_0 = 4250 \text{ volts}$$

$$I_0 = 0.350 \text{ amp}$$

$$B_0 = 675 \text{ Gauss} \quad .$$

The plasma frequency is obtained from the cyclotron frequency, since this is a Brillouin-focused device, and a knowledge of the approximate beam diameter as well as of the circuit dimensions allows an estimate of the space-charge reduction factor by means of curves such as are given by Beck.[39] It is found that the phase velocity of the slow space-charge wave is

$$\frac{v_p}{c} \approx 0.11 \quad ,$$

which is very close to the phase velocity of the first backward space harmonic in both the couplers and the quadrupole. Since these oscillations are a result of an unmodulated beam interacting with a single resonant cavity, they have been called monotron oscillations here. Since the interaction happens to be with a negative phase velocity component of

the circuit field, some might feel it preferable to call this backward-wave oscillation.

The main importance of these results is that they show that beam misalignment can cause oscillations. This would be particularly evident in long structures in which the coupling occurs over many wavelengths. However, the ordinary care that was exercised in the construction of the device described here was quite sufficient to avoid difficulties.

CHAPTER IX

SUMMARY

In general, the plan of the work presented in this report has been to use the coupled mode approach to describe certain classes of transverse-wave interactions, and then to experimentally investigate those interactions which appeared to be most likely to result in devices that perform a useful function. An outline of the major divisions of the work is presented below, along with a summary of the way in which each part represents a contribution to the understanding and utilization of transverse-wave interactions.

The purpose of Chapters II, III, and IV was to present an explicit and unified description of the various types of transverse-wave couplers that employ either traveling-wave or standing-wave circuits. The filamentary beam model has been used throughout the analysis and, although this represents a limitation, it is felt that a good qualitative description of the basic interactions is found in this way. The results derived in these chapters should serve as a useful guide to the design of couplers, and the description of both resonant and traveling-wave couplers in the same notation makes it easier to study transverse-field circuits without specifying the manner in which they are to be used. The coupled mode formulation of the twisted circuit interactions makes it possible to gain a better understanding of this class of couplers. In particular, it was observed that any two transverse waves of opposite polarization can be excited equally in a twisted coupler. On the other hand, the twisted coupler can be used to discriminate between waves with the same phase velocity and opposite polarization.

Chapters V and VI presented the coupled mode theory of transverse-wave frequency doublers. These devices consist of an input transverse-wave coupler and a quadrupole structure for the second harmonic power output cavity. The theory included a study of some new interactions as well as a new formulation of the fast cyclotron-wave doubler that has

been described before. Several of the new interactions have some promise as useful devices because they lead to high conversion efficiencies by means of an active process. The doublers employing both of the synchronous waves were of particular interest because of the opportunity to obtain gain in the input coupler and thereby increase the overall conversion efficiency of the device.

The studies reported in Chapters VII and VIII described some new transverse-field circuits, and the results of an experimental investigation of some of the interaction schemes that were considered in the first part of this report. The synchronous-wave klystron described in Chapter III was investigated and the observed 8 db gain is felt to be significant because this is the first experimental observation of this phenomenon. Frequency doubling by means of both the synchronous waves and the fast cyclotron wave was also observed. The conversion efficiency of the synchronous-wave doubler was much smaller than the value predicted on the basis of the theoretical work, while the experimental and calculated efficiencies of the cyclotron-wave doubler agreed very well. These results indicate that the filamentary beam model used in the theory is probably inadequate as far as quantitative descriptions of slow-wave interactions involving thick beams in quadrupole fields are concerned. The quadrupole conversion efficiency of 25 per cent that was obtained in the cyclotron-wave doubler does show that this interaction is practicable in devices that use periodic circuits to reduce the magnetic field requirement.

APPENDIX A

IMPEDANCES OF IDEALIZED SLOW-WAVE CIRCUITS

In order to compute the ultimate interaction impedance which might be obtained with a longitudinal-field traveling-wave circuit, Pierce[36] introduced a hypothetical circuit which had only the field of interest in the interaction, and the extraneous fields as required by Maxwell's equations (assuming slow waves). Then, by using the assumed field variations that are appropriate to the postulated cylindrical symmetry of the ideal circuit, it was possible to match the external and internal fields at the circuit by means of the continuity relations, and obtain the fields everywhere in terms of the axial electric field. The energy stored per unit length was then calculated and, by introducing the group velocity, the interaction impedance of the circuit was determined.

This same approach may also be applied in the case of transverse-field circuits. By doing this it will not only be possible to obtain an upper bound to the impedance of transverse-field circuits, but it will also allow some comparison of the ultimate capabilities of this class of circuits with those of the longitudinal-field circuits. We calculate here the impedance of an idealized TE circuit which is circularly polarized. The circularly polarized circuit is the interesting case since the transverse waves on a beam are circularly polarized.

We begin with the equations relating the electric fields to the longitudinal electric and magnetic fields in cylindrical coordinates:

$$E_r = -\frac{1}{k_c^2}\left[\gamma \frac{\partial E_z}{\partial r} + j\,\frac{\omega\mu_0}{r}\frac{\partial H_z}{\partial \theta}\right]$$

$$E_\theta = \frac{1}{k_c^2}\left[-\frac{\gamma}{r}\frac{\partial E_z}{\partial \theta} + j\,\omega\mu_0 \frac{\partial H_z}{\partial r}\right], \qquad \text{(A.1)}$$

where

$$k_c^2 = \gamma^2 + k^2 \quad .$$

We are assuming $e^{(j\omega t - \gamma z)}$ variation here. For slow waves $(v/c << 1)$, we define $\gamma = j\beta$ and Eqs. (A.1) are approximately

$$E_r = \frac{j}{\beta}\frac{\partial E_z}{\partial r} + j\frac{\omega\mu_0}{\beta^2 r}\frac{\partial H_z}{\partial \theta}$$

and

$$E_\theta = \frac{j}{\beta r}\frac{\partial E_z}{\partial \theta} - j\frac{\omega\mu_0}{\beta^2}\frac{\partial H_z}{\partial r} \quad . \tag{A.2}$$

For a circularly polarized circuit the θ-variation is chosen to be $e^{-j\theta}$. Then assuming that there is no axial electric field, Eqs. (A.2) become

$$E_r = \frac{\omega\mu_0}{\beta^2}\frac{1}{r}H_z$$

$$E_\theta = -j\frac{\omega\mu_0}{\beta^2}\frac{\partial H_z}{\partial r} \quad . \tag{A.3}$$

The appropriate solutions for H_z, with the z- and θ-variation suppressed, are

$$H_z^i = A\, I_1(\beta r)$$

$$H_z^o = B\, K_1(\beta r) \quad ,$$

where the superscripts indicate fields inside and outside of the cylindrically symmetric circuit, A and B are arbitrary constants, and I_1 and K_1 are the modified Bessel and Hankel functions. After substituting these fields into Eqs. (A.3), matching E_θ across the circuit boundary (at $r = a$), and choosing $E_r(0)$ to be unity, we obtain

$$E_r^i = 2 \frac{I_1(\beta r)}{\beta r}$$

$$E_\theta^i = -j2\, I_1'(\beta r)$$

$$E_r^0 = 2 \frac{I_1'(\beta a)}{K_1'(\beta a)} \frac{K_1(\beta r)}{\beta r}$$

$$E_\phi^0 = -\, j\, 2 \frac{I_1'(\beta a)}{K_1'(\beta a)} K_1'(\beta r) \quad . \tag{A.4}$$

The total average stored energy per unit length is twice the average electric energy stored, or

$$\mathcal{E} = \frac{\epsilon_0}{2} \int_{r=0}^{\infty} |\vec{E}|^2\, 2\pi r\, dr \quad .$$

By substituting Eqs. (A.4) into this expression, we obtain integrals which are simply evaluated by means of standard recurrence relations and integral formulas. The resulting expression for the energy stored per unit length in the hypothetical circuit is

$$\mathcal{E} = \pi \epsilon_0 a^2 I_0^2 \left[2 - \frac{I_1^2}{I_0^2} \left(1 + \frac{4}{(\beta a)^2} \right) \right.$$

$$\left. + \left(\frac{1 - (I_1/I_0)(1/\beta a)}{1 + (K_1/K_0)(1/\beta a)} \right)^2 \cdot \frac{K_1^2}{K_0^2} \left(1 - \frac{4}{(\beta a)^2} \right) \right] \quad . \tag{A.5}$$

The arguments of the cylinder functions are all βa and have been omitted. The transverse interaction impedance, defined by (2.18), is

$$K_T = \frac{E_r^2(0)}{4\beta^2 \varepsilon v_g} \quad ,$$

where v_g is the circuit group velocity. The final expression for the impedance is

$$K_T = 30 \frac{c}{v_g} \frac{1}{(\beta a)^2} \frac{1}{I_0^2} \left[2 - \frac{I_1^2}{I_0^2} \left(1 + \frac{4}{(\beta a)^2} \right) + \left(\frac{1 - (I_1/I_0)(1/\beta a)}{1 + (K_1/K_0)(1/\beta a)} \right)^2 \cdot \frac{K_1^2}{K_0^2} \left(1 - \frac{4}{(\beta a)^2} \right) \right]^{-1} \quad . \qquad (A.6)$$

If the longitudinal-field circuit (TM) impedance is defined in the same way as the transverse impedance K_T, we have

$$K_L = \frac{E_z^2(0)}{4\beta^2 \varepsilon v_g} \quad ,$$

so that, from Pierce's results,[1]

$$K_L = 30 \frac{c}{v_g} \frac{1}{\beta a} \frac{1}{I_0^2} \left[\frac{I_1}{I_0} + \frac{K_1}{K_0} \right]^{-1} \quad . \qquad (A.7)$$

Equations (A.6) and (A.7) are plotted in Fig. 7.2.

---

[1] Pierce's definition of impedance differs from that used here, since he employs the field at the circuit rather than on the axis.

APPENDIX B

MEASUREMENT OF INTERACTION IMPEDANCES

The interaction impedances of the circuits described in Chapter VII were determined by a frequency perturbation technique. A section of the slow wave structure, an integral number of periods long, was shorted at the ends to form a resonant cavity, and the shift in resonant frequency was noted when a metal needle was placed in the cavity field. It is noted below that the frequency perturbation produced by a thin needle is proportional to the square of that electric field component that is parallel to the needle. Consequently, a needle that is placed in the plane that is transverse to the axis of the cavity can be used to determine the axial distribution of the transverse field and to note the angular distribution of the field in any transverse plane. If it is desirable to have a frequency perturbation that is independent of the orientation of the perturbing object, a cross made of two needles that are perpendicular to each other may be used. This is useful since it is often desirable to support the needles on a thread so that the orientation cannot be controlled. A drinking straw was found to be a very suitable vehicle for the needle when it is desirable to control the orientation. The determined transverse-field distribution along the axis of the cavity can be used to compute the space harmonic amplitudes of the traveling-wave circuit by matching assumed space-harmonic series, composed of forward and reverse propagating waves, to the data in a manner very similar to that described by Gallagher.[40]

The traveling-wave interaction impedance is calculated from the frequency perturbation and the needle dimensions by means of an expression that is derived from an equation given by Ginzton.[41] The reference states that the shift in resonant frequency of a cavity when a needle of

length $2a$ and diameter $2b$ is placed parallel to a uniform electric field is given by

$$\frac{\omega_0^2 - \omega^2}{\omega_0^2} = F(b/a)\, E_0^2\, 4\pi a^3 \quad , \tag{B.1}$$

where ω_0 is the natural resonant frequency of the cavity and ω is the perturbed resonant frequency. The $F(b/a)$ is a shape factor for the needle that is given in the reference, and E_0^2 is given by

$$E_0^2 = \epsilon_0 \frac{E^2}{2U} \quad , \tag{B.2}$$

where E is the electric field at the needle and U is the energy stored in the cavity. Equation (B.1) is used below to relate the impedance of a coupler and a quadrupole type circuit to the perturbation data.

1. Impedance of a Linearly Polarized Coupler

If a circuit supporting a single traveling-wave is shorted to make a cavity, the peak field is related to the field of the forward wave component on the circuit by

$$E_f = \frac{1}{2} E_p \quad , \tag{B.3}$$

and the energy stored per unit length in the forward propagating wave is related to the total energy stored in the cavity by

$$U_f = \frac{1}{2} \frac{U}{L} \quad , \tag{B.4}$$

where L is the length of the cavity. The power that is carried by the forward propagating wave is

$$P_f = U_f v_g \quad , \tag{B.5}$$

where v_g is the group velocity. Finally, by combining these equations and using the definition of the transverse interaction impedance given in Chapter II,

$$K_t = \frac{E^2}{4\beta^2 P} \quad , \tag{B.6}$$

we obtain the impedance in terms of the known circuit and needle quantities and the frequency shift

$$\delta = \frac{\omega - \omega_0}{\omega_0} \quad . \tag{B.7}$$

For $\delta \ll 1$, we obtain

$$K_t = 15 \left[F(b/a) \frac{a}{L} (v_g/c)(\beta a)^2 \right]^{-1} \delta \quad . \tag{B.7}$$

In general, there will be space harmonic components in the field and (B.7) must be modified. The impedance of the n^{th} space harmonic is

$$K_{tn} = 15 \left(\frac{E_n}{E} \right)^2 \left[F(b/a) \frac{a}{L} \frac{v_g}{c} (\beta_n a)^2 \right]^{-1} \delta \quad , \tag{B.8}$$

where E_n/E is the ratio of the space harmonic amplitude to the amplitude of the field which gave the frequency perturbation.

2. Impedance of a Linearly Polarized Quadrupole

In the calculation of the gain of the quadrupole frequency doublers we need to use a value for R_q which is defined to be

$$R_q = \frac{V_q^2}{2P} \quad , \tag{B.9}$$

where V_q is the forward propagating voltage and P is the power which must be supplied by the beam to establish this V_q. An approximate determination of R_q can be made by means of the perturbation procedure described above.

A cross section of a quadrupole cavity and the needle orientation are shown in Fig. B.1. The unperturbed potential at the position of the needle is

$$\phi = V_q \frac{x^2}{r_0^2} \quad , \tag{B.10}$$

so that the field is

$$E = 2 \frac{V_q}{r_0} \frac{x}{r_0} \quad . \tag{B.11}$$

An effective uniform field for use in the perturbation equations is taken to be that field which gives the same energy stored in the volume to be removed by the needle that is stored there in the actual quadrupole field, that is,

$$E_{eff}^2 = \frac{2}{a} \int_0^a E^2 \, dx \quad . \tag{B.12}$$

The effective field is then

$$E_{eff}^2 = 4/3 \left(\frac{V_q}{r_0}\right)^2 \left(\frac{a}{r_0}\right)^2 \quad . \tag{B.13}$$

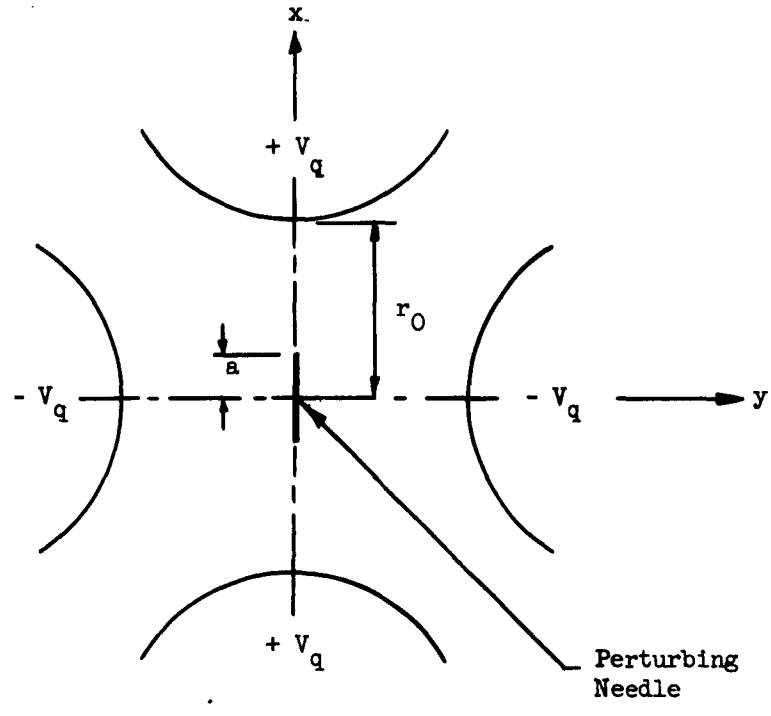

FIG. B.1--A schematic diagram of the quadrupole showing the needle orientation.

The quantity

$$\frac{(E_{eff})^2}{4\beta^2 v_g \left(\frac{U/2}{L}\right)} \tag{B.14}$$

is exactly the impedance K_n obtained in terms of the frequency perturbation in (B.8). Upon combining Eqs. (B.8), (B.9), (B.13), (B.14) and the definition of the Q of the cavity and its load,

$$Q = \omega U/P \quad , \tag{B.15}$$

we obtain

$$\frac{R_{qn}}{Q} = 22.5 \left[\frac{(p/a)(a/r_0)^5}{(v_p/c)\beta_n p\ F(b/a)}\right]\left(\frac{E_n}{E}\right)^2 \quad . \tag{B.16}$$

Thus, a perturbation measurement and determination of the Q of the cavity allows the calculation of R_q .

APPENDIX C

SPACE HARMONICS IN TRANSVERSE-WAVE COUPLERS

In order to calculate the amplitudes of the space harmonic components of the field to be expected in transverse-field couplers, we employ the model shown in Fig. C.1. It is assumed that there is no variation of the field in the y direction. Because the circuit is periodic in the z direction, we will have space harmonics with propagation constants

$$\beta_n = \beta_0 + \frac{2n\pi}{L} \quad , \tag{C.1}$$

where β_0 is the fundamental propagation constant. An appropriate expansion for the potential V at a point between the upper and lower halves of the circuit is, in rectangular coordinates,

$$V = - \sum_{n=-\infty}^{\infty} \frac{a_n}{\beta_n} \sinh \beta_n \times e^{-j\beta_n z} \quad , \tag{C.2}$$

so that the transverse field is

$$E_x = \sum_{n=-\infty}^{\infty} a_n \cosh \beta_n \times e^{-j\beta_n z} \quad , \tag{C.3}$$

To determine the amplitudes a_n , we match (C.2) to the assumed potential of the circuit at $x = a$:

$$V = V_0 \quad , \quad -\frac{d}{2} < z < +\frac{d}{2}$$

$$V = 0 \quad , \quad -\frac{p}{2} < z < -\frac{d}{2} \quad ; \quad \frac{d}{2} < z < +\frac{p}{2} \quad .$$

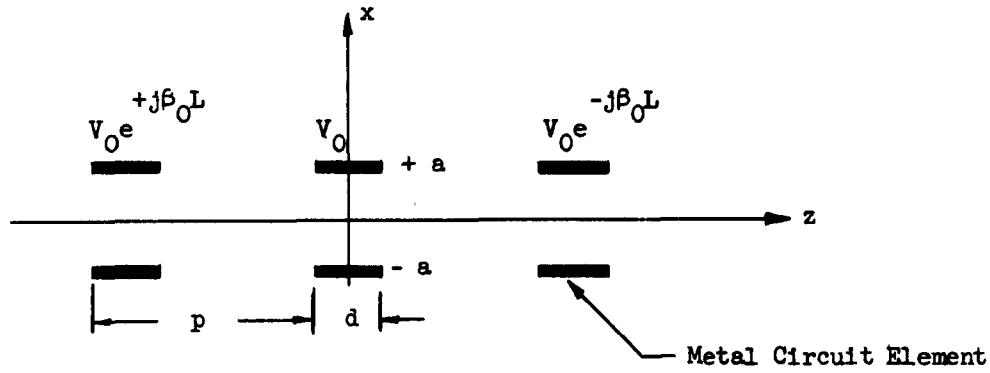

FIG. C.1--The circuit model used to calculate space harmonic amplitudes. The circuit is uniform in the y direction.

Then, using the orthogonality in z, we integrate over the period to obtain

$$a_n = \frac{V_0}{a}\frac{d}{p}\left(\frac{\sin\frac{\beta_n}{2}p\,d/p}{\frac{\beta_n}{2}p\,d/p}\right)\left(\frac{\sinh\beta_n a}{\beta_n a}\right)^{-1} \quad . \tag{C.4}$$

For small $\beta_n a$, the last factor in (C.4) is unity and to the same degree of accuracy the transverse variation of E in (C.3) may be neglected.

These results may be used to determine the requirements on d and p in order to maximize the impedance of a particular space harmonic. In order to do this for the space harmonic denoted by $n = k$, we maximize the ratio of the square of the harmonic amplitude to the average of the square of the electric field. That is, we look for the maximum of

$$\frac{a_k^2}{\frac{1}{L}\int_{-L/2}^{L/2}\left|\sum_{n=-\infty}^{\infty} a_n e^{-j\beta_n z}\right|^2 dz} = \frac{\theta_{gk}}{\theta_t}\left(\frac{\sin\theta_{gk}/2}{\theta_{gk}/2}\right)^2 , \tag{C.5}$$

where

$$\beta_k d = \theta_{gk}$$

$$\beta_k p = \theta_{tk} \quad .$$

This is exactly the result obtained by Pierce[42] for longitudinal field circuits and the solutions are:

$$\begin{aligned} \theta_{gk} &= \theta_{tk} \quad \text{if} \quad \theta_{tk} < 2.33 \\ \theta_{gk} &= 2.33 \quad \text{if} \quad \theta_{tk} \geq 2.33 \quad . \end{aligned} \tag{C.6}$$

REFERENCES

1. C. L. Cuccia and J. S. Donal, Jr., "The Electron Coupler - a Spiral Beam UHF Modulator," Electronics 23, 80 (1950).
2. C. L. Cuccia, "The Electron Coupler - a Developmental Tube for Amplitude Modulation and Power Control at Ultra-High Frequencies," RCA Rev. XIV, 72-99 (March 1953).
3. R. Adler, G. Hrbek, and G. Wade, "The Quadrupole Amplifier, a Low-Noise Parametric Device," Proc. IRE 47, 1713-1723 (October 1959).
4. E. I. Gordon, "A Transverse Field Traveling-Wave Tube," Proc. IRE 48, 1158 (June 1960).
5. T. J. Bridges and A. Ashkin, "A Microwave Adler Tube," Proc. IRE 48, 361-363 (March 1960).
6. T. Wessel-Berg and K. Blötekjaer, "A DC-Pumped Amplifier Using Space-Periodic Magnetic Field," Norwegian Defense Research Establishment Internal Report R-120 (June 1962).
7. L. Malter, "Deflection and Impedance of Electron Beams at High Frequencies in the Presence of a Magnetic Field," RCA Rev. V, 439 (April 1941).
8. L. P. Smith and C. I. Shulman, "Frequency Modulation and Control by Electron Beams," Proc. IRE 35, 644-657 (July 1947).
9. C. L. Cuccia, "The Electron Coupler - a Developmental Tube for Amplitude Modulation and Power Control at Ultra-High Frequencies," RCA Rev. X, 270-303 (June 1949).
10. A. E. Siegman, "The Waves on a Filamentary Electron Beam in a Transverse-Field Slow-Wave Structure," J. Appl. Phys. 31, 17-26 (January 1960).
11. R. W. Gould and C. C. Johnson, "Coupled Mode Theory of Electron Beam Parametric Amplification," J. Appl. Phys. 32, 248-258 (February 1961).
12. T. Wessel-Berg, "Electronic Interaction Theory for Transverse-Wave Couplers," Microwave Laboratory Report No. 922, Stanford University (June 1962).

13. E. I. Gordon, "Transverse Electron Beam Waves in Varying Magnetic Fields," B.S.T.J. 39, 1603-1616 (November 1960).
14. T. Wessel-Berg, "A Thick Beam Analysis of Transverse-Wave Propagation on Electron Beams," Microwave Laboratory Report No. 978, Stanford University (November 1962).
15. N. B. Chakrabortz, "Analysis of Fast Wave Couplers for Transverse Field Beam-Type Parametric Amplifiers," J. Electr. and Contr. 10, 147 (February 1961).
16. T. Wessel-Berg, "Transverse-Field Couplers for Electron Beams," Norwegian Defense Research Establishment Internal Report No. R-97 (July 1961).
17. E. I. Gordon, "A New Microwave Amplifier," Bell Labs. Internal Memorandum 59-124-24 (August 1959).
18. A. E. Siegman, "The DC Pumped Quadrupole - a Wave Analysis," Stanford EDL Technical Report No. 159-1 (March 1960).
19. K. Bløtekjaer and T. Wessel-Berg, "Some Aspects of Cyclotron-Wave Amplification in Time-Periodic and Space-Periodic Fields," presented at the International Congress on Microwave Tubes, Munich, Germany (June 1960).
20. C. L. Cuccia, "Parametric Amplification, Power Control, and Frequency Multiplication at Microwave Frequencies," RCA Rev XXI, 228-244 (June 1960).
21. A. Ashkin, "A Microwave Adler Tube," presented at the International Congress on Microwave Tubes, Munich, Germany (June 1960).
22. P. A. Lindsay and J. Caunter, "Crossed Field Frequency Doubler," General Electric Co., Ltd., Central Research Laboratories, Report No. 13, 877C (April 1961).
23. W. H. Louisell, Coupled Mode and Parametric Electronics, (John Wiley and Sons, New York, 1960), Section 1.7.
24. A. Nordbotten, "An Experimental Synchronous-Wave Amplifier," Norwegian Defense Research Establishment Report No. R-119 (June 1962).
25. T. Wessel-Berg, "Space-Charge Wave Theory of Interaction Gaps and Multi-Cavity Klystrons With Extended Fields," Norwegian Defense Research Establishment Report No. 32 (September 1960), Chapter 5.
26. G. Bernstein and J. Feinstein, "The Larmotron - a DC Pumped Quadrupole Amplifier," SFD Laboratories, Inc. Report (June 1961).

27. W. H. Louisell, op. cit., Sections 3.3 and 3.5.

28. D. A. Watkins, Topics in Electromagnetic Theory, (John Wiley and Sons, Inc., New York, 1958), p. 2.

29. K. Blφtekjaer and T. Wessel-Berg, private correspondence.

30. J. M. Manley and H. E. Rowe, "Some General Properties of Nonlinear Elements - Part I," General Energy Relations, Proc. IRE 44, 904-913 (July 1956).

31. K. Blφtekjaer, "A Proposed Harmonic Generator Based on Cyclotron Waves," IRE, Trans. PGED, ED-9, 27-32 (January 1962).

32. A. D. Wheelon, "A Short Table of Summable Series," Douglas Aircraft Co., Inc., Report No. SM-14642 (February 1953), Eqs. 13.108 and 13.112.

33. C. C. Johnson, "An Investigation of the Magnetic Transverse Waves on an Electron Beam," IRE, Trans. PGED, ED-9, 288-295 (May 1962).

34. R. C. Honey, "A TW Electron Deflection System," Stanford ERL Technical Report No. 63 (May 1953).

35. J. Sorland, "Investigation of a Periodic Transmission Line for Use as a Transverse-Wave Coupler," Norwegian Defense Research Establishment Internal Report No. R-110 (March 1962).

36. J. R. Pierce, Traveling-Wave Tubes, (D. Van Nostrand Co., Inc., Princeton, New Jersey, 1950), Appendix III.

37. M. Chodorow and C. Susskind, "Fundamentals of Microwave Tubes," Notes for a course given at Stanford University, Section 2.7.

38. G. C. Van Hoven and T. Wessel-Berg, "Negative Energy Fast Waves in Brillouin Flow Beams," Microwave Laboratory Report No. 990, Stanford University (December 1962).

39. A. H. W. Beck, Space-Charge Waves, (Pergamon Press, New York, 1958), p. 119.

40. W. J. Gallagher, "Measurement Techniques for Periodic Structures," Microwave Laboratory Report No. 767, Stanford University (November 1960).

41. E. L. Ginzton, Microwave Measurements, (McGraw-Hill Book Co., Inc., New York, 1957), pp. 448-51.

42. J. R. Pierce, op. cit., Section 4.4.

DISTRIBUTION LIST

CONTRACT NONR 225(48)

cc	Addresses
2	Chief of Naval Research Department of the Navy Washington 25, D. C. Attention: Code 427
1	Commanding Officer Office of Naval Research 1030 E. Green Street Pasadena, California
1	Commanding Officer Office of Naval Research Branch Office 346 Broadway New York 13, New York
	Director Naval Research Laboratory Washington 25, D. C.
1	Attention: Code 3400
1	3600
1	3900
1	3930
1	1940
2	Chief, Bureau of Naval Weapons Department of the Navy Washington 25, D. C. Attention: RREN
1	Director Naval Electronics Laboratory San Diego 52, California
10	ASTIA Arlington Hall Station Arlington 12, Virginia
1	Commanding Officer Office of Naval Research Branch Office 1000 Geary Street San Francisco 9, California
1	Commanding Officer Office of Naval Research Branch Office John Crerar Library Building 86 E. Randolph Street Chicago 1, Illinois
10	Commanding Officer Office of Naval Research Navy 100 Fleet Post Office Box 39 New York, New York
2	Chief, Bureau of Ships Navy Department Washington 25, D. C. Attention: Code 670
2	Chief, Bureau of Aeronautics Navy Department Washington 25, D. C. Attention: Code AV
	Chief, Naval Operations Navy Department Washington 25, D. C.
1	Attention: Code Op 30
1	Op 31
1	U. S. Naval Post Graduate School Monterey, California
1	Commander Naval Air Missile Test Center Point Mugu, California
1	Chief, European Office Air Research and Development Command 47 Rue Cantersteen Brussels, Belgium

cc	Addresses
	Commanding General Air Force Research Division Air Research and Development Command Bedford, Massachusetts
8	Attention: CRRE
1	ERRSA-1
1	Director Air University Maxwell Air Force Base Alabama Attention: Cr 4582
1	Assistant Secretary of Defense (Research and Development) Department of Defense Washington 25, D. C. Attention: Technical Library
1	Chief, West Coast Office USASRDL Building No. 6 75 South Grande Avenue Pasadena 2, California
1	Chief Signal Officer Department of the Navy Washington 25, D. C. Attention: SIGRD
1	Commanding Officer U. S. Army Signal Missile Support Agency White Sands, New Mexico
1	Commanding General U. S. Army Ordnance Missile Ground Huntsville, Alabama Attention: ORDAB-T
1	Commanding Officer U. S. Naval Proving Ground Dahlgren, Virginia
1	Commander U. S. Naval Air Development Center Johnsville, Pennsylvania

cc	Addresses
1	Commanding Officer Office of Ordnance Research Box CM, Duke Station Durham, North Carolina
1	Airborne Instrument Laboratory Comac Road Deer Park, L. I., New York Attention: John Dyer
1	U. S. Coast Guard 1300 E. Street, N.W. Washington 25, D. C. Attention: EEE
1	Secretary Commission on Electrics Office of the Assistant Secretary of Defense (Research and Development) Department of Defense Washington 25, D. C.
1	Director of Army Research Office, Chief of Research and Development Washington 25, D. C.
1	Chief Signal Officer Department of the Army Washington 25, D. C. Attention: SIGCO05b4
1	Commanding General U. S. Army Electronic Proving Ground Fort Huachuca, Arizona ATTN: Technical Library, Greely Hall
1	Commanding General Naval Ordnance Laboratory Corona, California
32	Signal Property Agent Building 2504, Watson Area Fort Monmouth, New Jersey Attention: Officer of Research Operations

cc	Addresses
1	Bell Telephone Laboratories Murray Hill Laboratory Murray Hill, New Jersey Attention: Dr. J. R. Pierce
1	Office of the Chief of Engineers Department of the Army Washington 25, D. C.
1	California Institute of Technology Department of Electrical Eng. Pasadena, California Attention: Professor L. M. Field
1	Commanding Officer Engineering Research and Development Laboratory Ft. Belvoir, Virginia
1	Ballistics Research Laboratory Aberdeen Proving Ground Aberdeen, Maryland Attention: D. W. W. Delsasso
2	Chief of Staff United States Air Force Washington 25, D. C. Attention: AFDRD-SC-3
2	Commanding General Rome Air Development Center Griffiss Air Force Base Rome, New York Attention: RCRW
5	Commander Air Force Office of Scientific Research Attention: SRYA Washington 25, D. C.
1	National Science Foundation 1951 Constitution Avenue, N. W. Washington 25, D. C.

cc	Addresses
1	Commander Air Force Armament Center Attention: Technical Library Elgin Air Force Base, Florida
1	Commander Air Force Missile Development Center Attention: Technical Library Holloman Air Force Base New Mexico
1	Hq. U.S. Army Material Command Building T-7 Attention: AMDRD-DE-MI Washington, D.C.
1	Commanding Officer Frankford Arsenal Bridesburg Philadelphia, Pennsylvania
	Commander Wright Air Development Division Wright-Patterson Air Force Base Ohio
2	Attention: WCLC
4	WCLRC
1	WCLRC
1	WPLJ
1	WCLJH
1	WCRE
2	WCRED
1	WCRET
1	AEMTC (AEMTC Technical Library-MU 135) Patrick Air Force Base Cocoa, Florida
1	Chief, Physics Branch, Division of Research U. S. Atomic Energy 1901 Constitution Avenue, N. W. Washington 25, D. C.

cc	Addresses
1	Commander Arnold Engineering Development Center Attention: Technical Library Tullahome, Tennessee
1	Commander Air Force Special Weapons Center Attention: Technical Library Kirtland Air Force Base New Mexico
1	Commandant Air Force Institute of Tech. Attention: MCLI, Tech. Library Wright-Patterson Air Force Base Ohio
1	Commander Air Force Ballistic Missile Division Headquarters ARDC Attention: WDSOT Post Office Box 262 Inglewood, California
40	Stanford University Stanford, California
1	Sylvania Electric Products, Inc. 500 Evelyn Avenue Mountain View, California Attention: Special Tube Operations
1	Ohio State University Department of Electrical Eng. Columbus 10, Ohio Attention: Professor E. M. Boone
1	University of Michigan Willow Run Research Center Engineering Research Institue Ann Arbor, Michigan Attention: Dr. H. Goode
1	Director Electronics Defense Group Engineering Research Institute University of Michigan Ann Arbor, Michigan
1	Columbia University Columbia Radiation Laboratory New York 27, New York Attention: Mr. Bernstein
1	Cruft Laboratory Harvard University Cambridge, Massachusetts
1	Dr. Winston H. Bostick Department of Physics Stevens Institute of Technology Hoboken, New Jersey
1	Sperry Gyroscope Company Great Neck, L. I., New York Attention: Technical Library
1	Sylvania Electric Systems Applied Research Laboratory 40bSylvan Road Waltham 54, Massachustts Attention: Charles E. Arnold
1	Varian Associates 611 Hansen Way Palo Alto, California Attention: Technical Library
1	University of Texas Defense Research Laboratory Austin, Texas Attention: Harold D. Krick, Sr.
1	Massachusetts Institute of Technology Research Laboratory of Electronics Cambridge 39, Massachusetts Attention: Mr. Hewitt Librarian

cc Addresses

1 Brooklyn Polytechnic Institute
Microwave Research Institute
55 Johnson Street
Brookly 1, New Jersey
Attention: Mr. Jerome Fox

1 Dr. John R Whinnery
Division of Electrical Eng.
University of California
Berkeley 4, California

1 Professor Hans Motz
Oxford University
Oxford, England

1 Lincoln Laboratory
Massachusetts Institute of Technology
P. O. Box 73
Lexington, Massachusetts

1 Gilfillian Brothers
1815 Venice Blvd.
Los Angeles, California
Attention: Countermeasures Laboratories

1 Hallicrafters
4401 West 5th Street
Chicago, Illinois
Attention: William Frankart

1 The Maxson Corporation
460 West 34th Street
New York 1, New York

1 Motorola, Incorporated
8330 Indiana Avenue
Riverside, California
Attention: Robert W. Barton

1 Raytheon Manufacturing Corp.
Waltham 54, Massachusetts
Attention: Research Division Library

cc Addresses

Sperry Gyroscope Company
Electronic Tube Division
Great Neck, L. I., New York
Attention: T. Sege

4 Office of Ordnance
U. S. Army
Box CM, Duke Station
Durham, North Carolina

1 Electron Tube Division of the Research Laboratory
General Electric Company
The Knolls
Schenectady, New York

1 Glenn L. Martin Company
Baltimore, Maryland
Attention: Mary E. Exxo

1 Hughes Aircraft Company
Florence Ave. and Teale St.
Culver City, California
Attention: Mr. Nicholas E. Devereux
Technical Document Center

1 The Rand Corporation
1700 Main Street
Santa Monica, California
Attention: Margaret Anderson
Librarian

1 Dr. Walter Higa
Engineering Specialist
Research Group Supervisor
California Institute of Technology
4800 Oak Grove Drive
Pasadena 3, California

1 General Electric Microwave Lab.
601 California Avenue
Palo Alto, California
Attention: Librarian

1 Pacific Union College
Physics Department
Angwin, California
Attention: Dr. Ivan Neilson

cc	Addresses
1	Dr. A. D. Berk 4134 Del Rey Avenue Venice, California
1	Dr. A. F. Pierce Imperial College of Science and Technology South Kensington London, S. W., England
1	The Mitre Corporation P. O. Box 208 Lexington 73, Massachusetts
1	Mr. Jack Summers Varian Associates 611 Hansen Way Palo, Alto, California
1	General Electric Company Power Tube Division Electronic Components Division Building 269, Room 205 One River Road Schenectady 5, New York
1	Litton Industries Electron Tube Division 960 Industrial Road San Carlos, California
1	Eitel-McCullough, Inc. Research Library 301 Industrial Way San Carlos, California
1	Stanford Research Institute Menlo Park, California Attention: Documents Center
1	Bendix Corporation Red Bank Division Eatontown, New Jersey Attention: Mr. S. Barbasso

cc	Addresses
1	High-Power Klystron Department G.38 Attention: Dr. John Romaine Sperry Gyroscope Company Great Neck, L. I., New York
1	Dr. Bertil Agdur Microwave Department Royal Institute of Technology Stockholm, Sweden
1	California Institute of Technology Electron Tube Laboratory Pasadena, California
1	Robert Vehn Watkins-Johnson Company 3333 Hillview Avenue Palo Alto, California
1	Sperry Electronic Tube Division Sperry Rand Corporation Gainesville, Florida
1	Research Division Library Raytheon Company 28 Seyon Street Waltham 54, Massachusetts
1	Mr. J. F. Kane Kane Engineering Laboratories 845 Commercial Street Palo Alto, California
1	Phillips Laboratoties Division of North American Phillips Company, Inc. Irvington-on-Hudson New York Attention: Robert C. Bohlinger
1	Director U. S. Naval Research Labs. Washington 25, D. C. Attention: Code 5300

cc	Addresses
1	Sperry Phoenix Company Division of Sperry Rand Corp. Phoenix, Arizona Attention: Tech. Librarian
1	TUCOR, Incorporated 18 Marshall Street South Norwalk, Connecticut Attention: Mrs. Marion Osband
1	Professor H. W. Konig Institute fur Hochfrequenztechnik Technische Hochschule Vienna 4, Gusshausstrasse 25 Austria
1	Dr. V. L. Stout, Manager Physical Electronic Research P. O. Box 1088 Schenectady, New York
1	Institute for Defense Analysis Research and Engineering Support Division 1825 Connecticut Ave., N. W. Washington 25 D. C. Attn: Technical Information Office
1	Director National Security Agency Fort George G. Meade, Maryland Attention: CREF-332 (Rm. 2C087) Miss Creswell Librarian
1	Research Center for the Airtron Division of Litton Industries 200 East Hanover Avenue Morris Plains, New Jersey Attention: J. W. Neilson, Manager Solid State Materials Laboratory

cc	Addresses
1	Commanding Officer U. S. Army Research Office Durham Box CM, Duke Station Durham, North Carolina Attention: CRD-AA-IP, Mr. Ulsh
1	Cornell University School of Electrical Engineering Ithaca, New York Attention: Professor G. C. Dalman
1	Carlyle Barton Lab. The Johns Hopkins University Charles and 34th Streets Baltimore 18, Maryland Attention: Librarian
1	Professor Sanai Mito Osaka City University Department of Engineering 12 Nishi-Ogimachi, Kitaku Osaka, Japan
1	CERN Service d'Information Scientifique Attn: Mme L. Goldschmit-Clermont Geneva 23, Switzerland
1	Amphenol-Borg Electronics Corporation 2801 South 25th Avenue Broadview, Illinois ATTN: Mr. R. C. Becker Senior Staff Engineer
1	Mr. Glen Wade Spencer Laboratories Burlington, Massachustts
1	Scientific Attache Swedish Embassy 2249 R. Street, N. W. Washington 8, D. C.

cc	Addresses
1	Dr. Yen Department of Electrical Eng. University of Toronto Toronto 5, Ontario Canada
1	M. A. Allen Microwave Associates Inc. Burlington, Massachusetts
3	Commanding Officer U. S. Army Research Office (Durham) ATTN: CRD-AA-IP, Box CM Duke Station Durham, North Carolina
1	Raytheon Company Research Division Waltham 54, Massachusetts ATTN: Mrs. Madaleine Benett Librarian
1	USNPG Monterey, California ATTN: Prof. Gray Electronics Department
1	Dr. E. A. Ash Standard Telecommunications Lab., Ltd. London Road Harlow, Essex, England
1	Dr. W. Veith Siemens and Halske Aktiengesell- schaft St. Martin Strasse 76 Munchen 8, Germany
1	Dr. Humio Inaba Electrical Engineering Department Tohoku University Sensai, Japan
1	Dr. T. Rossing St. Olaf College Northfield, Mennesota

cc	Addresses
1	Carnegie Institute of Technology Department of Electrical Eng. Schenlay Park Pittsburgh 13, Pennsylvania
1	U. S. Atomic Energy Commission Research Division Washington 25, D. C. Attn: Mr. Wm. C. Gough